TECHNISCHE UNIVERSITÄT MÜNCHEN

Department Chemie

Lehrstuhl für Anorganische Chemie

Water-insoluble and water-soluble NHC complexes and their applications in hydrogenation reactions

Esther Bayón Castañón

aus León

Vollständiger Abdruck der von der Fakultät für Chemie der Technischen Universität München zur Erlangung des akademischen Grades eines

Doktor der Naturwissenschaften (Dr. rer. nat.)

genehmigten Dissertation.

Vorsitzender: Prof. Dr. Lukas Hintermann

Prüfende der Dissertation: 1. Prof. Dr. Fritz E. Kühn

2. Prof. Dr. Klaus Köhler

Die Dissertation wurde am 18.06.2018 bei der Technischen Universität München eingereicht und durch die Fakultät für Chemie am 12.07.2018 angenommen.

Abstract

The use of *N*-heterocyclic carbenes (NHCs), particularly as ligands in metal complexes, has attracted considerable attention during the recent two decades. So far, the use of most organometallic complexes in catalysis is restricted to organic solvents due to their low solubility and limited stability in aqueous solutions. However, water presents several advantages over organic solvents. The development of water-soluble complexes is not only interesting due to the "green chemistry principles", but also for the establishment of processes that allow the application of highly selective molecular catalysts under mild conditions, e.g. for biphasic processes associated with easy catalyst/product separation. Therefore, a series of analogous new water-insoluble and water-soluble NHC complexes is developed in order to compare their different catalytic activities.

The synthesis of novel Ru(II), Os(II), Rh(III) and Ir(III) mono *N*-heterocyclic carbene (NHC) complexes with a pyridine substituent is reported. Reaction of the imidazolium salts bearing *N*-alkyl and sulfonated *N*-alkyl substituents with Ag_2O leads to the formation of the corresponding Ag(I) complexes. The metal complexes are available in good yields via transmetallation reactions from the corresponding silver complexes and $[ArMCl_2]_2$, where Ar = p-cymene or Cp* and M = Ru, Os, Rh or Ir. While N-alkyl substituted NHC complexes are almost insoluble in water (1.55 mg/ml), sulfonated *N*-alkyl substituted NHC complexes display good solubility in water (up to 400 mg/mL). All complexes have been characterized by means of spectroscopic methods. Molecular structures of all the silver, rhodium and iridium complexes, together with the water-soluble osmium compound were determined by single crystal X-ray diffraction analysis.

All complexes were examined in the catalytic transfer hydrogenation of acetophenone, which is quantitatively and highly selective reduced to 1-phenylethanol. Tests for water-insoluble compounds were studied under inert atmosphere in a KOH/^{i}PrOH reaction mixture and yields determined by ^{1}H NMR spectroscopy. The ruthenium (water-insoluble) catalyst was found to be the most active catalyst, followed by its analogous rhodium and iridium catalysts. The osmium based complex displays a comparatively low activity. When water-soluble catalysts were applied for transfer hydrogenation of acetophenone, an aqueous buffer solution of HCO_2Na/HCO_2H was used as hydrogen source. In this case, the rhodium catalyst appears to be the most active one, followed by iridium and ruthenium. The osmium complex showed again comparatively low activity. Yields were determined by ^{1}H NMR spectroscopy and GC-MS measurements.

Additionally, the water-soluble complexes were examined in the complete hydrogenation of acetophenone with hydrogen in an autoclave system. First experiments revealed ruthenium to be the most active catalyst followed by rhodium. Both compounds were able to hydrogenate the aromatic ring displaying an induction period of about 3 h. However, this period can be avoided by activation of the pre-catalysts in aqueous solution. For both catalytic reactions, higher conversions with lower catalyst loadings are obtained as compared to literature-known complexes.

Zusammenfassung

Der Einsatz *N*-heterozyklischer Carbene (NHCs) als Liganden in Metallkomplexen hat in den letzten zwei Dekaden stetig an Beachtung gewonnen. Bisher war die Verwendung der meisten organometallischen Komplexe als Katalysatoren aus Gründen der Löslichkeit und Stabilität vor allem auf organische Systeme beschränkt. Wasser hingegen bietet einige bedeutende Vorteile, und zwar nicht nur im Hinblick auf die „Green chemistry principles“. Es ermöglicht auch den Einsatz hoch selektiver Katalysatoren unter milden Bedingungen bei einfacher Trennung von Katalysator und Produkt im Zweiphasensystem.

In dieser Arbeit wurden mehrere neue wasserlösliche NHC Komplexe hergestellt und mit ihrem wasserunlöslichen Analog verglichen. Im Vordergrund steht die Synthese neuer Ru(II), Os(II), Rh(III) und Ir(III) mono-NHC Komplexe mit einem Pyridinsubstituenten. Sulfonierte und nicht sulfonierte *N*-Alkyl Substituenten aus Imidazoliumsalzen reagieren mit Ag_2O zu den entsprechenden Ag(I) Komplexen. Ihre Transmetallierungsreaktionen mit $[ArMCl_2]_2$, wobei Ar für *p*-Cymol oder Cp* und M für Ru, Os, Rh oder Ir steht, erzielten hohe Ausbeuten. Während *N*-Alkyl substituierte NHC Komplexe fast wasserunlöslich sind (1.55 mg/ml), zeigen die sulfonierten Analoge eine hohe Wasserlöslichkeit (bis zu 400 mg/ml). Alle untersuchten Komplexe wurden spektroskopisch charakterisiert. Die molekularen Strukturen der Ag, Rh und Ir Komplexe, sowie die der wasserlöslichen Os Verbindung wurden anhand von Einkristall-Röntgenbeugungsanalyse bestimmt.

Alle Komplexe wurden für den Einsatz in der quantitativen und hochselektiven Transfer-Hydrierung von Acetophenon zu 1-Phenylethanol getestet. Experimente mit wasserunlöslichen Verbindungen wurden unter inerter Atmosphäre in einer KOH/^{i}PrOH Mischung durchgeführt und die Ausbeuten per ^{1}H NMR Spektrometrie bestimmt. Dabei war die Reihenfolge vom aktivsten zum am wenigsten aktiven Katalysator Ru – Rh – Ir – Os Für die wasserlöslichen Katalysatoren bei den Tranfer-Hydrierungsreaktionen wurde eine wässrige HCO_2Na/HCO_2H Pufferlösung als Wasserstoffquelle verwendet. Hierbei zeigte Rh die höchste Aktivität, gefolgt von Ir, Ru und zuletzt Os. Die Produktausbeuten wurden mittels ^{1}H NMR Spektrometrie und GC-MS Messungen bestimmt.

Weiterhin wurden die wasserlöslichen Komplexe für die vollständige Hydrierung von Acetophenon im Autoklaven getestet. In ersten Experimenten zeigte Ru die höchste Aktivität, gefolgt von Rh, wobei beide Katalysatoren eine Induktionsperiode von 3 h präsentierten. Diese Zeit konnte jedoch verhindert werden indem die Vorläufer der Katalysatoren zuvor in wässriger Lösung aktiviert wurden. Sowohl bei den untersuchten Transfer-Hydrierungsreaktionen als auch bei der vollständigen Hydrierung erzielten die in dieser Arbeit entwickelten Katalysatoren höhere Umsätze beim Einsatz von niedrigeren Katalysatormengen im Vergleich zu Literatur bekannten Komplexen.

Acknowledgements

My very special gratitude goes to my doctoral supervisor **Prof. Dr. Fritz E. Kühn** for the opportunity to realize my doctoral studies in his group, as well as for his most valuable and highly appreciated guidance and supervision during my research.

Also very special thanks to the “Bayerische Forschungsstiftung” for the financial support.

I further want to express my deepest and sincere thanks to all those persons who have contributed to this work. Especially I thank and give significant recognition to Dr. Mirza Cokoja and Dr. Alexander Pöthig for their valuable support during these years.

I thank Dr. Karl Öfele for his help and support with the autoclave system.

Big thanks also to Marlene Kaposi for her work in X-Ray diffraction studies and Robert Reich for his support in the PhD and publication writing processes.

I would also like to thank the technicians of the department, above all Jürgen Kudermann, who supported me with a big variety of themes and help me to solve a lot of autoclave problems ; Maria Weindl for the preparation of various NMR spectra ; and Rodica Dumitrescu for her nice attention and quick FAB and ESI analysis results. I also thank Marianne Hanzlick for the support with the TEM measurements and also the elemental analysis team for their quick work, always really helpful.

I would like to extend my gratitude to my department colleges and especially to my laboratory mates, Florian Groche and Sophie Jürgens, who made every day different, for our talks and for helping each other. And also to Dominik Jantke, who introduced me in this research field.

Of course, I want to thank my family and friends for their support and notably to my husband David for his help, understanding and affection.

Table of Contents

Abstract ..... **i**

Zusammenfassung ..... **ii**

Acknowledgements ..... **iii**

Table of Contents ..... **iv**

1 Introduction **1**

1.1 Carbenes 1

1.2 *N*-Heterocyclic carbene complexes 4

1.3 Water as solvent and water-soluble NHC complexes 6

1.4 Objectives 8

2 Synthesis of *N*-Heterocyclic carbene complexes with later transition metals **9**

2.1 Imidazolium salts and metal precursors 18

2.1.1 Ligand precursors 18

2.1.2 Non-sulfonated imidazolium salts 20

2.1.3 Sulfonated imidazolium salts 22

2.2 Metal precursors 23

2.3 Silver(I) NHC complexes 24

2.4 Water-insoluble 1-(2-pyridinyl)-3-n-butyl)imidazol-2-ylidene metal complexes 27

2.5 Water-soluble 1-(2-pyridinyl)-3-(sulfonatepropyl)imidazol-2-ylidene metal complexes 30

2.6 Solid state structures of Osmium, Rhodium and Iridium complexes 32

3 Catalytic hydrogenation of acetophenone **35**

3.1 Catalytic transfer hydrogenation of acetophenone with water-insoluble 1-(2-pyridinyl)-3-(*n*-butyl)imidazol-2-ylidene metal complexes 44

3.1.1 Experimental 44

3.1.2 Proposed mechanism 49

3.2 Catalytic transfer hydrogenation of acetophenone with water-soluble 1-(2-pyridinyl)-3-(sulfonatepropyl)imidazol-2-ylidene metal complexes 50

3.2.1 Experimental 50

3.2.2 Proposed mechanism 58

3.3 Complete hydrogenation of acetophenone in water 60

3.3.1 First experiments in an autoclave system 60

3.3.2 Optimization of the catalysis for ruthenium and rhodium catalysts 63

3.3.3 Characterization of the active species in catalysis 65

4 Conclusion and outlook 67

A. Annex 69

A.1 Experimental methods 69

A.1.1 General remarks 69

A.1.2 Analytical methods 69

A.1.3 Synthesis of catalysts 70

A.1.4 Representative procedure for catalytic experiments 88

A.3 Supporting information 89

A.3.1 ^{1}H and ^{13}C NMR spectra 89

A.3.2 X-Ray crystallographic data 99

Notations 104

References 106

List of Schemes **114**

List of Figures **116**

List of Tables **120**

1 Introduction

1.1 Carbenes

Carbenes are defined as the electrically neutral species $:CH_2$ and its derivatives, in which the carbon is covalently bonded to two univalent groups of any kind or a divalent group and bears two nonbonding electrons, which may be spin-paired (singlet state) or spin-non-paired (triplet state). In systematic name formation, carbene is the name of the parent hydride $:CH_2$, e.g. $:CCl_2$ is named dichlorocarbene. However, names for acyclic and cyclic hydrocarbons containing one or more divalent carbon atoms are derived from the denomination of the corresponding all-λ^4-hydrocarbon using the suffix "–ylidene".[1,2]

On the other hand, the term metal-carbene complexes refers to compounds of the general type:

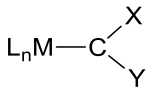

in which a carbene :CXY, is coordinated to a metal atom M, and L simply represents the various other coordinated ligands.[3]

Although they were not recognized until 1970, first carbene complexes were prepared in 1915.[4–6] Fischer and Maasböl revolutionized the organometallic chemistry in 1964 with the discovery of some metal carbenes (Figure 1 (a))[7,8] which led to a huge number of applications in synthesis and catalysis. Heterocyclic carbenes derived from imidazolium and pyrazolium salts were first used in 1968 to form stable complexes with some transition metals. Wanzlick and Öfele synthesized the first chromium and mercury *N*-heterocyclic carbene complexes (Figure 1 (b) and (c)).[9–11] In 1974, Schrock reported the first synthesis of a high oxidation state (d^0) metal-alkylidene complex by an α-hydrogen abstraction on the tris(2,2-dimethylpropyl)methyl tantalum(V) dichloride precursor (Figure 1 (d)).[12] It was not until 1991, when for the first time Arduengo *et al*. reported remarkable stable free carbenes (Figure 1 (e)), which have been used to prepare metal complexes.[13,14]

At this point, it is important to explain the main differences between the different type of carbenes, their properties and their different reactivities. There is more than one unique carbene to be considered in the field of organometallic chemistry. The carbonic atom can be nucleophilic or electrophilic. Attending to their electronic configuration singlet and triplet carbenes are distinguished (Figure 2).[15]

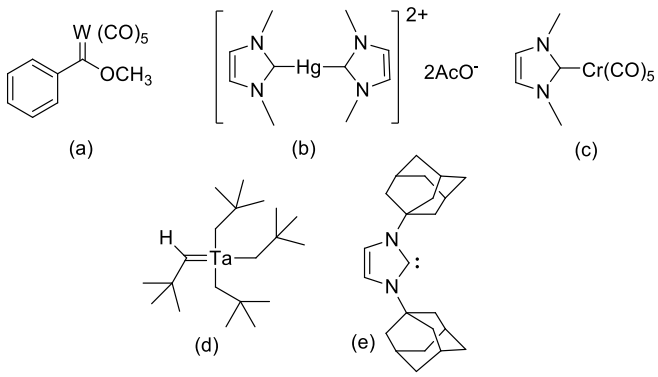

Figure 1. Fischer (a) first carbene compound, Wanzlick (b) and Öfele (c) first *N*-Heterocyclic compounds, first Schrock alkylidene–metal (d^0) complex (d) and first stable free carbene synthesized by Arduengo *et al*. (e)

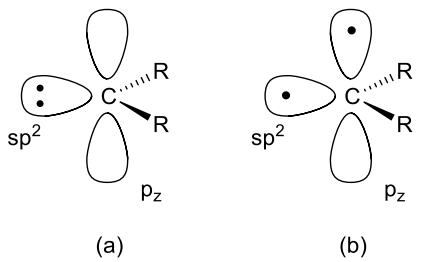

Figure 2. Singlet (a) and triplet (b) forms of a carbene.

Singlet carbenes: Carbene multiplicity can be determined by the electronegativity of both *α*-substituents (X and Y). *σ*-electron withdrawing groups (negative inductive effect: -*I*) favor the singlet state by stabilizing the filled non-bonding orbital, increasing its *s*-character. On the other hand, electronic delocalizations (mesomeric effects: ±M) between the methylene and its *σ*-substituents determine the carbene geometry (linear or bent) and play an active role in its thermodynamic stabilization.[15]

Triplet carbenes: Diazo compounds, most of which are very fragile and prone to degradation, are used to generate triplet carbenes by photolysis. They usually bear two *α*-phenyl groups, as most *α*-di-alkylmethylenes appear to be singlet carbenes. Their diradical behavior makes them very reactive and difficult to isolate.[15]

Carbene complexes are commonly differentiated depending on their electronic properties. These differences correspond to both, an energy level splitting and to different chemical properties.

Fischer carbenes: They belong to the electrophilic carbene types (singlet carbenes) and form a metal–carbon bond constituted by mutual donor–acceptor interaction of two closed-shell (singlet) fragments. The dominant bonding arises from carbene–metal *σ*-donation and

simultaneously from metal–carbene π-back donation (Figure 3 (a)). The π-electrons are usually polarized toward the metal, having the carbon–metal bond a partial double bond character that diminishes with the stabilization of the carbene by its α-groups.

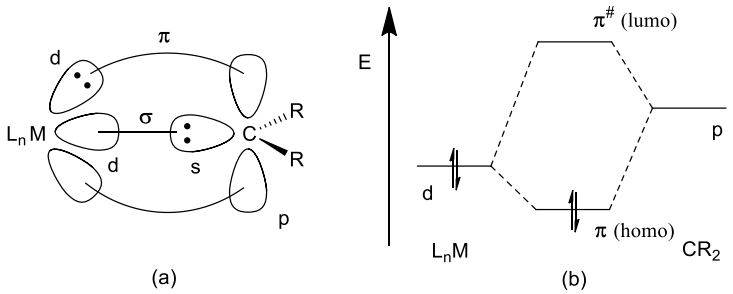

Figure 3. Bond of a singlet carbene with a metal to form a Fischer carbene (a) and OM diagram of the π- contribution of the M-C bond (b).

As it can be observed in the orbital molecular (OM) diagram of the π-contribution to the meta-carbon bond (Figure 3 (b)), the lumo orbital is closer to the *p* orbital of the "carbenic" carbon than to the *d* orbitals of the metal. This behavior usually arises with transition metals located on the right in the periodic table (groups 6, 7, 8…) or with low oxidation state metals. Due to this characteristic, Fischer carbene complexes are electrophilic at the carbon-metal bond and are prone to nucleophilic attack at the carbene center.

Schrock carbenes: They belong to the nucleophilic carbene types (triplet carbenes) and form a covalent metal–carbon bond in nature created by the coupling of two triplet fragments (Figure 4 (a)). The π-electrons are nearly equally distributed between the carbon and the metal, and the metal–carbon bond is seen as a true double bond.

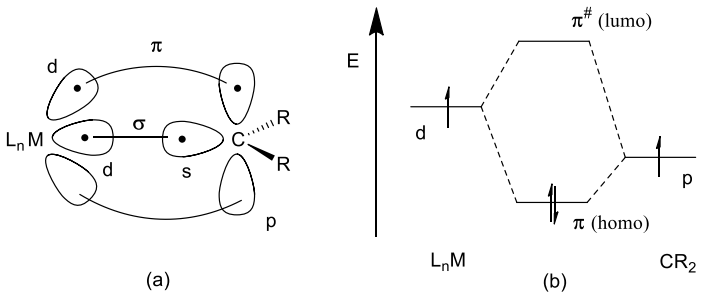

Figure 4. Bond of a triplet carbene with a metal to form a Schrock carbene (a) and OM diagram of the π- contribution of the M-C bond (b).

The OM presented in Figure 4 shows that in this case the homo orbital is closer to the *p* orbital of the "carbenic" carbon whereby the electron density delocalizes preferably on the *p* orbital. The homo orbital is negatively charged with respect to the metal, which makes Schrock carbene complexes nucleophilic at the carbon–metal bond and thus susceptible to react at the carbene center with electrophiles. They are found exclusively among early transition metals (where *d* orbitals are more destabilized; groups 4, 5) with the highest oxidation state (d^0).

Other type of meta-carbene complexes: There are complexes which are between Fischer- and Schrock-type compounds and which fit partially the definition of both categories. Non-heteroatom stabilized carbenes can be bond to late-transition metals and low oxidation state early transition metals. The complexes formed are usually electrophilic at the metal–carbon bond in contrast to Schrock carbene complexes. Schrock mentioned that in such complexes, the carbene moieties should be called phenylcarbenes and alkylcarbenes since benzylidenes and alkylidenes stand for Schrock carbene complexes.

The group of ***N*-Heterocyclic carbene (NHC) complexes** were initially not considered so interesting for their catalytic behavior, which may be debt to their differences in their properties as compared to the other, more common types of carbene ligands (Fischer and Schrock carbenes). NHCs are generally spectator ligands, while the other ones are reactive substituents. However, since they are focus of the presented work, the NHC complexes are described in more detail in the next sections.

1.2 *N*-Heterocyclic carbene complexes

NHC complexes, also called "Arduengo carbenes", are diamino-carbenes and form Fischer-type complexes with transition metals. Since the synthesis of free and stable carbenes, initially discovered by Arduengo *et al*. in 1991, [13,14] the development of this type of compound has significantly increased during the last decades. A huge variety of different NHCs have been synthesized and bonded to transition metals leading to well-defined complexes.

NHC complexes are neutral two-electron donors that form σ-bonds, but they can also engage in π-backbonding to accept any transfer of electron density from the metal. In metal complexes, NHCs share together with phosphines the characteristics of being monodendate two-electron donor ligands, hence they can be considered as an alternative to this family of compounds. However, experiments and calculations have shown that the σ-donor character of NHCs is often stronger than that of most basic phosphane ligands.[16] On the other hand, the π-accepting ability of NHC complexes decreases when compared to Schrock and Fischer carbene complexes. Except of the relation with group 11 transition metals (Cu, Ag, Au) it even can be considered negligible.[15,17,18]

Another important aspect to be considered in relation to the π-backbonding properties of NHCs is the nature of the ring system. It has been proved that π-back donation is favored in saturated imidazolylidenes when compared to their unsaturated analogues.[19] The unsaturated carbenes render the metal center a better σ-acceptor and π-donor, which renders coordination of substrates usually more facile. However, due to the weaker bond that they form with the metal, this could give rise to stability issues. Conversely, saturated NHCs, which are more strongly bound ligands, stabilize the catalyst, but they may also lower its reactivity. This is probably because they make the metal center a worse σ-acceptor and π-donor, which results in weaker interactions with many substrates. The electronic properties of NHCs can be tuned by varying the 4,5 position on the heterocycle or the substituents of the hetero atoms, but also steric properties can be varied by applying bulky ligands. In addition, chirality can be induced by employing chiral substituents. Furthermore, complex solubility can be increased and complex stability enhanced by choosing the right NHC ligand.[20] NHCs react with acids to form iminium salts due to their high pK_a values (pK_a = 20-30 in water), [21,22] but at the same time they are very powerful neutral organic bases, comparable to DBU and pentacyclic vinamides.[23,24]

NHC complexes can be synthesized through many different routes,[25] as for example by use of protected forms or performed isolated free carbenes, by oxidative additions of an imidazolium cation, insertion of metals into a double C=C bond of bis(imidazolidin-2-ylidene)olefins, etc. The most famous and widely applied routes are named below.

The *in situ* deprotonation of an azolium salt with external bases is very frequently used method. Another alternative is the use of metal complexes containing a basic ligand, as for example acetate (AcO^-) or acetylacetonate (acac). Probably one of the most applied methods in the last years is the transmetallation reaction from a silver-NHC complex to other metals, due to the less sensitive character of these compounds to moisture or air.

NHC complexes have been widely used for a plethora of catalytic applications,[26 27–32], including cross coupling (M=Pd),[33] cycloisomerizations (M=Au),[34] isomerization of allylic alcohols (M=Ru)[35], *N*-alkylation of amines (M=Ru, Ir),[36] hydrogenation (M=Ru, Ir)[37], [38] and transfer hydrogenation reactions (M=Ru, Ir).[36], [39] NHC metal complexes have been also studied in fields as photophysics and medicinal chemistry.[40] The strength of the σ-donor characteristic of NHCs can be considered as the origin of high energy emissions, which represents a fundamental requisite to obtain complexes emitting in the blue region (most attractive color for the development of an efficient OLED device). On the other hand, gold and silver are actually the most studied metal centers concerning the medical properties of the corresponding NHC complexes. Both can act as antitumorals, while silver compounds can be used also as antimicrobials.

1.3 Water as solvent and water-soluble NHC complexes

For long time, the use of organometallic complexes in catalysis has been restricted mainly to organic solvents due to their low solubility and limited stability in aqueous solutions. However, water presents several advantages over organic solvents[41]. Being the most abundant liquid on earth it is relatively cheap, non-toxic and it can be used in large amounts without health hazards. The development of water-soluble complexes is not only interesting due to the so called "green chemistry principles",[42] but also for the establishment of processes that allow the application of highly selective molecular catalysts under mild conditions, e. g. for biphasic processes associated with easy catalyst/product separation which is one of the most notorious challenges in homogeneous catalysis.

Green Chemistry is defined as the ''design of chemical products and processes to reduce or eliminate the use and generation of hazardous substances". [42] The Twelve Principles of Green Chemistry are ''design rules'' to help chemists achieve the intentional goal of sustainability. Because of this goal, its application in all industrial sectors is not surprising. From aerospace, automobile, cosmetic, electronics, energy, household products, pharmaceutical, to agriculture, there are hundreds of examples of successful applications of award winning, economically competitive technologies.[42] The Twelve Principles are: prevention of waste, atom economy, less hazardous chemical synthesis, design of safer chemicals, use of safer solvents and auxiliaries, design for energy efficiency, use of renewable feedstocks, reduce unnecessary derivatization, use of selective catalysts, design of chemical products for innocuous degradation, real-time analytic methodologies for pollution prevention and inherently safer chemistry for accident prevention. In this light it is worth mentioning that nowadays, most of the solvents used in academia are organic and associated with significant risks since they are harmful, if not toxic, carcinogenic, flammable, or explosive. The same accounts for "volatile organic compounds" (VOCs) which are being used in most industrial processes. Focusing on environmental concerns, the chemical industry is a major contributor to environmental pollution which is why the development of nonhazardous alternatives is of great importance.[41] The use of water as solvent reveals saving potential for the chemical industry.[43]In this context water presents various advantages related to its physical and chemical properties. It has a high dielectric constant ($\varepsilon_{25º}$=78.5) which favors ionic reactions. It has the ability to solvate cations as well as anions. Its strong O-H bonds (enthalpy 436 kJ/mol) makes water the ideal solvent for radical reactions since O-H bonds are not easily attacked. It also has a high heat capacity, strong pressure dependency of the viscosity and high cohesive energy density.[44]

The field of chemical catalysis can be divided into homogeneous and heterogeneous catalysts. In homogeneous catalysis the catalyst is completely miscible with the solvent while in heterogeneous catalysis, substrate and catalysts are present in different phases. Heterogeneous catalysis permits an easy separation of the catalyst, but the reactions are often associated with lower activities and/or selectivities. On the other hand, the absence of mass transfer resistances in homogeneous operations permits the achievement of superior activity and selectivity.

However, the major bottleneck consists in the separation of the catalyst separation from reaction products, as well as in the lowered activity of the recovered catalysts. In order to avoid such problems, the use of water-soluble catalysts under biphasic conditions has become an attractive alternative, since the catalysts can be recovered (and re-used) by simple phase separation, filtration or decantation.

In this light, different NHC complexes, which have been found to present high stability in water, are promising candidates for homogeneous catalysis. Their high complex stability is debt to their high electron donation to the metal center. There are different ways to obtain water-soluble catalysts. Focusing on the ligand design and more concrete, on the use of NHC ligands, a detailed review which describes perfectly the different synthetic ways to achieve water-solubility through special features on the NHCs is presented in [43]. Commonly, NHCs have been synthesized containing either aliphatic or aromatic substituents, which enhance their hydrophobic properties. This may be omitted by finding an ionic or strongly polar functionalization of the NHCs in order to increase their solubility in water prior to metal complexation. With this purpose, various authors have investigated the use of different functionalization, such as carbonate/carboxylate, sulfonate, amine/ammonium, alcohol/ether, water-soluble macrocycle/polymer, natural-product-based and charged ligands and proton functionalization (Figure 5).

Water-soluble transition metal-NHC complexes have been applied for different catalytic or medical studies since they fulfill the above-mentioned advantages of high stability and easy catalyst separation. For example, Palladium catalysts have been mainly used for Suzuki, Heck and Sonogashira C-C coupling reactions, Pt and Rh have more impact in hydrosilylation, while Ru and Ir have shown to be very active in hydrogenation reactions; at the same time, ruthenium has important applications in olefin metathesis. Medicinal application has been widely studied with water-soluble silver complexes because of their antimicrobial activities and cytotoxicity.[45]

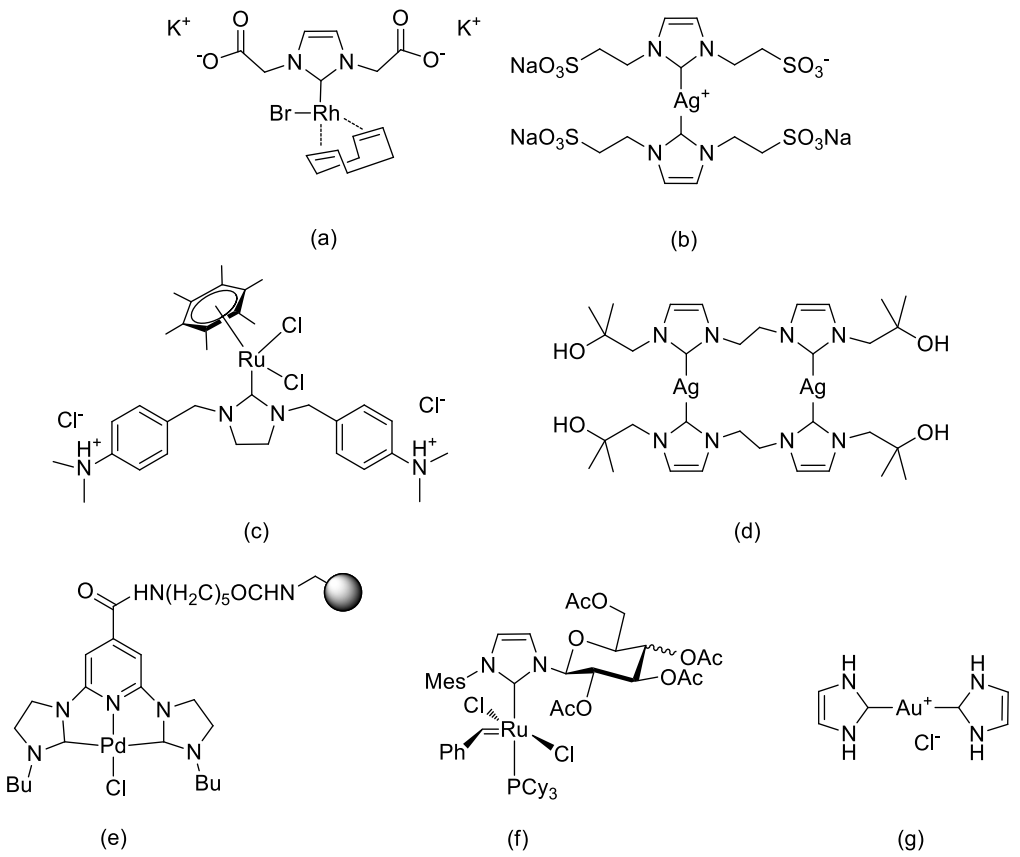

Figure 5. Examples of synthesized water-soluble NHC-metal complexes containing different functionalization of the NHC moieties: carboxylate (a), sulfonate (b), ammonium (c), alcohol (d), water-soluble polymer (e), natural product based (f) and charged ligand (g).

1.4 Objectives

The aim of this work is the synthesis of different water-insoluble and water-soluble NHC catalysts containing almost identical structures. Their different properties should be based in their different solvent solubility in order to be able to compare first, their synthetic procedures and second and most important, their different catalytic abilities. Both types of catalysts are tested in same catalytic applications (transfer hydrogenation reactions) under proper conditions, since we are limited by the different solubility and stabilities of the new synthesized catalysts. Furthermore, water-soluble complexes are also tested in catalytic hydrogenation reactions. More details are specified and will be considered in further chapters.

2 Synthesis of *N*-Heterocyclic carbene complexes with later transition metals

The focus of this work is the synthesis of new catalysts containing ruthenium, osmium, rhodium and iridium metal centers. For this purpose, transmetallation reaction from a silver-NHC complex to the other metals is the chosen method. In this case, silver-NHC intermediates are also isolated and characterized, proving that such compounds are not as sensible to moisture or air as when other synthetic methods are used (see section 1.2). In this introduction, some representative examples of literature known water-insoluble and water-soluble complexes that contain the same metal centers and similar structures to the new synthesized catalysts are presented. The main similarity is sought on the structure of the used NHCs (Figure 6) since they confer different properties to the compounds (completely different solubility) and consequently a different catalytic activity. Catalytic applications are described in the next sections.

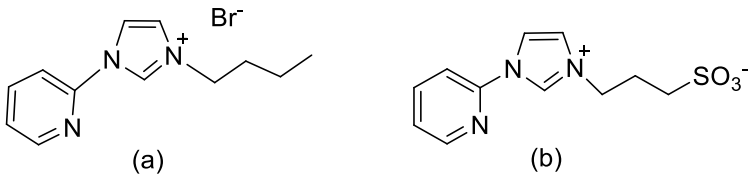

Figure 6. Used NHC ligands for the synthesis of new catalysts

Both ligands employed to synthesized the new catalysts are already known in the literature [34,46] and have been used for the preparation of metal-NHC compounds. Llobet *et al.*[47] describes the synthesis of ruthenium NHC compounds containing the 2-(Imidazole-1-yl-3-*n*-butyl)pyridine together with a tridentate NHC ligand. The synthetic route is shown in Scheme 1. After steps 1 and 3, purification by column chromatography is required to obtain the pure intermediate obtaining just only 10% yield after the first step. Finally, after the treatment of the intermediate complex containing bromide as ligand with silver(I) nitrate, the authors obtained a mixture of *cis* and *trans* isomers with a yield of 95%. Later on, they were able to obtain de *cis* isomer in a quantitative manner by irradiating *trans* isomer by means of a tungsten lamp.

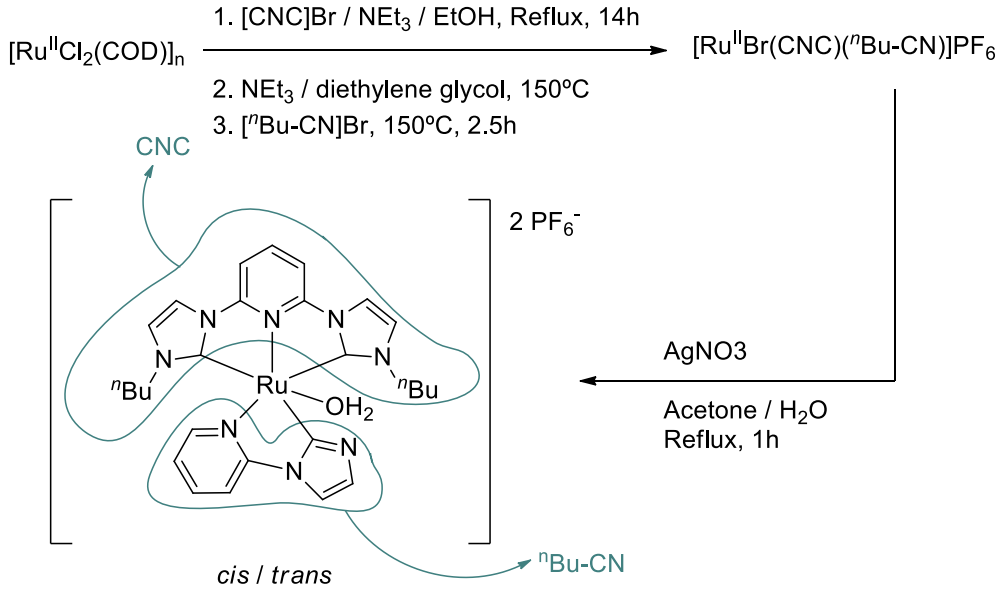

Scheme 1. Synthesis of a ruthenium (II) NHC complex reported by Llobet *et al.*[47]

Another example of similar ruthenium catalysts, but employing a simpler synthetic pathway is presented by Zi-Ling Xue *et al.*[48] in 2009 (Scheme 2). A mixture of the imidazolium salt with an excess of Ag_2O was stirred to afford the corresponding silver NHC compound, which, after filtration through Celite, was directly treated with the polymeric metal precursor $[Ru(CO)_2Cl_2]_n$. However, the authors did not characterize the silver NHC intermediate and also temperature and reaction time specifications for the synthesis are missing. Nevertheless, ruthenium final *cis* and *trans* isomers could be isolated and separated by column chromatography. Solvent and temperature of this second step may affect *cis*/*trans* ratio. It was found that the reactions in CH_2Cl_2 at room temperature gave the *trans* isomers as main product (yield 60-70%) while for the *cis* isomers lower yields were obtained (10-20%). The reactions in toluene at refluxing temperature on the other hand, afforded the *trans* isomers with only 5-10% yield and *cis* isomers with 70-80% yield respectively.

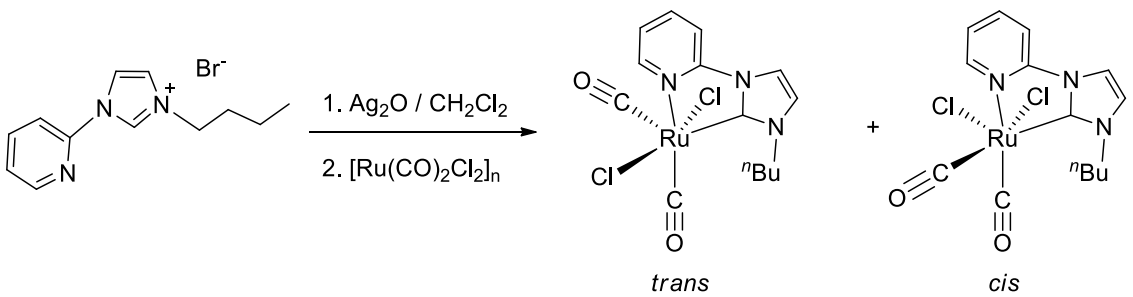

Scheme 2. Synthesis of a ruthenium (II) NHC complex reported by Zi-Ling Xue *et al.*[48]

Although in the case of Zi-Ling Xue *et al*.[48] the structure of the silver intermediate complex is not studied, previous works have synthesized silver compounds containing very similar NHC ligands. The complexes described by Eastham *et al*. in 2000 (Scheme 3)[49] were obtained by stirring the silver and ligand salts in CH_2Cl_2 under reflux for two days, achieving quantitative yields of all compounds.

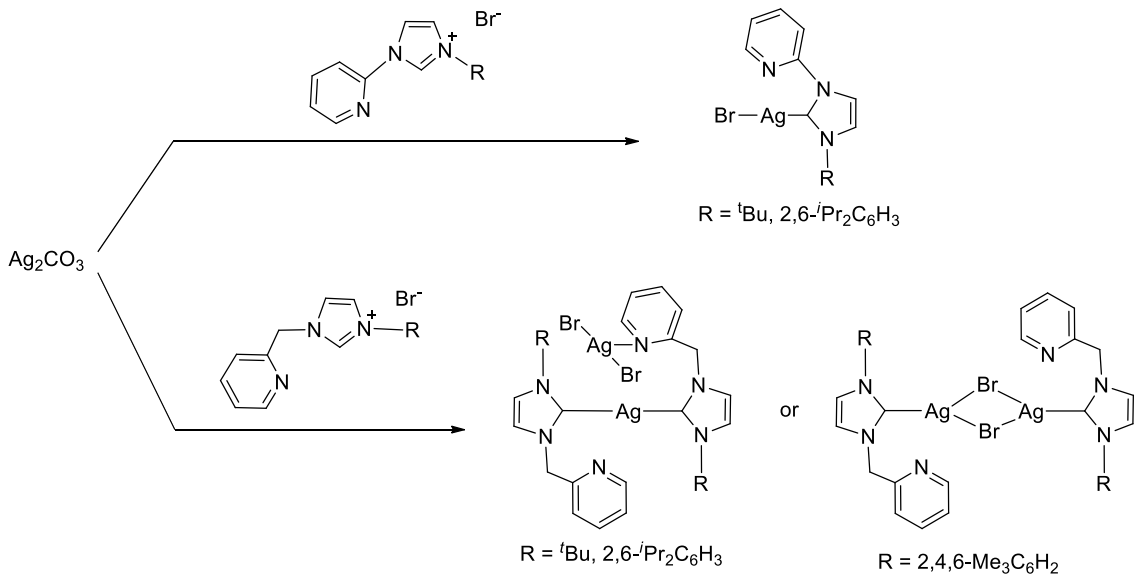

Scheme 3. Synthesis of silver (I) complexes reported by Eastham *et al*.[49]

Crabtree *et al*.[36] presented ruthenium and iridium complexes (Scheme 4) with almost identical structure to two of the new presented in this work. Ruthenium and iridium catalysts were prepared by *in situ* transmetallation from the silver carbene complexes of the different presented ligands. Treatment with Ag_2O under light-free conditions in CH_2Cl_2 at room temperature formed the presumed silver carbenes, which were filtered and directly added to the corresponding metal precursors and KPF_6. The mixture was stirred for 2 h, then filtered through Celite and concentrated, yielding yellowish-orange solids with good yields.

A summary of further ruthenium metal complexes containing chelating NHC ligands can be found in the book "N-Heterocyclic Carbenes".[50] Some examples are presented in Figure 7. All of them contain a *N*-functionalization on a side chain of the NHC which confers the ligand a chelating effect to the metallic center.

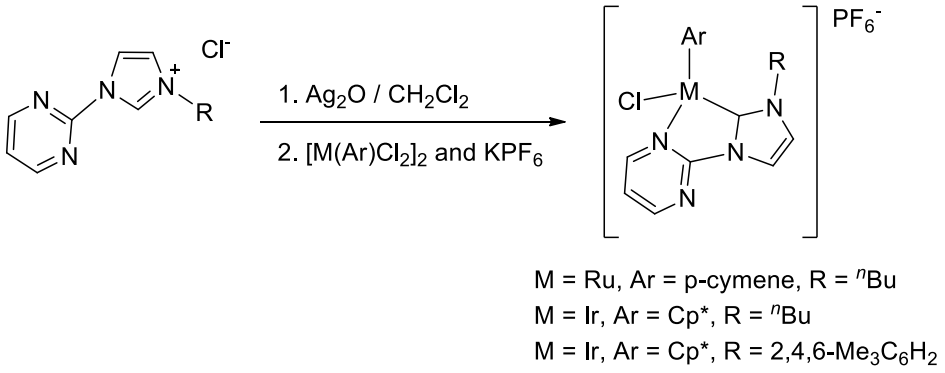

Scheme 4. Synthesis of ruthenium (II) and iridium (III) NHC complex reported by Crabtree *et al*.[36]

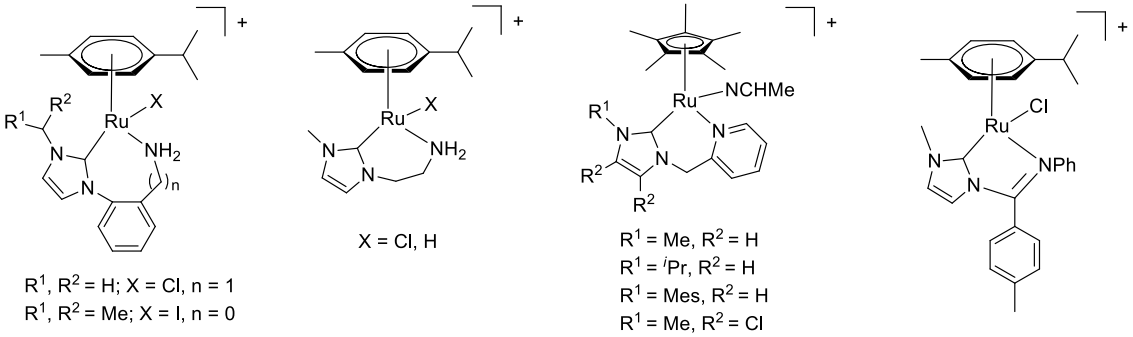

Figure 7. Some examples of chelating ruthenium NHC complexes.

In case of osmium metal NHC catalysts with these specific structures, much fewer examples can be found in literature. Some examples are described by Lai-Hon Chung *et al*. (Figure 8 (a)) [51] and Chun-Yuen Wong *et al*.[52] (Figure 8 (b)) in which tridentate chelating NHC ligands are bonded to the metallic center. In this last work, analogous complexes, in which ruthenium is the metal center, are also described including some examples with more variety of ligands. Nevertheless, for rhodium and iridium, some more examples can be found in literature. In some cases it can be found for some rhodium complexes also pincer tridentate ligands, where two NHC units are bound by a bridge pyridine group (Figure 8 (c)),[53] tridentate mono NHC ligands containing two pyridine groups (Figure 8 (d)),[53]or even complexes containing derived tridentate CNC macrocycles (Figure 8 (e)).[54] For iridium complexes there is already a detailed summery in which where pincer NHC ligands are present in the molecules, also containing *N*-functionalization of the side chains. [50] Some of these examples are presented in Figure 8 (f-h). Another illustration containing a more similar NHC ligand to the new presented catalysts in this chapter has been described by Baranoff *et al*. in 2013 (Figure 8 (i)).[55]

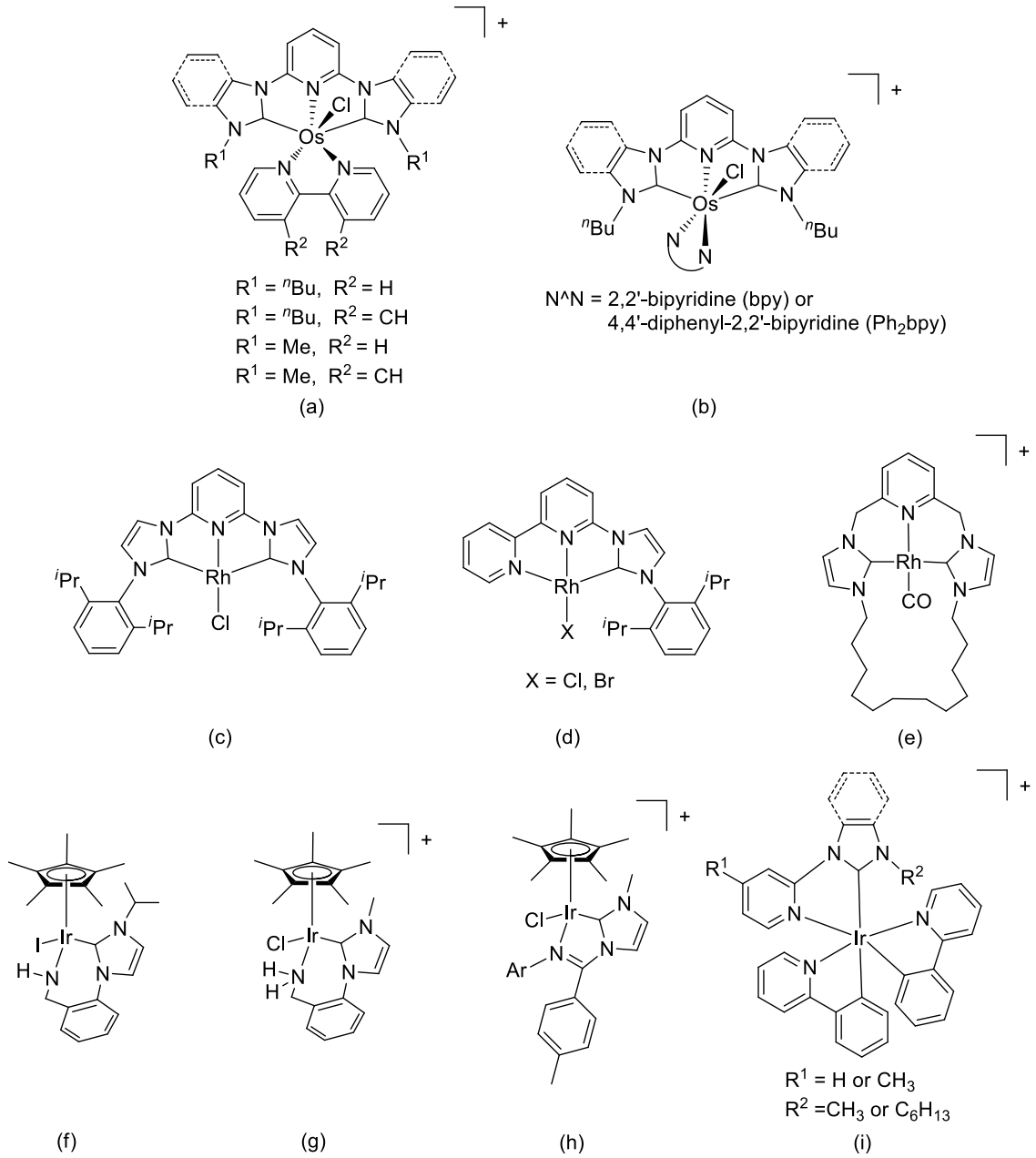

Figure 8. Some examples of osmium, rhodium and iridium NHC complexes.

Focusing on the preparation of water-soluble complexes containing a NHC ligand where at least one side chain presents a sulfonate group, the number of published synthesized compounds, when compared to water-insoluble NHC complexes, decreases. Confining the literature research to those containing chelating NHCs functionalized with a pyridine group, the results are even more reduced. As described in section 1.3, there are several ways to induce the solubility in aqueous solutions to organometallic species. In this work, the attention is centered on sulfonate

NHC compounds since the synthetic methods offer the opportunity to obtain analogous compounds to the new synthesized water-insoluble catalysts.

In 2013, Cadierno *et al.*[34] published the synthesis of water-soluble gold catalysts in which exactly the same NHC ligand is present as used in this work, but with a different metal center. A series of Au(I)-NHC complexes were synthesized through a silver-carbene transfer method (Scheme 5). Treatment of dichloromethane solutions of the ligands (including the one used in this research work) with Ag_2O in the presence of tetrabutylammonium chloride (TBACl), and [AuCl(SMe_2)], followed by addition of *p*-toluene sulfonic acid, leads to the precipitation of gold (I) complexes (obtained as air-stable solids, 68-88% yield). However, the silver(I) intermediate was not isolated and characterized. Based on this on this work of Cadierno *et al.*[34], the synthesis and characterization of the silver(I) NHC compound containing a pyridine functionalizated NHC is attempted in this research work. Treatment of gold (I) compounds with the oxidant agent iodobenzene dichloride lead to the gold (III) species. All the presented gold complexes are soluble in water. It has been observed that, when some of the gold (III) species are dissolved in water, an equilibrium with the corresponding chelate derivatives establishes (Scheme 6).

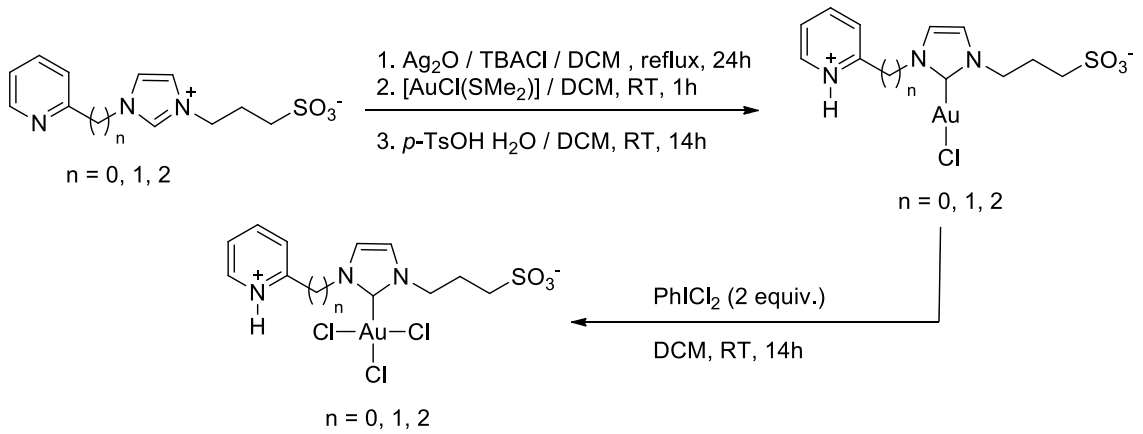

Scheme 5. Synthesis of gold NHC complexes.

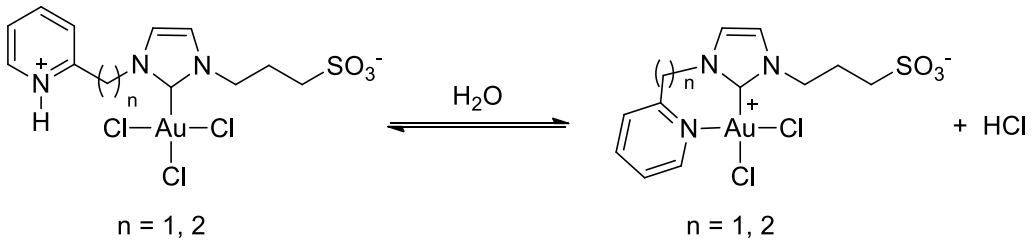

Scheme 6. Equilibria of gold (III) complexes dissolved in water.

In the same year, a review[43] was published which summarizes a series of water-soluble NHC complexes through special features on the NHC ligands. Considering those in which side chains contain a sulfonate group, many examples can be found with silver, palladium, rhodium and iridium as metal centers.

Silver carbenes functionalized with alkylsulfonates are also proved available through the reaction of ligand precursor salts with silver oxide in water, followed by addition of NaCl. Some examples are presented in Figure 9. As explained above for the silver water-insoluble silver complexes, they can be used for further transmetallation reactions to other metals. More examples containing palladium, ruthenium and iridium centers are summarized in Figure 10 Apart from the ionic character that sulfonated groups confer to the complexes, they are often preferred by virtue of their non-coordinating behavior. However, there are some examples in which an oxygen is coordinated to the metallic center (Figure 9 (e) and Figure 10 (c)). The use of bases for the carbene generation is also suitable to sulfonate functionalized NHCs, as Azua *et al*. [35,39] proved by means of mild bases, such as cesium carbonate ($CsCO_3$) or sodium acetate (MeCOONa) for the synthesis of ruthenium and iridium compounds (Figure 10 (d-f)) obtaining the first abnormal iridium *bis*-NHC complex.

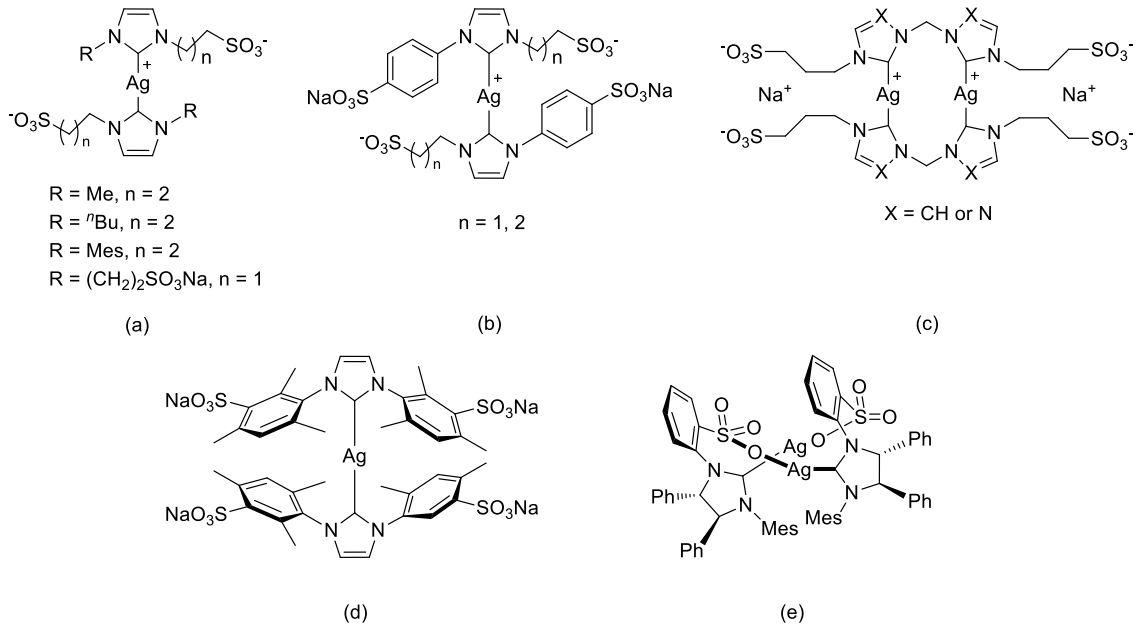

Figure 9. Some examples of silver-NHC complexes containing sulfonate groups.

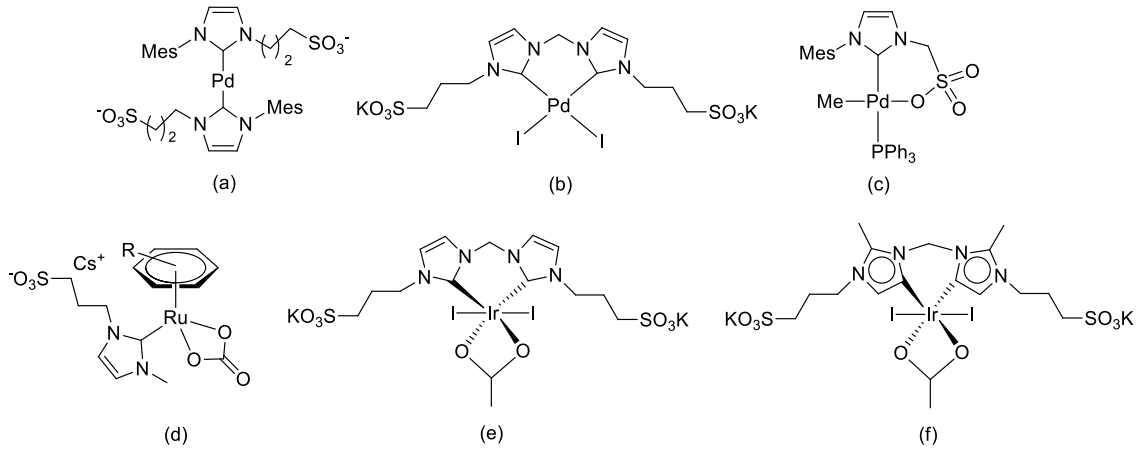

Figure 10. Some examples of palladium, ruthenium and iridium NHC complexes containing sulfonate groups.

The research group of Kühn has published in the last years a series of ruthenium, osmium, rhodium and iridium sulfonated NHC complexes. In 2012, the synthesis of new ruthenium, rhodium and iridium catalysts was described.[56] Scheme 7 (a) shows the synthesis of a ruthenium compound by *in situ* deprotonation of 1-methyl-3 (butyl-4-sulfonate) benzimidazolium betaine azolium salt to form free carbene and subsequent reaction of the ruthenium precursor $[RuCl_2(p\text{-cymene})]_2$. A different synthetic procedure was established for the synthesis of rhodium and iridium catalysts (Scheme 7 (b - c)). With this purpose, respective metal precursors ($[Rh(COD)Cl]_2$ and $[Ir(COD)Cl]_2$) were stirred at room temperature in a sodium ethoxide/ethanol solution and followed by further addition of the respective azolium precursor (1-methylimidazolium-3-butylsulfonate or 1-methyl-3 (butyl-4-sulfonate) benzimidazolium betaine). In the first reaction step, bridge chlorides were substituted by acetate groups in the metal precursor molecules, favoring later on the *in situ* deprotonation of the NHC ligand, which coordinates to the metal centers.

On the other hand, the group of Kühn also published in 2013 the synthesis of ruthenium and osmium water-soluble compounds (Scheme 8, synthesis A and C).[57] Both routes follow a similar reaction pathway in which the initial ligand is transformed into the corresponding silver-NHC complex by reaction with Ag_2O in water at 50°C and under exclusion of light, followed by the addition of NaCl. Such silver intermediates are not isolated but directly used for the reaction with the corresponding metal precursor ($[(p\text{-cymene})RuCl_2]_2$ or $[(p\text{-cymene})OsCl_2]_2$) in aqueous solutions to obtain the desired complexes. In 2016, the same author published the synthesis and catalytic application of rhodium and iridium catalysts (Scheme 8, synthesis B)[58] applying a similar procedure for the synthesis of ruthenium and osmium analogues. The reaction consisted in one-pot procedure using respective imidazolium salts, silver(I)oxide and the corresponding metal precursors, but in this case, a H_2O/DMSO mixture was required as reaction media.

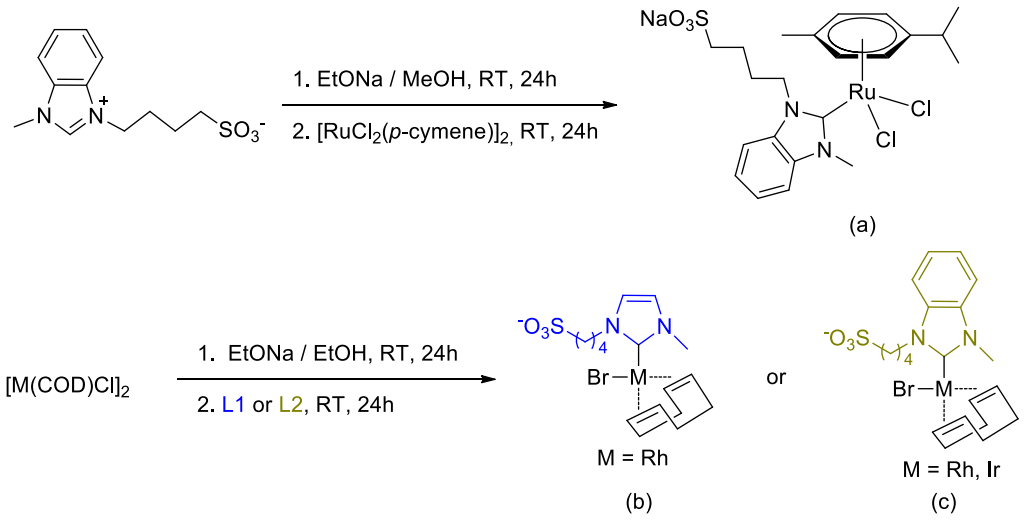

Scheme 7. Synthesis of ruthenium, rhodium and iridium complexes developed by Kühn *et al.*[56]

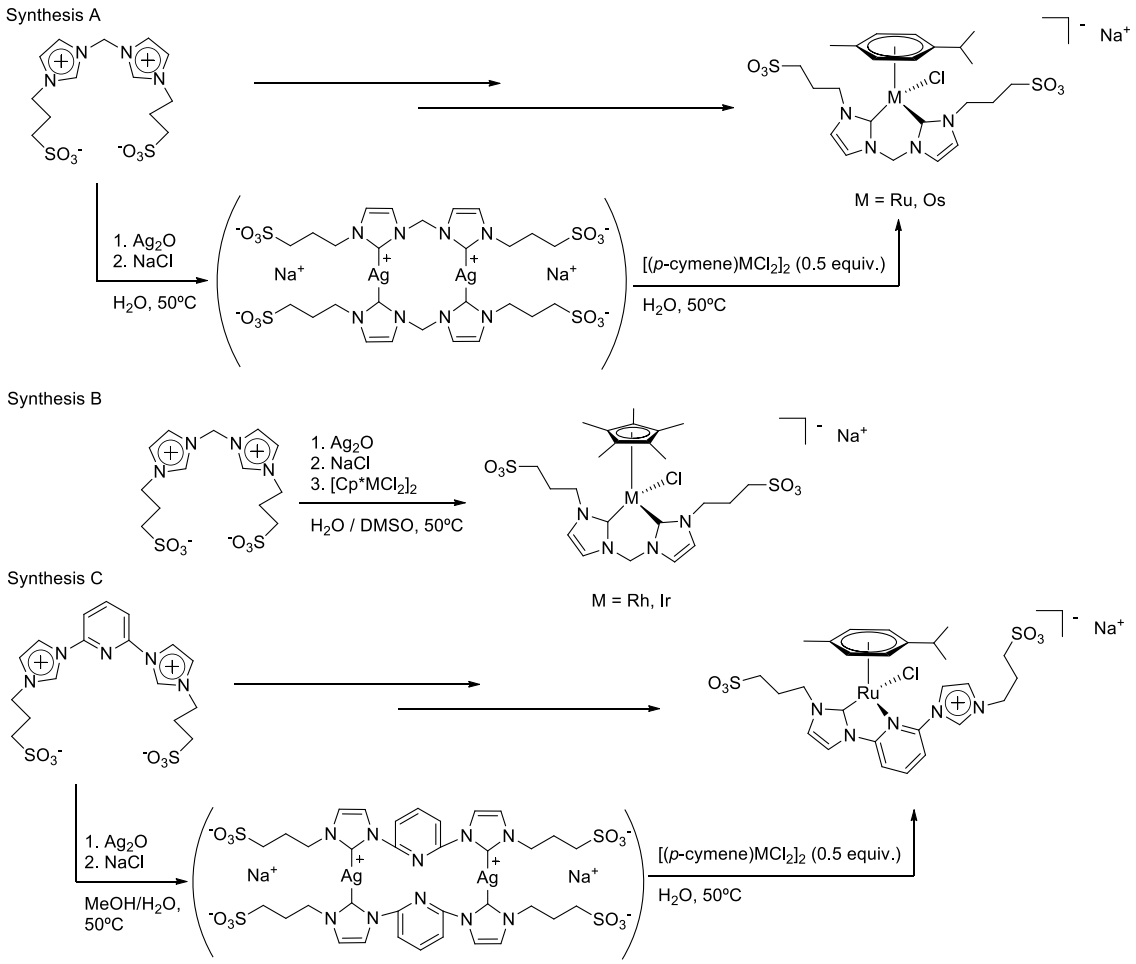

Scheme 8. Synthesis of ruthenium, osmium, rhodium and iridium complexes developed by Kühn *et al.*[57,58]

In this chapter a series of new water-insoluble and water-soluble chelating NHC complexes are described. The main objective is to obtain the most similar complexes with completely different solubilities, since that would give a big influence to their catalytic applications that will be discussed in the following chapters. With this purpose, a ligand design has been considered, which permits this solubility change. Therefore, the modification of a side chain of the NHC ligand by substitution of a terminal methyl group by a sulfonate group was chosen. The optimized synthetic routes for different metal complexes are presented in the next sections.

2.1 Imidazolium salts and metal precursors

As described above, the use of bridged imidazolium salts has the significant advantage that after complexing with the transition metal precursor a chelate complex is obtained which is has an increased stability. For this reason, a selection of bridged imidazolium compounds has been synthesized in the course of this work, which are described in more detail below.

2.1.1 Ligand precursors

The synthesis of 2-(imidazole-1-yl)pyridine (**1**) was carried out according to the procedure described above (Scheme 9). Our research group has described the synthesis of different 2-imidazole pyridines in 2013.[59] The reaction of 2-bromopyridine (1 equiv.) with a slight excess of H-imidazole (3 equiv.) and potassium carbonate (2 equiv.) under argon atmosphere at 190°C for 18 h gives the desired product in good yields (94%). The reaction follows a nucleophilic aromatic substitution with no necessity of additional solvents. An excess of imidazole is required for a faster reaction and in order to avoid a second nucleophilic attack that leads to the formation of an imidazolium salt. Potassium carbonate as base is necessary to increase the nucleophilic character of the free imidazole by deprotonation. After cooling the mixture to room temperature, the solid is dissolved in 40 mL H_2O and the aqueous solution is extracted with chloroform. The combined organic phases were washed with water and with a saturated aqueous Na_2CO_3-solution for the extraction of the excess of imidazole. After removing the solvent under reduced pressure and drying under vacuum the product was obtained as an off-white solid.

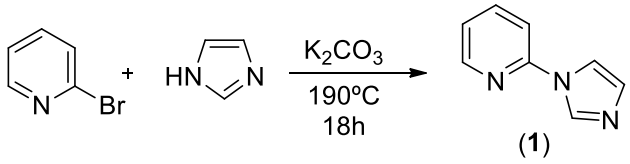

Scheme 9. Synthesis of 2-(imidazole-1-yl)pyridine (**1**).

For the synthesis of bis (imidazol-1-yl) methane (**2**) (Scheme 10), H-Imidazole (1equiv.) and the phase transfer tetrabutylammonium bromide salt (0.03 equiv.) are dissolved in a biphasic medium containing dichloromethane and NaOH-aqueous solution (45%). The resulting two-phase mixture is stirred and heated under reflux for 17 h. After cooling the sample to room temperature, the phases are separated and the aqueous phase is extracted with CH_2Cl_2. Unreacted imidazole can be removed by extraction of the organic phase with saturated sodium bicarbonate solution. The combined organic phases are dried with $MgSO_4$ and filtered. The product which is dried under vacuum is obtained as a white solid (31%). This synthesis has been previously described in literature[60,61] by different research groups since 1983.

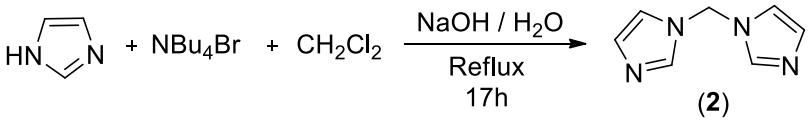

Scheme 10. Synthesis of bis(imidazol-1-yl) methane (**2**).

The mono-substituted product cannot be detected, which can be seen as a consequence of activation after a first substitution with imidazole on dichloromethane. The resulting imidazol-1-ylmethylene chloride is highly activated and is rapidly substituted by a second molecule of imidazole, thus the second step in the reaction is significantly faster. Here, the desired product was obtained in a large batch (~1 mol) with a yield of 36% and unequivocally identified by NMR spectroscopy. A slight contamination with the phase transfer catalyst TBAB was also observed, which, however, should not influence the subsequent synthetic steps and therefore the product was used without further purification.

The synthesis of Bis(1,2,4-triazol-1-yl)methane (**3**) compound is shown in Scheme 11 and has been previously described in literature by Gural'skiy *et al*. in 2012.[62] 1,2,4-triazole (1 equiv.), NBu_4Br (0.03 equiv.) and KOH (2 equiv.) are added to 0.3 mL of H_2O. The resulting mixture is stirred at room temperature for 1 hour. Then, CH_2Br_2 is added and the resulting mixture is stirred at room temperature for 48 h. Afterwards, the mixture is extracted with CH_2Cl_2. The combined organic phases are dried with $MgSO_4$, filtered and dried under vacuum. The product is obtained as a white solid (35%). Only the 1,2,4-substituted isomer shown is formed, since here too the activation of the nitrogen atoms only allows the substitution shown.

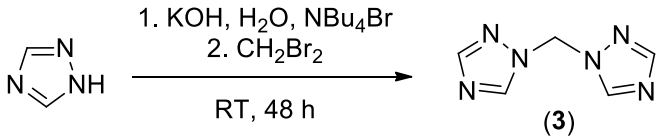

Scheme 11. Synthesis of bis(1,2,4-triazol-1-yl)methan (**3**).

The preparation of 2,6-Bis(imidazol-1-yl)pyridine (**4**) (Scheme 12) is based on previously published work of our research group,[59] where the possibility of a two-fold substitution is carried out by the reaction of H-imidazole (6.0 equiv.) and 2,6-bromopyridine (1.0 equiv.) in solvent-free conditions. Both compounds are mixed with K_2CO_3 (4 equiv.) under vacuum and subsequently heated to 190°C and reacted for 24 h. After cooling to room temperature, the solid was suspended in chloroform. The organic phase is extracted with saturated aqueous $NaHCO_3$-solution (to remove excess of imidazole) and the combined aqueous phases are extracted with $CHCl_3$. The combined organic phases were dried with $MgSO_4$. After removing the solvent under reduced pressure and drying under vacuum the product is obtained as an off-white solid in good yields (97%).

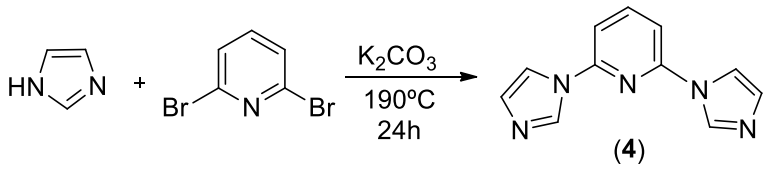

Scheme 12. Synthesis of 2,6-Bis(imidazol-1-yl)pyridine (**4**).

2.1.2 Non-sulfonated imidazolium salts

All the synthetic procedures employed for the synthesis of non-sulfonated imidazolium salts are based on literature known pathways. In 2002 Crabtree *et al*. have published the experimental procedure of the synthesis of 2-(Imidazole-1-yl-3-*n*-butyl)pyridine (**5**) and 2,6-Bis(imidazol-1-yl-3-*n*-butyl)pyridine (**6**) ,[46] while Bis(imidazol-1-yl-3-butyl)methane dibromide (**7**) can be found more recently described by Elsevier *et al*. in 2013.[63] None of the synthesis requires the use of previously described ligand precursors.

For the synthesis of 2-(Imidazole-1-yl-3-*n*-butyl)pyridine (**5**) a mixture of 1-butylimidazole (1.0 equiv.) and 2-bromopyridine (1.0 equiv.) are heated at 160°C and stirred at that temperature for 20 h (Scheme 13). After cooling to room temperature, the mixture is dissolved in CH_2Cl_2 and precipitated with Et_2O. The obtained brown solid is re-dissolved in CH_2Cl_2 and re-precipitated

and washed with pentane. After drying under vacuum, the product is isolated as a brown solid (10%).

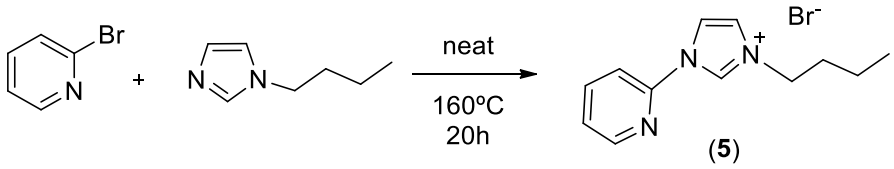

Scheme 13. Synthesis of 1-(imidazole-1-yl-3-n-butyl)pyridine (**5**).

In case of d 2,6-bis(imidazol-1-yl-3-n-butyl)pyridine (**6**) (Scheme 14)**,**2,6-dibromopyridine (1.0 equiv.) and an excess of 1-butylimidazole (4.0 equiv.) are heated neat to 150°C and react for 20 h. After cooling to room temperature, the mixture is dissolved in 25°mL $CHCl_3$ and Et_2O is added to precipitate a grey solid. After several re-precipitation processes using chloroform and methanol combined with diethyl ether the product is isolated (70%).

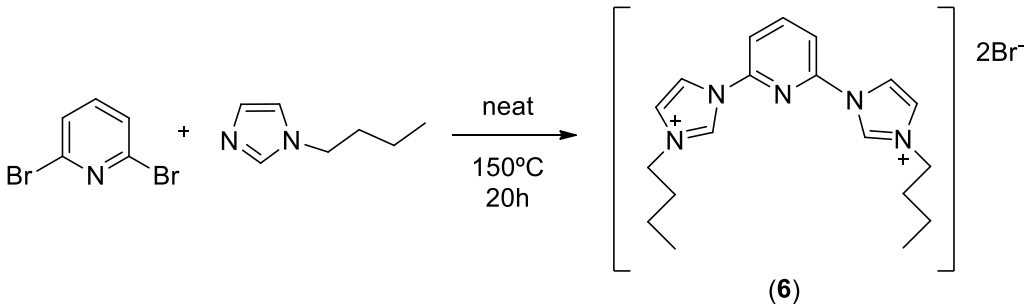

Scheme 14. Synthesis of 2,6-bis(imidazol-1-yl-3-n-butyl)pyridine (**6**).

Bis(imidazol-1-yl-3-butyl)methane dibromide (**7**) can be synthesized by dissolving 1-butylimidazole (1.0 equiv.) in dibromomethane (6.24 equiv., Scheme 15). The mixture is stirred at 75°C for 40 h. After cooling to room temperature, the solvent is removed and the resulting solid is washed with THF and dried under vacuum. The product is obtained as a white solid (94%).

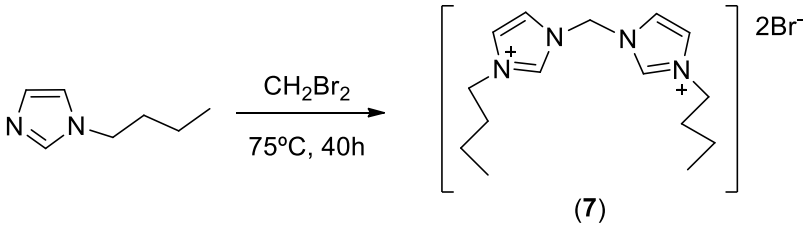

Scheme 15. Synthesis of bis(imidazol-1-yl-3-butyl)methane dibromide (**7**) ligand.

2.1.3 Sulfonated imidazolium salts

The synthetic routes to obtain sulfonated imidazolium salts follow a similar pathway. For all of them, the respective precursor and an excess of 1,3-propanosultone are mixed in MeCN and heated up in an ACE pressure tube at T≥90°C and reacted for different reaction times (Table 1). The reactions are carried out according to slightly modified procedures previously described in literature.[33–35,64] Thus, the characterization of all these ligands is carried out only by ^{1}H and ^{13}C NMR spectroscopy. If, as in the case of bridged ligands, a double alkylation has to be carried out, the reaction time increases due to the low solubility of the mono-alkylated intermediate in acetonitrile, but here too the desired products can be obtained in very good yields and purities.

Table 1. Overview of the synthesis of the different water-soluble ligands (**8**-**11**).

Entry	Ligand	Precursor	Ratio[a]	T (ºC)	t (h)	Yield (%)
1	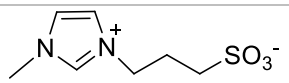 (**8**)	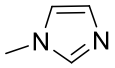	1:3	100	1.5	85
2	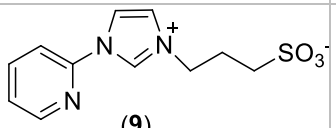 (**9**)	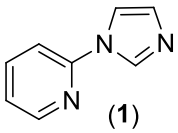 (**1**)	1:2	90	18	98
3	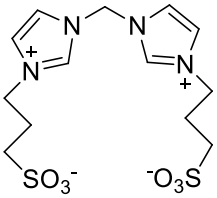 (**10**)	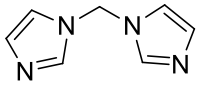 (**2**)	1:6.5	100	48	89
4	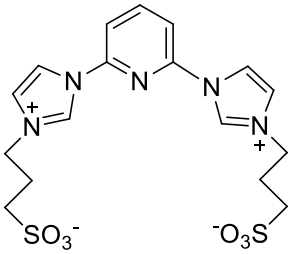 (**11**)	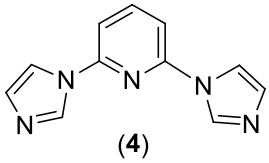 (**4**)	1:6	110	5 days	95

[a]Ratio between the two reagents, ligand precursor to 1,3-Propanesultone, which is always in excess.

In all cases, the new described synthetic routes exhibits some advantages to the already published procedures. For the synthesis of 1-methylimidazolium-3-propylsulfonate (**8**),[35] and considering that 1,3-propanosultone is an alkylating, genotoxic and carcinogenic compound, it is important to remark that in our developed synthesis less excess of this compound is required (1:3 instead of 1:6 ratio). In our case, the reaction is finished after 90 min at 100°C. It considerably reduces the reaction time, although the temperature is higher as in the published reaction (15 h, 60°C). Focusing on 2-(imidazole-1-yl-3-propylsulfonate)pyridine (**9**),[34] the reaction time is decreases from one week to 18 h and no inert atmosphere is required. Solvent and temperature are modified using MeCN instead of acetone and the reaction is heated to 90°C instead of room temperature. In case of Bis(imidazol-1-yl-3-propylsulfonate)methane (**10**),[64] we are able to reduce the reaction time from 5 days to 48 h and increase the yield from 69% to 89%. For 2,6-Bis(imidazol-1-yl-3-propylsulfonate)pyridine (**11**)[33] only the reaction time was influenced, obtaining higher yields (95% instead of 85%), increasing the reaction time (5 days instead of 12 h).

2.2 Metal precursors

A series of analogous metal complexes has been synthesized as precursor for the catalysts, (applied later in this work) in hydrogenation catalysis. Ruthenium, osmium, rhodium and iridium were the desired metal centers. In case of ruthenium, rhodium and iridium, which are commercially available, the prices are quite expensive and their synthesis straightforward. Therefore, all of the presented metal precursors were synthesized according to literature procedures. [65–67]

For the synthesis of $[(\eta^6\text{-p-Cymene})RuCl_2]_2$ (**12**)[65] and $[(\eta^6\text{-p-Cymene})OsCl_2]_2$ (**13**)[66] very similar reactions are carried out (Scheme 16). The starting materials are ruthenium and osmium chloride respectively, which react with excess of α-terpinene. The oxidation state of both metals is reduced from +III to +II, where these species form chlorine-bridged, aromatic, dimeric complexes. In case of the ruthenium compound, the reagents are heated up to reflux in ethanol and stirred for 4h and in case of osmium, the solvent used is isopropanol, and the reaction mixture is heated up to reflux and reacted for 17h. Both complexes are obtained in high purity.

In case of both, $[(\eta^5\text{-Cp*})RhCl_2]_2$ (**14**)[67] and $[(\eta^5\text{-Cp*})IrCl_2]_2$ (**15**)[67], the respective hydrated chloride salts are heated up to reflux in methanol together with pentamethylcyclopentadiene and maintained at the desired temperature for 24 and 48 h respectively (Scheme 17). Oxidation states of rhodium and iridium do not change, both obtained as +III species forming chlorine-bridged, aromatic, dimeric complexes in high purity.

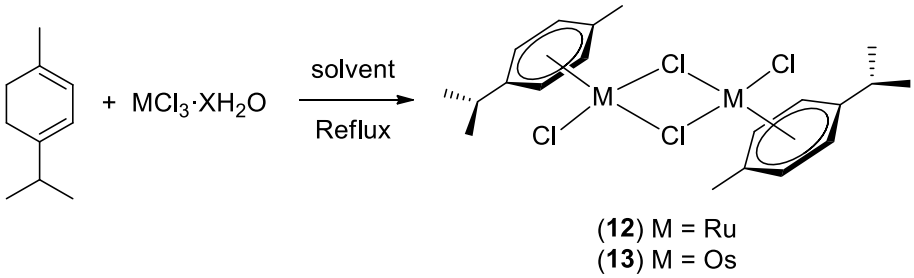

Scheme 16. Synthesis of ruthenium (**12**) and osmium (**13**) metal precursors.

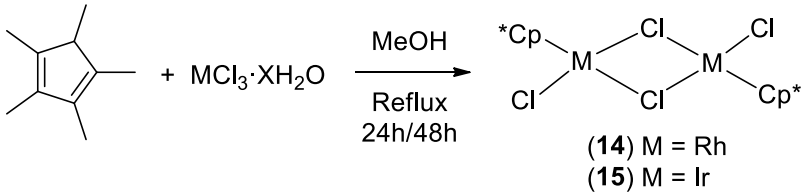

Scheme 17. Synthesis of rhodium (**14**) and iridium (**15**) metal precursors.

2.3 Silver(I) NHC complexes

For the synthesis of NHC complexes *N*-alkyl (**5**) and sulfonated N-alkyl imidazolium (**9**) salts were used. In this work, Ag_2O has been used to generate Ag-NHC complexes (Scheme 18). Complex **16a** was synthesized by stirring ligand **16a** with Ag_2O in dichloromethane under exclusion of light at room temperature for 2 h. Silver hexafluorophosphate ($AgPF_6$) was then added to replace the bromide counterion by the precipitation of silver bromide. It was not possible to isolate the pure silver intermediate (**16a**) confirming the elemental analysis the presence of 0.55 mol equivalents of AgCl, which could not be removed. The treatment of Ag_2O with the sulfonated imidazolium salt **9** by refluxing in dichloromethane results in the analogous water-soluble $[Ag(NHC)_2]$ complex **16b** in high yield. There are some cases already known where a sulfonate group can coordinate to metallic centers.[68] In order to avoid the coordination of the sulfonate groups to silver(I) and to provide Na^+ as counterion, sodium chloride was added in a second step since the coordination of sulfonate groups to sodium is preferred.

Some other silver based sulfonated NHC complexes reported previously are not particularly stable for a longer period and it is necessary to apply them for carbene transfer immediately.[69] Especially, as compared to the reported synthesis for *in situ* carbene transmetallation to gold complexes with the same ligand and theoretically silver intermediate, the synthetic route, developed in this work presents important advantages.[34] It avoids the use of tetrabutylammonium chloride (TBACl), which cannot be separated from the final desired final gold compounds.

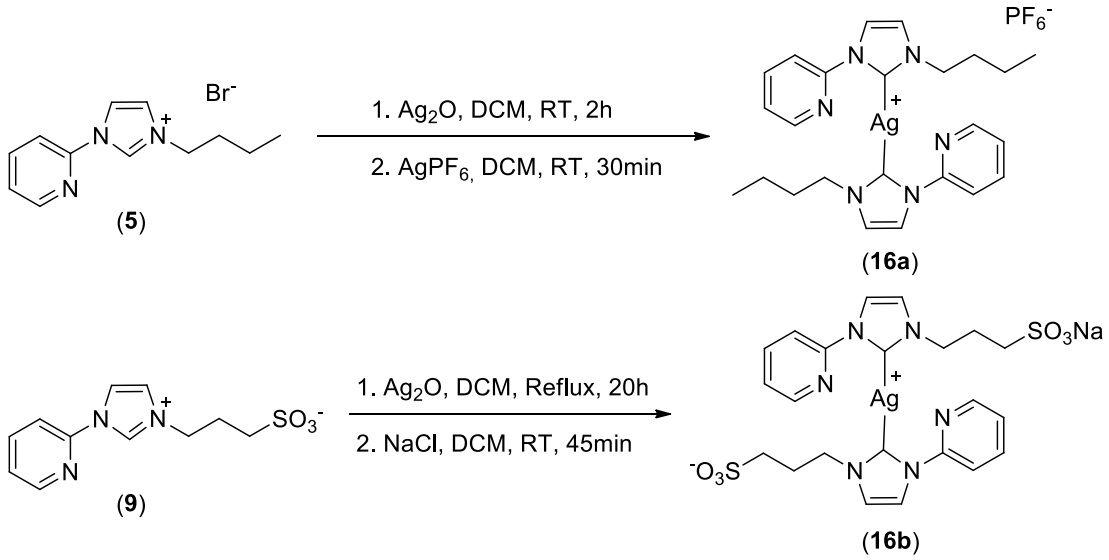

Scheme 18. Synthesis of Ag-NHC complexes (**16a**-**b**).

Complex **16b** could be isolated as stable white solid and was used for further transmetallation reactions. Both silver complexes **16a** and **16b**, were characterized by X-Ray single-crystal diffraction analysis (Figure 11 and Figure 12). Crystals of **16a** and **16b**·MeOH were obtained by slow diffusion of diethyl ether into a saturated solution of the respective complex in methanol.

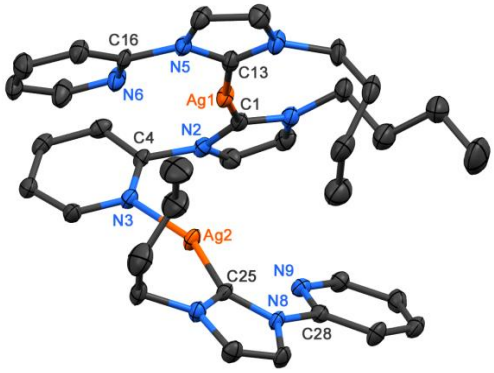

Figure 11. ORTEP style representation of the cation of **16a** (thermal ellipsoids are shown at a 50% probability level). Hydrogen atoms and two PF6- are omitted for clarity. Selected bond lengths (Å) and angles(º): Ag(1)–C(1) 2.090(4), Ag(1)–C(13) 2.094(4), Ag(2)–C(25) 2.078(3), Ag(2)–N(3) 2.156(3), Ag(1)–Ag(2) 3.3456(4), C(1)–Ag(1)–C(13) 166.72(14), N(3)–Ag(2)–C(25) 158.87(13), C(13)–N(5)–C(16)–N(6) -10.60(5), C(1)–N(2)–C(4)–N(3) -67.6(4), C(25)–N(8)–C(28)–N(9) -13.7(5).

Single crystal X-ray crystallographic studies reveal that complex **16a** exists in dinuclear form in solid state. The metallic centers Ag(1) and Ag(2) are arranged in a pseudo-linear environment. Ag(1) is coordinated to two carbene carbon atoms, while Ag(2) is coordinated to a carbon carbene atom and to the pyridine nitrogen of one of the NHC ligands coordinated to Ag(1). This pseudo-linear coordination (CNHC–Ag–CNHC 166.72(14)° and 158.87(13)°) is in accord with several previously reported polymetallic structures[70–74].

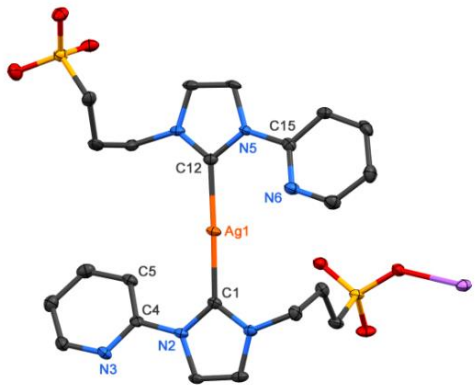

Figure 12. ORTEP style representation of **16b**·MeOH (thermal ellipsoids are shown at a 50% probability level). Hydrogen atoms and co-crystallized solvent are omitted for clarity. Selected bond lengths (Å) and angles(°): Ag(1)–C(1) 2.088(3), Ag(1)–C(12) 2.094(3), C(1)–Ag(1)–C(12) 173.21(12), C(1)–N(2)–C(4)–C(5) 28.6(4), C(1)–N(2)–C(4)–N(3) -153.2(3), C(12)–N(5)–C(15)–N(6) -10.9(4).

Complex **16b** displays a mononuclear structure. The metallic center is coordinated to two carbene carbon atoms in a linear fashion. The environment is less distorted than in **16a**. Such differences can be observed for many silver complexes, where monometallic biscarbene moieties display angles C_{NHC}–Ag–C_{NHC} closer to linearity (171.3° – 180.0°)[49,69,75–79] than polymetallic structures (165.5° – 173.42°)[49,70–73,78].

For both, **16a** and **16b**, the Ag–C_{NHC} distances are in the range of 2.078(3) – 2.094(3) Å. Similar bond lengths have been reported for other Ag-NHC complexes.[49,69–81] Torsion angles found in the pyridinyl imidazole suggest that the ligands are not completely planar, rising to 28.66° for **16b**.

The solid phase structure of **16a** is not in accord with the spectroscopic data obtained by ^{1}H, ^{13}C NMR, mass spectrometry (FAB-MS) and elemental analysis, which suggest $[Ag(NHC)_2]PF_6$ as the main species in solution. The ^{1}H, ^{13}C $\{^{1}H\}$ liquid phase spectroscopic studies of **16a** indicate equivalence of two imidazolium ligands, which is consistent with mass spectrometry and elemental analysis results. ^{1}H variable temperature NMR experiments (20°C to -90 C) were performed in order to explore potential equilibria between different species in solution. However, shift migration was observed when temperature was varied. Furthermore,

considering the asymmetric unit of **16a** (Figure 11), it can be assumed that the complex adopts in its bimetallic structure only in the solid state. The formation of this dinuclear species may be caused by the presence of $AgPF_6$, where Ag^+ in solution is available to provide additional interaction sites with donor atoms of the NHC ligand. In solution, the proposed monometallic biscarbene structure is formed, as evidenced by $\{^1H\}$ NMR measurements. The view of the crystal structure **16b** along the crystallographic *a* axis highlights the interaction of the sulfonated groups with the Na^+ counter-ions and their positions (Figure 13).

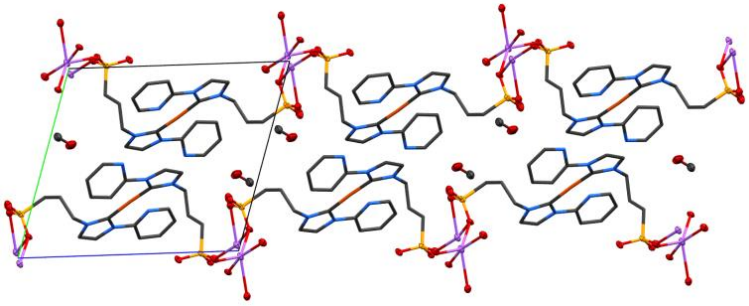

Figure 13. View of the crystal structure **16b**·MeOH along the crystallographic *a* axis.

2.4 Water-insoluble 1-(2-pyridinyl)-3-n-butyl)imidazol-2-ylidene metal complexes

NHC ligand **5** was transferred from silver(I) (**16a**) to ruthenium(II) (**17a**), osmium(II) (**18a**), rhodium(III) (**19a**) and iridium(III) (**20a**) via transmetallation (Scheme 19). All reactions were carried out in dichloromethane as solvent under light exclusion at room temperature. Complexes **17a** and **19a** are obtained as orange solids, while compounds **18a** and **20a** are obtained as yellow powders. All solids were found to be air stable for weeks in solution and at elevated temperatures (>100°C) in solid state. Complexes **17a-20a** are characterized by NMR spectroscopy, elemental analysis and mass spectrometry (FAB-MS).

Crabtree *et al*.[36] have previously published the synthesis of a series of ruthenium and iridium complexes with almost identical structure to some of the new water-insoluble synthesized complexes of this work (Scheme 4). In this case, the authors do not isolate or characterize the silver intermediate. However, the obtained yields for ruthenium (73%) and iridium (80%) are higher than the obtained in this work, where both ruthenium and iridium complexes were obtained with a yield of 50%. This loss may be due to the isolation of the silver intermediate.

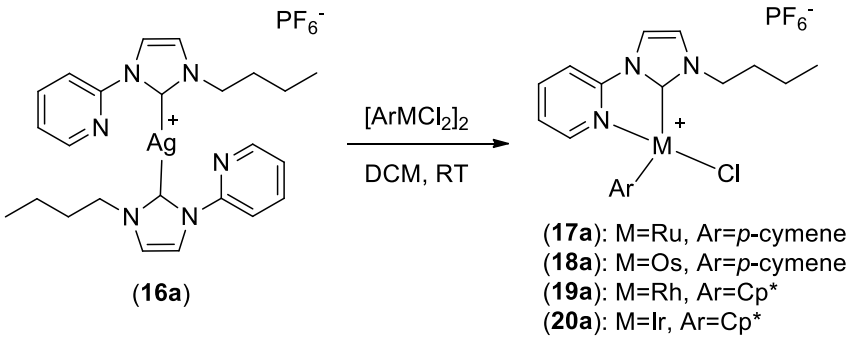

Scheme 19. Synthesis of ruthenium(II) (**17a**), osmium(II) (**18a**), rhodium(III) (**19a**) and iridium(III) (**20a**) complexes.

^{1}H NMR spectra for complexes **17a** and **18a** show the in-equivalence of all protons of the p-cymene ring. In ^{13}C NMR spectra more than one peak appears for this ring, indicating a rotational barrier for the p-cymene ring. ^{13}C NMR spectra indicate a stronger electron donation from ruthenium to the carbene ligand, than in the analogous osmium complex.[82] For **17a**, the carbene carbon signal appears at 184.63 ppm while for complex **18a** it appears at 170.80 ppm (Figure 14). Similar shifts were previously observed for comparable compounds.[57] These findings are also observed, although less significantly pronounced, in ^{1}H NMR.

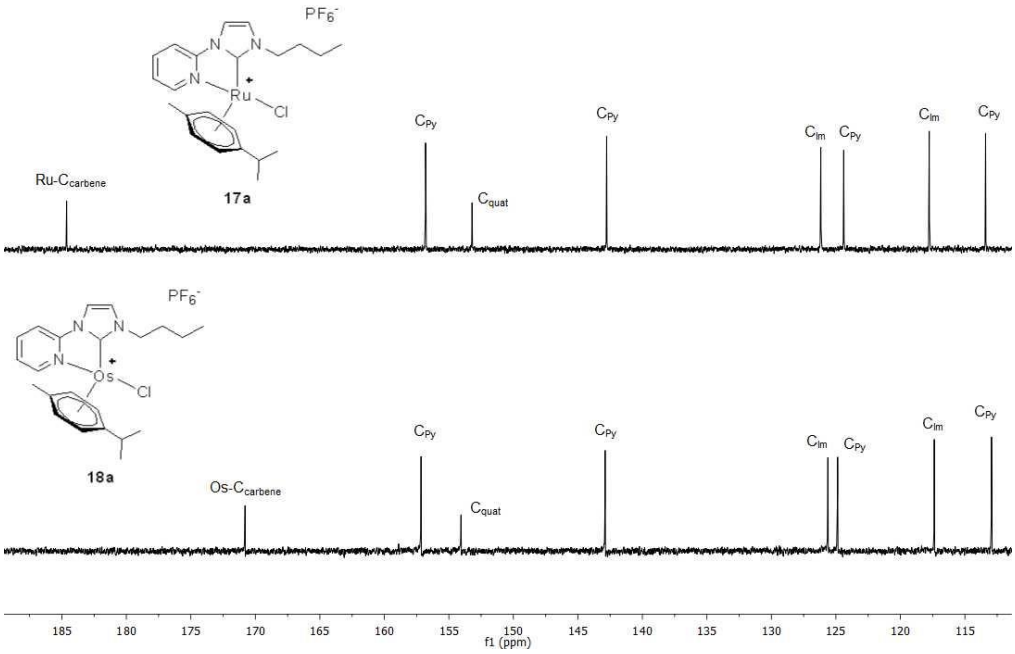

Figure 14. ^{13}C NMR shifts of the aromatic carbon resonances of complexes **17a** and **18a**.

For complexes **19a** and **20a**, all protons of the pentamethyl-cyclopentadienyl ligand are equivalent. The strong electron donation from one metal to the carbene ligand, observed for complexes **17a** and **18a**, is also supported by the ^{13}C NMR spectra of **19a** and **20a**. The carbene carbon resonance signal for **19a** appears at 179.22 ppm, while the Ir-$C_{carbene}$ signal appears at 166.08 ppm indicating that the Rh-C interaction is stronger than the Ir-C interaction (Figure 15).

Potential hemilability of the pyridine group in complexes **17a**-**20a** was studied by variable temperature NMR experiments. No changes were observed in the ^{1}H NMR spectra, recorded between 25 and 80°C, suggesting a chelating ligand. The chelating behavior of the ligand is further supported by X-ray diffraction studies for complexes **19a** and **20a**.

All complexes are soluble in methanol, acetonitrile, tetrahydrofuran, acetone and dichloromethane. Toluene, diethyl ether and *n*-hexane do not dissolve complexes **17a-20a**. However, solubility of these complexes in water is low, only 1.55 mg/ml for complex **17a**. Therefore, the synthesis of water-soluble derivatives was attempted.

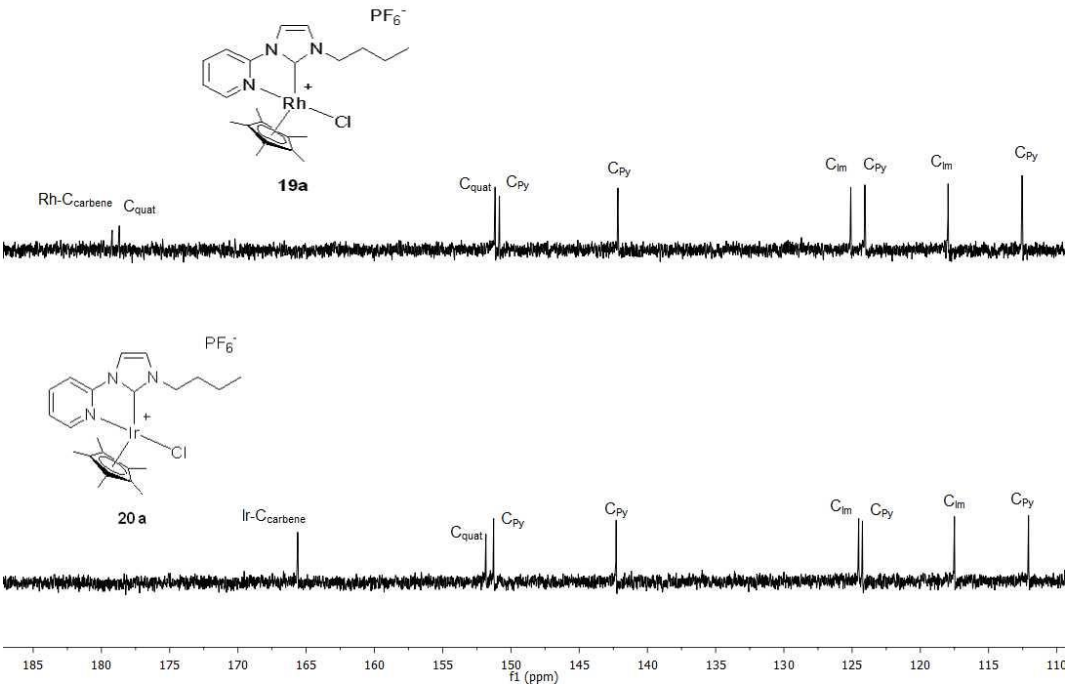

Figure 15. ^{13}C NMR shifts of the aromatic carbon resonances of complexes **19a** and **20a**.

2.5 Water-soluble 1-(2-pyridinyl)-3-(sulfonatepropyl)imidazol-2-ylidene metal complexes

The ruthenium (**17b**) and osmium (**18b**) complexes are obtained by transmetallation of the silver carbene (**16b**) with $[Ru(p\text{-cymene})Cl_2]_2$ (**12**) and $[Os(p\text{-cymene})Cl_2]_2$ (**13**) in acetonitrile at 50 °C. Both complexes are isolated in good yields as air stable, orange (**17b**) and yellow (**18b**) solids. Complexes **19b** and **20b** are available from silver complex **16b** by transmetallation in the absence of light at room temperature with the corresponding metal precursors (Scheme 20). Rhodium (**19b**) and iridium (**20b**) complexes are obtained in good yields as air stable orange and yellow solids, respectively. Complexes were characterized by X-Ray single crystal diffraction, NMR spectroscopy and elemental analysis.

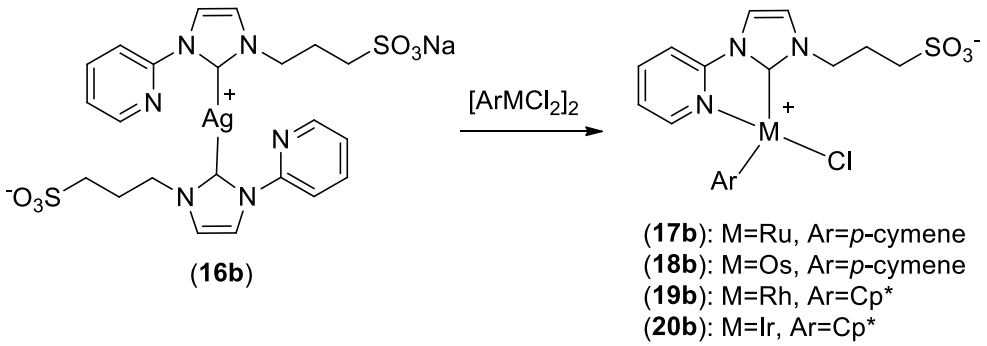

Scheme 20. Synthesis of water-soluble NHC ruthenium(II) (**17b**), osmium(II) (**18b**), rhodium(III) (**19b**) and iridium(III) (**20b**) complexes.

The ^{1}H NMR spectra of **17b**-**20b** are similar to their non-sulfonated derivatives. Differences can be observed in the proton resonances for the hydrogens in the hydrocarbon chain, which are shifted to lower fields due to the presence of the sulfonated group. Stronger electron donation from ruthenium and rhodium metal centers is observed compared to the osmium and iridium derivatives (**17a**–**20a**) which is also supported by ^{13}C NMR spectra for complexes **17b**-**20b** (Figure 16 and Figure 17). The M-$C_{carbene}$ resonance peak for both the osmium **18b** (171.4 ppm) and the iridium **20b** (167.2 ppm) complex are shifted high field compared to the ruthenium and rhodium derivatives **17b** (185.3 ppm) and **19b** (181.0 ppm).

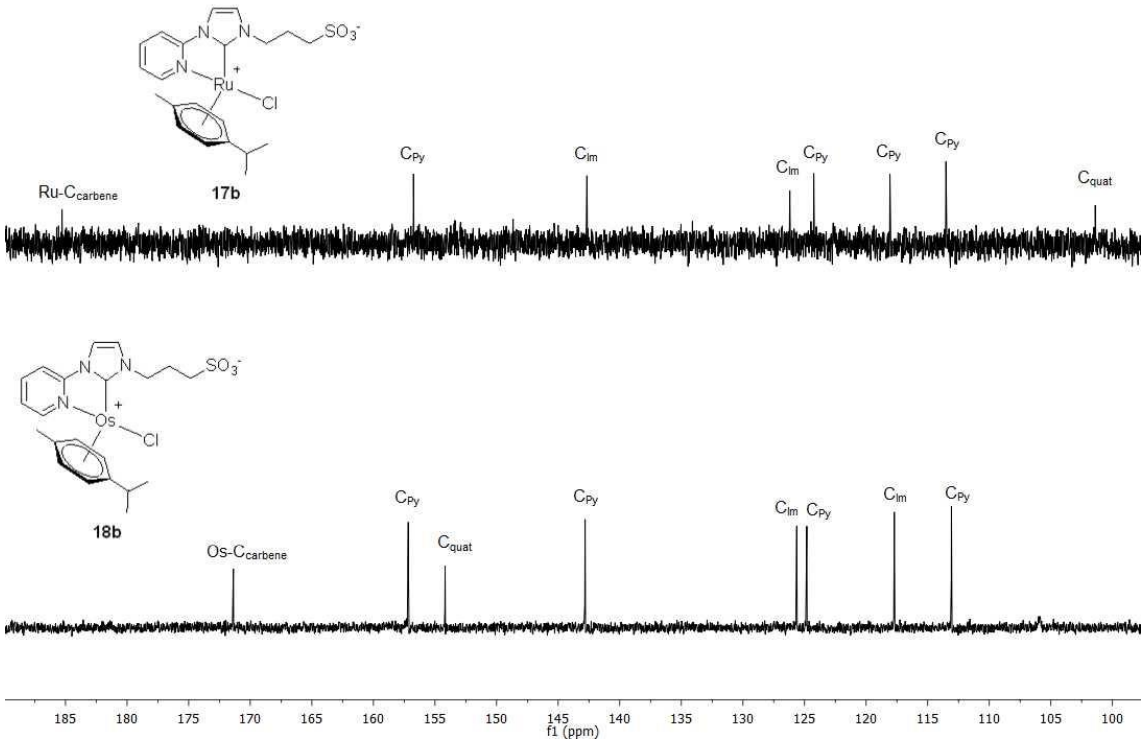

Figure 16. ^{13}C NMR shifts of the aromatic carbon resonances of complexes **17b** and **18b**.

In contrast to complexes **17a**-**20a**, compounds **17b**-**20b** exhibit good solubility in water, ca. 400 mg/mL of compound **17b** and ca. 300 mg/mL of compound **18b**. These results are in accord with values obtained for, previously reported sulfonated complexes.[57] However, compounds **19b** and **20b** exhibit lower solubility in water (~100 mg/mL). All complexes also dissolve in polar solvents (methanol, DMSO), but not in toluene, acetone, dichloromethane, tetrahydrofuran, diethyl ether or *n*-hexane. Their solubility in acetonitrile follows a slightly different order, being **17b** the most soluble, followed by **18b**, **19b** and **20b**, which is the least soluble. In general, complexes **17b**-**20b** were found to be air stable in solid state and in solution dissolved in any polar solvent with the only exception of **17b** and **18b**, which are not stable for longer periods in water. After 2 to 3 days, orange aqueous solutions of ruthenium (**17b**) and osmium (**18b)** complexes turn to darker colors. When aqueous solutions of **17b**-**20b** are treated with organic solvents, the complexes remain in the aqueous phase, indicating that a simple workup procedure, e.g. after application in catalysis, is possible.

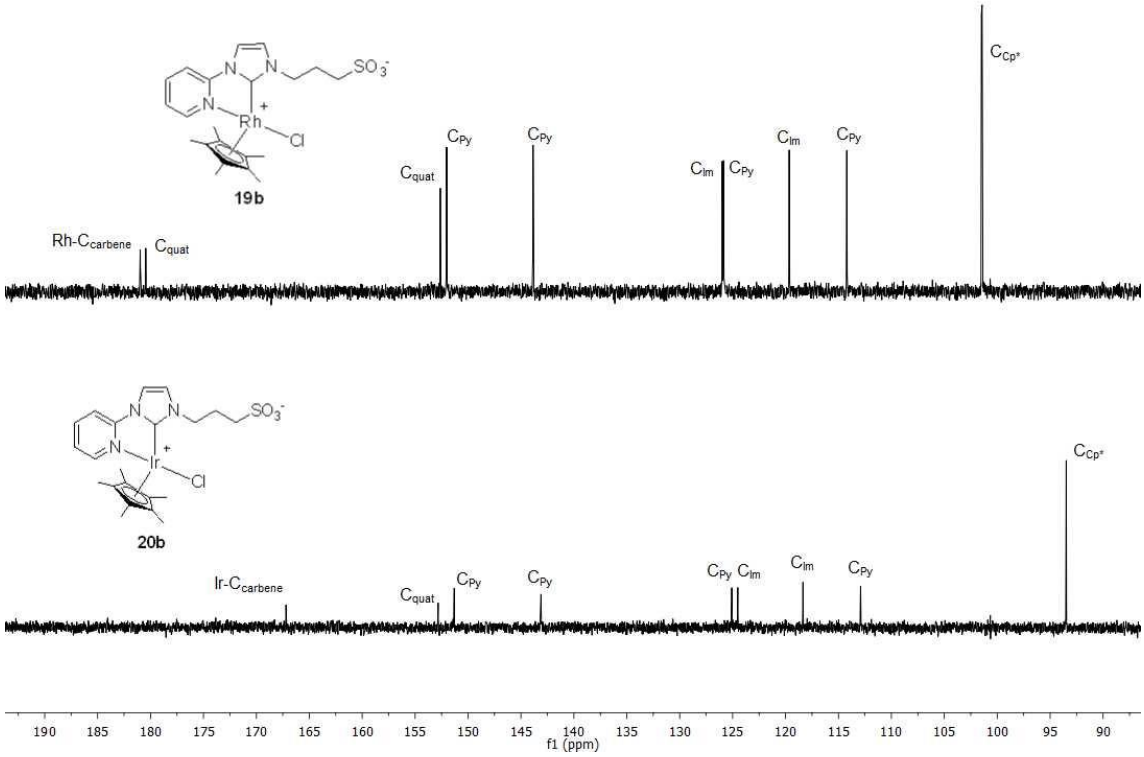

Figure 17. ^{13}C NMR shifts of the aromatic carbon resonances of complexes **19b** and **20b**.

2.6 Solid state structures of Osmium, Rhodium and Iridium complexes

Complexes **18b**, **19a**, **19b**, **20a** and **20b** were analyzed by single-crystal X-ray diffraction. Crystals of complex **18b**·MeOH (Figure 18) were obtained by vapor diffusion of diethyl ether into a saturated methanol solution, **19a** and **20a** (Figure 19) by slow evaporation of acetonitrile, and **19b**·2.10 H_2O and **20b**·2.10 H_2O (Figure 19) by slow evaporation of concentrated water solutions.

The molecular structures reveal the expected pseudo-octahedral structural motif. The metal center is coordinated to the carbene carbon atom of the NHC ligand, a pyridine nitrogen atom, chloride and the corresponding aromatic group (p-cymene for **18b** and Cp* for rhodium and iridium complexes). In the crystal structures of 1-(2-pyridinyl)-3-sulfonatepropyl)imidazol-2-ylidene metal complexes, no intra- or intermolecular interactions is observed between the nucleophilic sulfonated groups and the metal centers. The distortion of the octahedral environment of the metal is stronger in the osmium complex ($C_{carbene}$-Os-Cl = 96.01(14)°), which is likely caused by the steric demand of the p-cymene ligand.

The M-$C_{carbene}$ bond distances for rhodium and iridium complexes (Table 7, section A.3.2) are similar and slightly shorter than the Os-$C_{carbene}$ distance found for **18b** (2.037(3)Å). Similar bond-

lengths have already been reported for osmium[51,52,83–86], rhodium[53,87–91] and iridium[36,55,90,92–98] complexes. The M(1)–N(3) distances range between 2.107(2) – 2.128(3)Å[51–53,55,83–103]. The same holds for the metal−chloride bond length[84,86] and the bis-NHC chelated[52] osmium structures. Complexes **19a**, **19b**·2.1H_2O, **20a** and **20b**·2.1H_2O display M(1)-Cl(1) distances (see section A.3.2), which are in accord with literature known distances for rhodium[104–106] and iridium[34,59,72,78,107] M-Cl complexes. Similar $C_{carbene}$–M–N bond angles were observed for all complexes, from 75.60(12)° to 76.82 (4)°. Torsion angles C(1)–N(2)–C(4)–N(3) between the pyridine and the imidazole ring reveal the planarity of the ligand, with a maximal deviation found for **19a** (-2.2(4)°) and **20a** (-2.0(3)°).

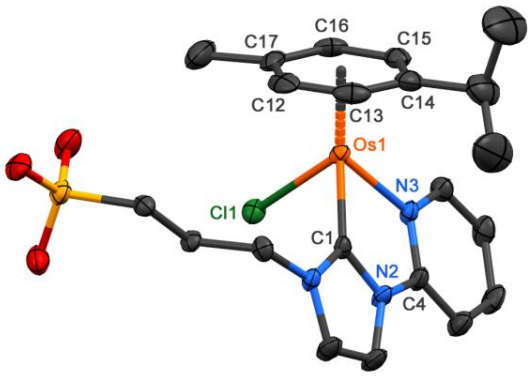

Figure 18: ORTEP style representation of the cation in **18b**·MeOH (thermal ellipsoids are given at a 50% probability level). Hydrogen atoms and co-crystallized solvent are omitted for clarity. Selected bond lengths (Å) and angles (°): Os(1)–C(1) 2.037(3), Os(1)–N(3) 2.103(3), Os(1)–Cl(1) 2.4006(8), Os(1)–C(12) 2.197(4), Os(1)–C(13) 2.161(4), Os(1)–C(14) 2.199(4), Os(1)–C(15) 2.199(4), Os(1)–C(16) 2.241(4), Os(1)–C(17) 2.233(4), C(1)–Os(1)–N(3) 75.60(12), C(1)–Os(1)–Cl(1) 81.84(10), C(1)–Os(1)–C(13) 96.01(14), N(3)–Os(1)–C(15) 92.89(12), Cl(1)–Os(1)–C(17) 87.95(10), N(3)–Os(1)–Cl(1) 84.25(8), C(1)–N(2)–C(4)–N(3) 0.7(5).

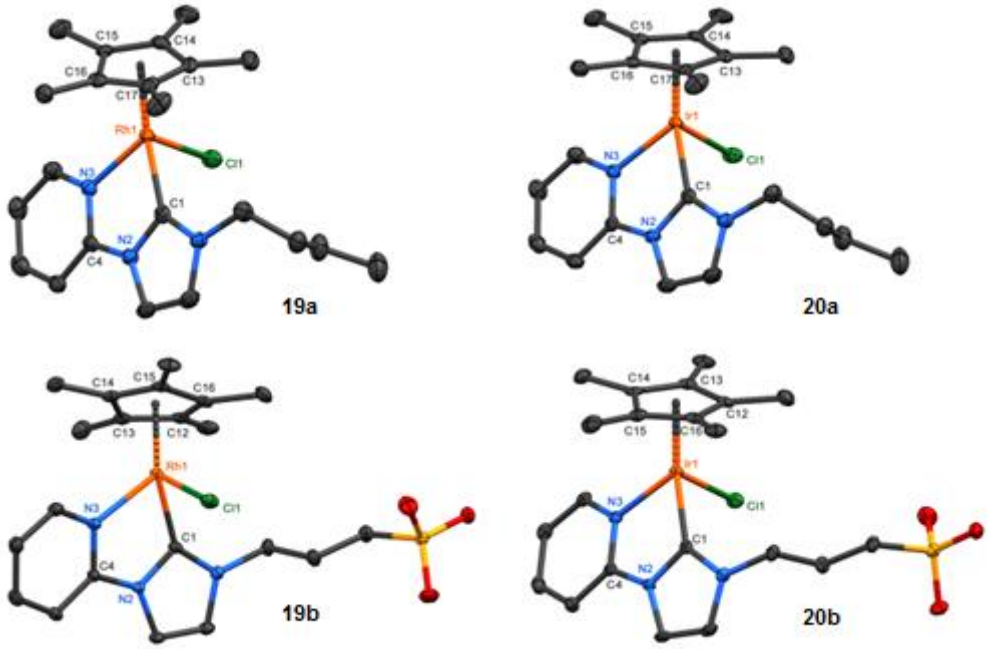

Figure 19. ORTEP style representation of the cations **19a**, **19b**·2.10H_2O, **20a** and **20b**·2.10H_2O (ellipsoids are set at 50% probability). Hydrogen atoms and co-crystallized solvent are omitted for clarity.

3 Catalytic hydrogenation of acetophenone

In this chapter, catalytic applications of the new synthesized complexes are presented. In a first step, the applications in transfer hydrogenation (TH) reactions of acetophenone by water-insoluble and water-soluble catalysts are explored. At continuation, the complete hydrogenation of the same substrate with the water-soluble catalysts is investigated in an autoclave for which the reaction parameters finally have been optimized. These reaction systems are of the most frequently transformations in chemical synthesis and hence, offer a good opportunity to compare with other studies.

N-Heterocyclic carbenes have superior properties as ligands in catalytic processes. The ability of the ligand to transfer electron density to the metal center implies an advantage in the catalytic process due to the more stable characteristics when compared to e.g. phosphines (see section 1.2). The development of functionalized NHCs requiring chelate ligands to improve catalytic processes has been studied during the last years. [108] In this work, the application of chelating NHC complexes containing a pyridine functionalization of the ligand is presented.

Hydrogenation and transfer hydrogenation are catalyzed by both homogeneous and heterogeneous catalysts. Heterogeneous catalysts are easy to use, recyclable and durable because of which they have been widely used in industrial chemical production, e.g. the synthesis of ammonia, methanol, cyclohexane, etc. Nevertheless, homogeneous catalysis presents several advantages , as for example excellent selectivity under mild conditions and high atom economy.[109]

Hydrogenation is probably the most studied reaction in aqueous media and consists in reduction by activation of molecular H_2 accompanied by oxidation of the hydrogen atoms and consequently, reduction of unsaturated organic molecules. In transfer hydrogenation, the hydrogen source is not gaseous H_2. A donor, typically alcohols (e.g. 2-propanol) or formic acid, transfer the hydrogen to an acceptor molecule, mostly in the presence of a base. It is easier to operate since it does not require gaseous hydrogen or pressure vessels and it has been more widely studied for organic solvents.[110] First studies with water-soluble catalysts appeared in the late 1980s while the study of aqueous phase hydrogenation has been less developed until recently. However, hydrogenation of olefins by simple water-soluble metal salts, such as $[Co(CN)_5]_3$ and $RhCl_3$ were already studied in the 1960s and 1970s.[109]

In this work, for the transfer hydrogenation reactions catalyzed by water-insoluble catalysts the standard reduction of acetophenone to 1-phenylethanol using 2-propanol as hydrogen donor in the presence of a base has been chosen. Likewise, for transfer hydrogenation catalytic tests by water-soluble complexes, an aqueous solution containing HCO_2Na/HCO_2H as hydrogen source and acetophenone as model substrate was used. Moreover, for the complete hydrogenation of acetophenone, a KOH basic aqueous system was used in an autoclave using H_2 (g) as hydrogen source. Scheme 21 shows these three studied catalytic reactions.

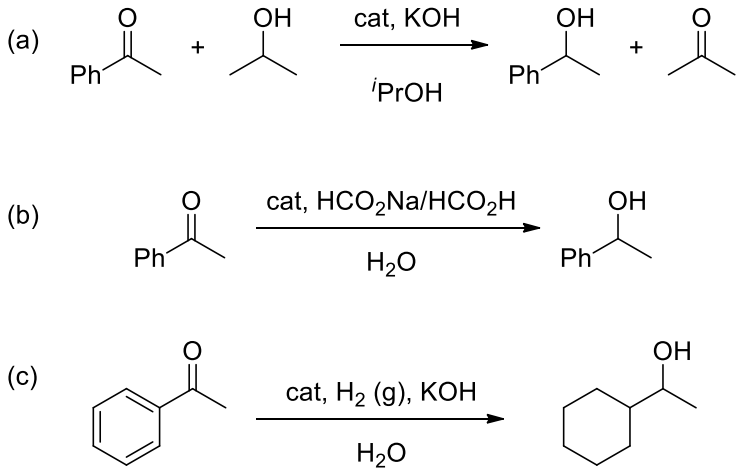

Scheme 21. Transfer hydrogenation of acetophenone in a basic ^{i}PrOH solution (a), in an aqueous solution containing sodium formate and formic acid (b) and hydrogenation of acetophenone using H_2(g) as hydrogen source (c).

As already described in chapter 2, there are some examples of organometallic compounds containing similar structures to those presented in this work and some of them are also applied in hydrogenation or transfer hydrogenation reactions. In the book titled "*N*-Heterocyclic Carbenes", edited by Steven P. Nolan,[50] a big variety of examples for transfer hydrogenation catalysis can be found. Moreover, it presents a more extended comparison of different catalyst properties, such as counterion effect, *N*- and backbone substituents or change of the aromatic ligands bounded to the metal center.

In this section only a small selection of literature examples is presented in which the catalysts and their application were most similar to that of the present work. In 2009, Zi-Ling Xue *et al*.[48] published the transfer hydrogenation of acetophenone to 1-phenylethanol in a basic isopropanol solution by a series of ruthenium carbonyl complexes containing pyridine-functionalised NHCs (Figure 20). For the catalytic tests, an isopropanol solution of KOH was added to another isopropanol solution containing catalyst and substrate. The mixture has been stirred at 82°C for 2 h 20 min, with a catalyst : base : substrate ratio of 1 : 25 : 500. In general, these ruthenium complexes achieved better results, when n = 0. In this case, complexes **B1** and **B2** of [48]are the most similar to the new synthesized in this work. A conversion > 90 % was obtained for the *trans* isomer **B1**, while approximately 75 % conversion was reached using the *cis* analogous isomer.

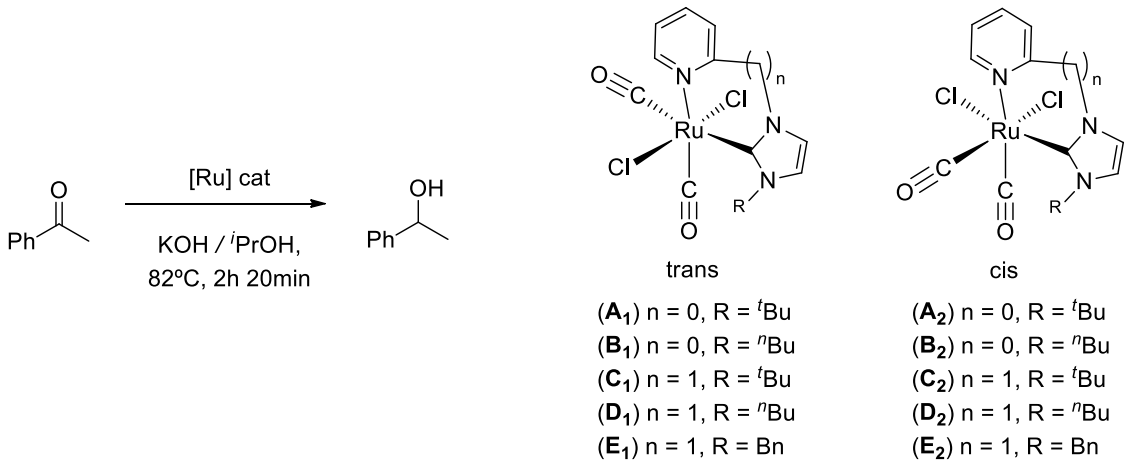

Figure 20. TH of acetophenone catalyzed by ruthenium (II) carbonyl chloride complexes containing pyridine-functionalized NHCs described by Zi-Ling Xue *et al*.[48]

In 2009, Crabtree *et al*.[36] also published a series of iridium and ruthenium complexes with chelating NHCs for the transfer hydrogenation, the *β*-alkylation of alcohols and the *N*-alkylation of amines. The structures of the organometallic compounds presented in the work of Crabtree *et al*.[36] are almost equal to the new synthesized water-insoluble catalysts of this work. In order to have comparable results, in this work, the same catalytic conditions were applied for the transfer hydrogenation of acetophenone. Crabtree *et al*.[36] found that both, iridium and ruthenium catalysts, are successful in catalyzing the transfer hydrogenation of acetophenone in KOH/^{i}PrOH basic solution at 82°C for 3 h (Figure 21). The applied catalyst : base : substrate ratio was 1 : 10 : 100. When iridium complexes were applied, 98% (R = ^{n}Bu) and 86% (R = Ar) yield of the hydrogenated product were obtained, while 98% yield was obtained for the ruthenium compound.

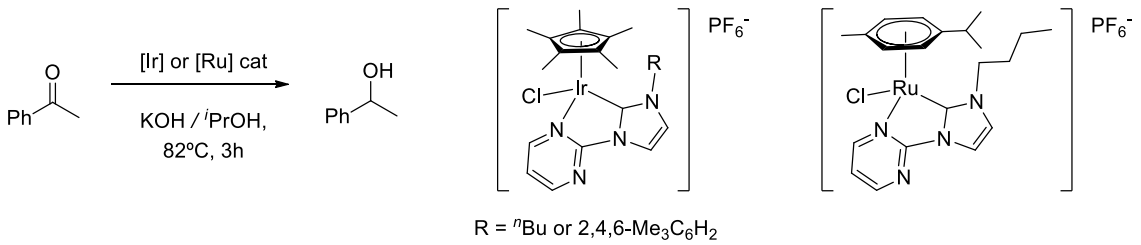

Figure 21. TH of acetophenone catalyzed by iridium (III) and ruthenium (II) complexes with chelating pyridine-functionalised NHCs described by Crabtree *et al*.[36]

More recently, in 2016, Gençay Çoğaşlioğlu *et al.*[111] described the transfer hydrogenation of acetophenone under similar catalytic conditions (Figure 22). The catalytic experiments were carried out using a catalyst : base : substrate ratio of 1 : 10 : 200 in isopropanol, by stirring the

solution at 82°C for 4 h. The authors studied the role of the base present in the catalysis. In contrast to KOH, other bases such as Na_2CO_3, NaOAc, triethylamine, pyridine, and K_2CO_3 showed less conversion and the completion of the reaction took much longer as compared to KOH. It was also observed that the activity of the complexes depends on the nature of the *N*-substituents and decreases in the order **d₁**>**c₁** and **d₂**>**b₁**>**a₁** (Figure 22) indicating that **d₁** presents the most noticeable activity and a maximum yield of 93% is achieved after 4 h. The essential features for efficient transfer hydrogenation with these Ru-NHC catalysts appear to include a sterically demanding benzyl substituent on the *N* atom of NHC.

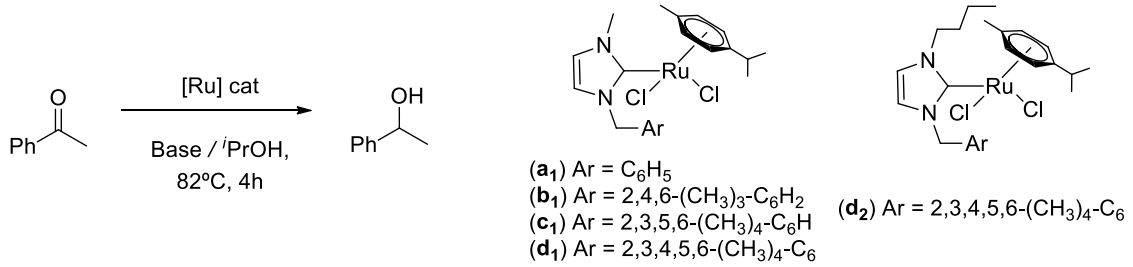

Figure 22. TH of acetophenone catalyzed by ruthenium (II) complexes without chelating functionalised NHCs described by Gençay çoğaşlioğlu et al.111

An interesting research from 2004[112] presents the catalytic properties of ruthenium complexes. It is worth noting that one of the presented compounds (Figure 23 (a)) has a similar structure to the **d₂** compound of [111] (Figure 22), but interestingly, it dissolves well also in water. When the ruthenium (II) compound is dissolved in D_2O and analyzed by ^{13}C NMR spectroscopy, two different singlet resonances were observed. When NaCl is added to the aqueous solution, only one of the signals appeared. These observations can be explained by the equilibrium presented in Figure 23 (b). Furthermore, aqueous solutions of the catalyst react with H_2 (g) with a color change from orange to deep red and the resulting solutions show considerable catalytic activity in the hydrogenation of various unsaturated substrates. In case of acetophenone, a conversion of 28% after 1 h was measured.

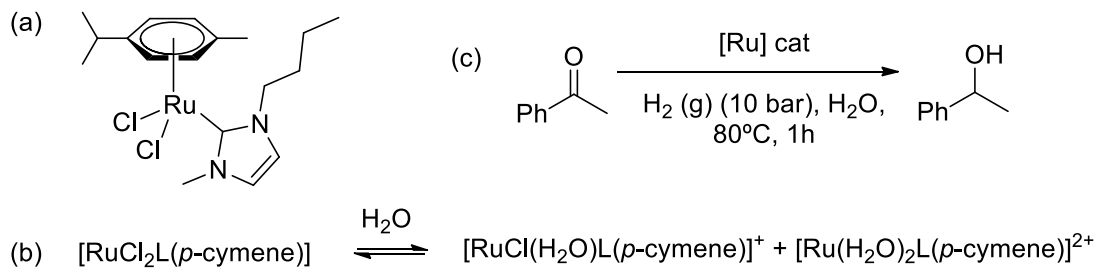

Figure 23. Structure of a ruthenium (II) complex (a), its equilibrium in water (b) and ketone catalytic hydrogenation of acetophenone (c) developed by Péter Csabai and Ferenc Joó.[112]

The development of aqueous-phase hydrogenation and transfer hydrogenation reactions do not only involve a contribution to a more sustainable process (see section 1.3). It also facilitates some tedious processes in the laboratory, such as catalyst/product separation. Having in mind that most organic compounds are insoluble or only slightly soluble in water, the utilization of water-soluble homogeneous catalysts in aqueous or multiphase media offers the opportunity to exploit new and efficient ways of chemical operations, as for example easy separation by phase separation or extraction.[26,109] In any case, engineering aspects are also important and should not be underestimated. It is important to note that two liquids are not completely "immiscible" but have limited miscibility in each other. Therefore, the insolubility of many organic compounds in water implies possible diffusion control if the reduction occurs in the aqueous phase. [113]

Two-phase catalytic processes retain many advantages of homogeneous catalysis such as efficient use of the molecularly dispersed catalyst, high selectivity and the possibility of tailoring the catalyst to the particular substrate by modification of the ligand environment, and combine those with the ease of recovery of a heterogeneous catalyst. For an efficient recovery, the catalyst must be insoluble in one of the phases, which in turn should preferentially dissolve the substrates and products. Ideally, the interaction of the catalyst with the substrates and products will not change its solubility properties and no leaching of the catalyst to the other phase should take place.[113]

Transfer hydrogenation reactions are usually performed in isopropanol that acts as both, solvent and hydrogen source. However, formic acid and its salts are viable hydrogen sources and soluble in water. Aqueous formate has been used by enzymes for reduction reactions for millions of years, but not until recent years, the asymmetric transfer hydrogenation in water received significant attention. This reflects the relatively limited research into aqueous transfer hydrogenation undertaken in the past decades.[109]

In the last years, some studies have revealed that ketones can be reduced by HCOONa or HCOOH in water with water-soluble half-sandwich ruthenium (II) and iridium (III) complexes. Some of them contain multidentate pyridine-type ligands and their catalytic results showed depend on the pH. [109] Further studies, as for example published by Mengping Zhu,[114] examine the effects of various different system parameters, like substrate inhibition due to the low solubility of the organic substrate in aqueous solutions, and the use of phase-transfer catalysts to overcome this issue. On the other hand, for HCO_2Na/HCO_2H aqueous systems, the base/acid concentration was found to be crucial in determining the catalytic performance. With respect to temperature, volume of water and stirring speed it was found that the reaction rate could be enhanced with increasing temperature and stirring rate. Transformation of formate to the organic phase depends on how well these two layers are mixed. Their better mixing can increase the interfacial area, which might be the active site of the hydrogenation.

A summary of various different examples of aqueous-phase transfer hydrogenation catalytic reactions can be found in different books, as for example "Aqueous-Phase Organometallic Catalysis" published in 2004 and edited by Boy Cornils and Wolfgang A.Herrmann[44] or "Metal-

Catalyzed reactions in water" published in 2013 and edited by Pierre H. Dixneuf and Victorio Cadierno.[109] Focusing on transfer hydrogenation of acetophenone in aqueous media catalyzed by water-soluble NHC complexes, less results are found. For the present work, catalytic applications of complexes containing a sulfonate functionalization of the NHC ligand are focus of interest. Nevertheless, aqueous transfer hydrogenation of acetophenone catalyzed by water-soluble sulfonated NHC complexes has not been reported to date to the best of my knowledge.

In 2009, Zhongqiang Zhou and Yong Sun[115] published the transfer hydrogenation of different ketones in water using HCO_2Na/HCO_2H as hydrogen source. The catalytic studies were performed in a *one-pot* reaction, since the corresponding water-soluble ligand (**L1** or **L2** in Figure 24) and $[RuCl_2(p\text{-cymene})]_2$ metal precursor were dissolved in degassed water and stirred at 40°C for 1 h under argon atmosphere, followed by consequent addition of HCO_2Na and the corresponding ketone to the mixture. No isolation or characterization of the active catalysts was carried out. Finally, the organic compounds were extracted with hexane. All catalytic reactions were performed using a substrate/catalyst ratio of 100 under argon atmosphere for 2 h at 40°C. With acetophenone as substrate, full conversion to 1-phenylethanol wass obtained with both ligands.

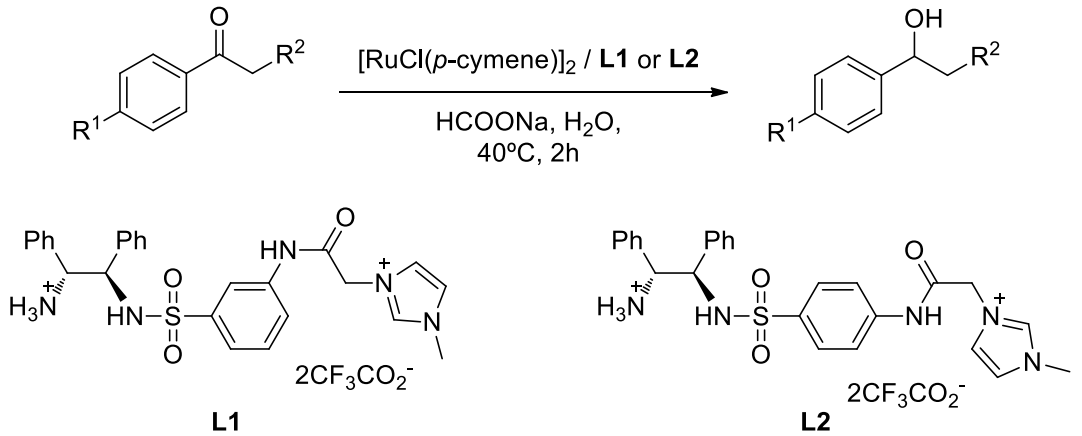

Figure 24. Catalytic transfer hydrogenation of ketones in water developed by Zhongqiang Zhou and Yong Sun[115]

Transition metal water-soluble NHC complexes containing a chelating alkanesulfonated imidazolium ligand have found different applications. For example, palladium compounds are able to catalyze Suzuki-Miyoura cross-coupling reactions in water(Figure 25 (a))[33], iridium successfully reduce CO_2 to formate under basic aqueous conditions (Figure 25 (b))[39] and ruthenium isomerizes allylic alcohols in water (Figure 25 (c)).[35] Nevertheless, the use of ruthenium in hydrogenation reactions is the most extended application. The research group of Kühn has reported results for the aqueous hydrogenation of acetophenone catalyzed by ruthenium, rhodium and iridium water-soluble complexes (Figure 26).[56] At room temperature

and a hydrogen pressure of 40 bar, good yields of up to 87% could be obtained for the ketone hydrogenation after 21 h with a ruthenium catalyst loading of 2.5 mol%. Similar results were obtained when a rhodium catalyst containing benzimidazolium ligand was applied (89% yield), while other rhodium and iridium complexes showed to be less active under the same catalytic conditions.

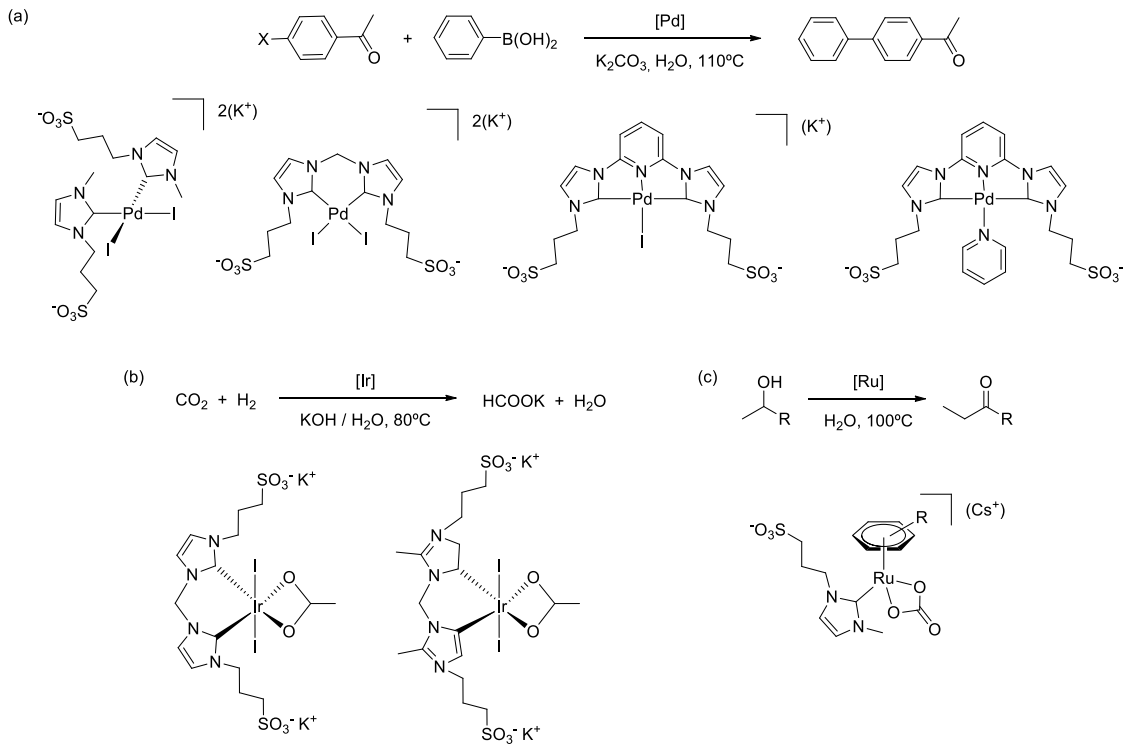

Figure 25. Some examples of catalytic applications of palladium (a)[33], iridium (b)[39] and ruthenium (c)[35] complexes containing a chelating alkanesulfonated NHC ligand.

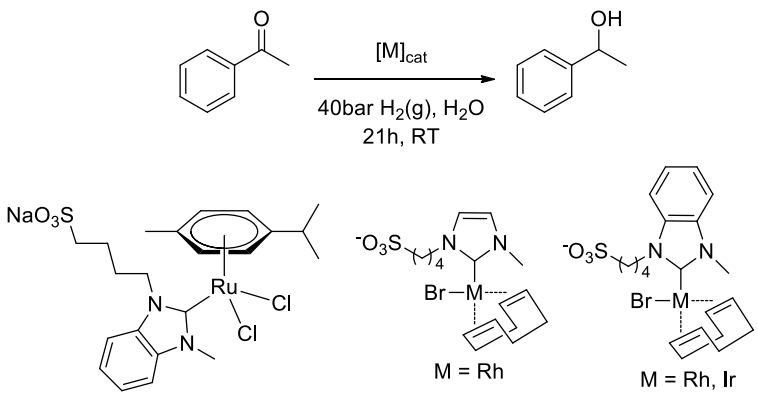

Figure 26. Catalytic hydrogenation of acetophenone by ruthenium, rhodium and iridium water-soluble catalysts developed by Kühn *et al.*[56]

In more recent studies the synthesis and application of different metal complexes with chelating alkanesulfonated NHC ligands was successfully applied. Kühn *et al.*[58] synthesized a series of ruthenium, rhodium and iridium compounds, which have shown to be efficient catalysts for the reduction of bicarbonate to formate, as well as for the hydrogen generation from formic acid (both processes in water) with the objective to establish a hydrogen production and storage on a formic acid/bicarbonate platform(Figure 27 (a) and (b)). The same ruthenium catalyst was previously tested in the complete hydrogenation of phenol (Figure 27 (c)) and acetophenone (Figure 27 (d)) obtaining good conversions. For the catalytic runs, a preactivation of the ruthenium catalysts solution (40 bar H_2 pressure, 60°C and 1 mol% of the catalyst) is necessary. Almost quantitative yield of cyclohexanol was obtained when the same conditions were applied for the catalytic runs after 2 h. For the acetophenone hydrogenation, best results were obtained with the same catalytic conditions as used for phenol. However, both catalytic studies always gave a mixture of products. In case of phenol, a mixture of cyclohexanone and cyclohexanol was detected, as well as for acetophenone, where a mixture of 1-phenylethanol, cyclohexylmethylketone and 1–cyclohexylethanol always appeared as product. The formation of ruthenium nanoparticles (Ru^0) appeared not to be the catalytic species, although the nature of the formed active catalysts remained elusive and was not definite. ^{1}H NMR measurements of reaction solutions after phenol hydrogenation showed three different signals corresponding to hydride species, which agrees to ESI-MS results. Interestingly, when acetophenone was used as substrate, only the first two signals were observed. Adding mercury to the catalytic solutions strongly decreased the activity of the ruthenium catalyst, suggesting the reaction of Ru^0 with Hg. On the other hand, TEM measurements did not show the formation of Ru^0 NPs at least larger than 1 nm, except of the case of acetophenone reduction.

The hydrogenation of arenes and heteroaromatics to partially or fully saturated cyclic hydrocarbons is a reaction of paramount industrial importance, typically catalyzed in heterogeneous phase by a number of transition metals. Some examples are the hydrogenation of benzene (on Raney nickel for nylon production) or fossil fuels as coal (to remove sulfur, nitrogen and oxygen from various heteroaromatics).[113] A promising alternative to petrochemical fossil resources for the production of biofuels and bio-based products consists in lignocellulosic biomass. It includes hardwood, softwood and grasses, which are an abundant renewable resource mainly composed of cellulose, hemicelluloses and lignin. Lignin depolymerization and conversion has a significant potential as a sustainable source for the production of fuels and bulk chemicals, and so as a direct alternative to the petrochemical industry. Lignin is the major aromatic resource of the bio-based economy since it owns a unique polyaromatic structure, where a wide variety of bulk and fine chemicals can be potentially be obtained.[116]

Aromatic rings are difficult to saturate and the hydrogenation is generally performed with heterogeneous catalysts being one of the most suitable alternatives to solve the separation problems presented by homogeneous catalytic systems. Most of the reported soluble metal complexes to catalyze arene hydrogenation in water lead to decomposition into heterogeneous metal particles.[109]

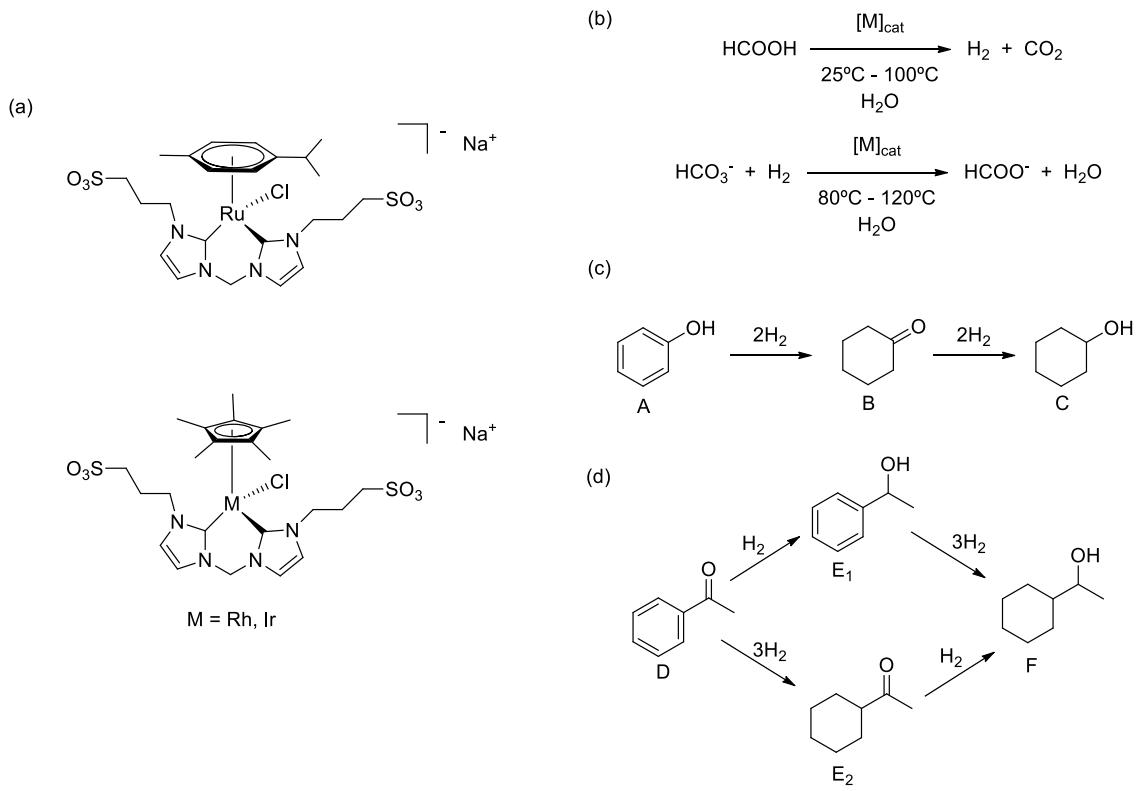

Figure 27. Catalytically active Ru, Rh and Ir complexes with sulfonate functionalized NHC ligand (a), hydrogen production and storage formic acid/bicarbonate platform (b), hydrogenation of phenol (c) and acetophenone (d) developed in our research group.[37,58]

The use of transition metal nanoparticles (NPs), also sometimes called “semi-heterogeneous” or “nanoheterogeneous” catalysts due to their particular matter state between homogeneous and heterogeneous, [117] have become an attractive alternative when compared to heterogenized catalysts, e.g. based on silica supports. For this type of heterogeneous systems, only sites on the solid surface are available for catalysis. However, NPs are robust, provide high surface area and their activity and selectivity can be manipulated by tailoring chemical and physical properties such as size, shape, composition and morphology.

Transition metal nanoparticles present some advantages over classical colloids and have different characteristics. They are smaller (1-10 nm),[117] their synthesis is reproducible, they are isolable and redissolvable in both organic and aqueous solvents and they display reproducible activities.[109] Ru and Rh are the most widely used metal NPs in hydrogenation reactions, especially in olefin and alkyne hydrogenation. Soluble metal NPs are considered as a reference in monocyclic arene catalytic hydrogenation.[117]

Metal nano-catalysts can be synthesized via two main methods:[109,117]

- Reduction of metal salts. The chemical reduction of commercial and various transition metal salts such as rhodium or ruthenium chloride species is probably the most common

synthetic route to colloids. However, in these processes, salts, water and by-products often remain in contact with the surface of the particles, thus passivating them, leading to the production of surface oxides or hydroxides, and potentially modifying their reactivity in catalysis.

- Decomposition of organometallic complexes. This strategy permits the control of particle dispersity, size, shape, organization and nature of the chemical species present at their surface.

Stabilization of the NPs is also important in order to avoid the formation of bulk metal:

- Electrostatic stabilization can be obtained using ionic compounds as protecting agents in aqueous solutions.
- Steric stabilization can be achieved by the use of neutral molecules (polymers or bulky molecules) and can be used in both organic and aqueous solvents.

The different catalytic applications of the new synthesized water-insoluble and water-soluble complexes in transfer hydrogenation and hydrogenation reactions are presented below. The water-insoluble compounds are applied in acetophenone transfer hydrogenation under inert conditions in isopropanol, while their water-soluble analogues are studied in the transfer hydrogenation and hydrogenation of the same substrate on air in a HCOONa/HCOOH aqueous solution or under H_2 pressure in a basic water solution respectively. In all cases, a proposal of the mechanistic pathway of the reactions is proposed.

3.1 Catalytic transfer hydrogenation of acetophenone with water-insoluble 1-(2-pyridinyl)-3-(*n*-butyl)imidazol-2-ylidene metal complexes

3.1.1 Experimental

Complexes **17a**-**20a** were successfully applied in transfer hydrogenations of acetophenone as model substrate. The ruthenium complex **17a** displays the highest activity (reaction conditions: ^{i}PrOH/KOH, T = 82°C, Table 2). The catalytic activity is comparable to that observed in previously published work of Crabtree *et al*.[36], who used related catalysts. However, a distinct advantage of the catalytic system presented is that lower reaction times are required. Crabtree *et al* described the transfer hydrogenation of acetophenone by a series of iridium and ruthenium complexes. Such ruthenium catalyst is able to hydrogenate the ketone after 3 h, obtaining 98 % yield of the hydrogenated product. However, complex **17a** is able to obtain 92% yield after only 1 h 10 min.

Table 2. Catalytic transfer hydrogenation with water-insoluble catalysts **17a**-**20a**.

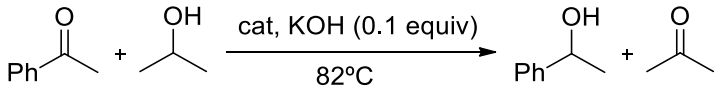

Entry	Catalyst	Catalyst loading (mol%)	Yield (%)[b]
1	17a	1	92
2	17a	1	79
3	17a	0.5	76
4	18a	1	60
5	19a	1	89
6	20a	1	85

[a] 2.00 mmol of ketone, KOH (10 mol %) in 3.0 mL of ^{i}PrOH at 82°C for 70 min. [b]yields were determined by ^{1}H NMR spectroscopy, using 1,3,5-trimethoxybenzene as an external standard. [c] reaction conducted at 60°C.

Catalyst **17a** (as most active compound) was used as model catalyst to determine the most favorable reaction conditions, which were found to be 1 mol% of the catalyst and a temperature of about 80°C. The optimized conditions were subsequently applied to samples of catalysts **18a** - **20a** in order to evaluate and compare their activity. The ruthenium complex **17a** is the most active one (entry 1, Table 2), followed by rhodium **19a** (entry 5, Table 2) and iridium **20a** (entry 6, Table 2) catalysts. The osmium-based catalyst **18a** displays a comparatively low activity.

^{1}H NMR studies show the different stabilities and behavior in isopropanol (neat or in presence of base). Catalyst **17a** is not completely soluble in neat isopropanol although the ^{1}H NMR of the catalysts measured in ^{i}PrOD shows the intact structure of the catalyst (Figure 28). When the complex is dissolved in a basic solution of ^{i}PrOD, containing KOH (using the same ratio KOH : catalyst as in the catalytic runs), the solution turns from yellow to dark brown. ^{1}H NMR of this solution was recorded, showing a completely different spectrum (Figure 29).

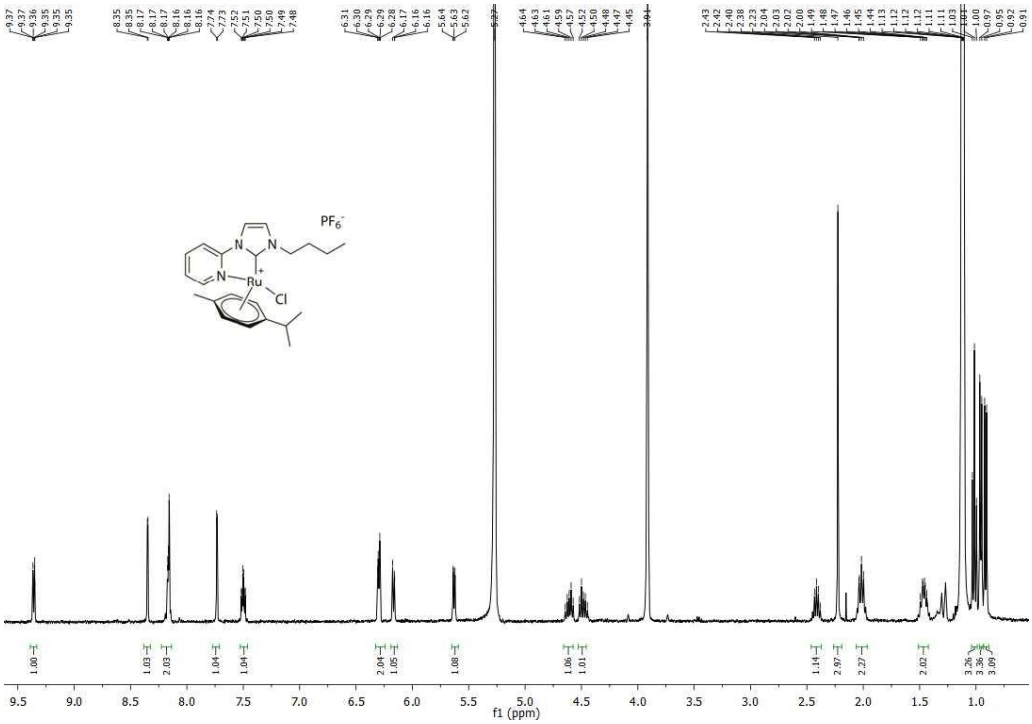

Figure 28. ^{1}H NMR spectrum of **17a** in ^{i}PrOD.

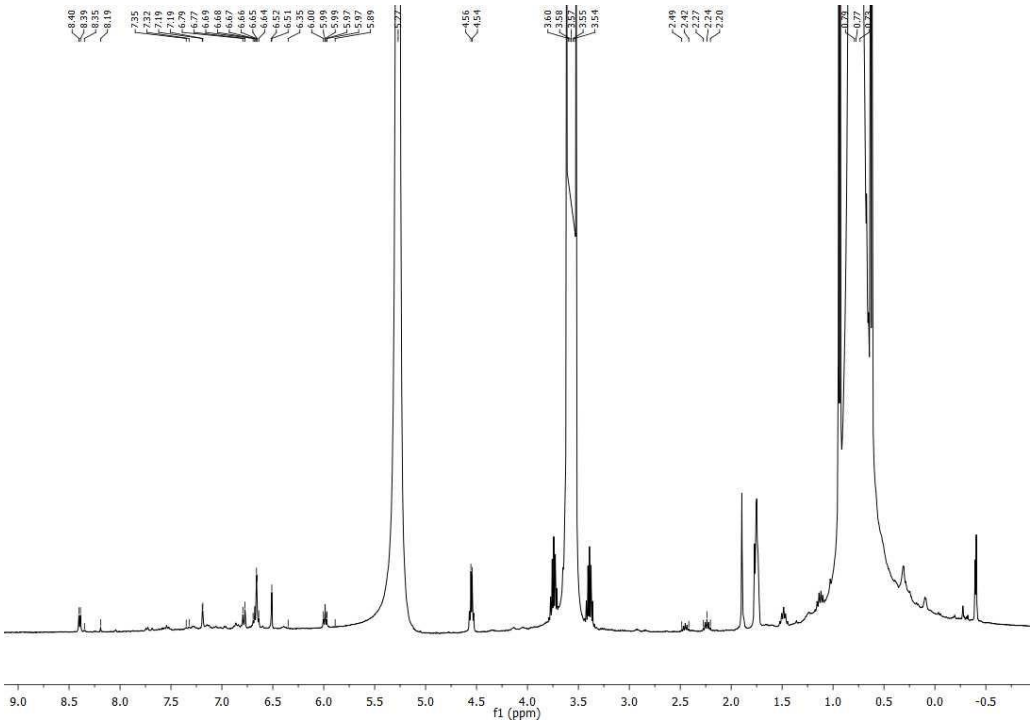

Figure 29. ^{1}H NMR spectrum of **17a** in the mixture KOH/^{i}PrOD.

Rhodium catalyst **19a** is not soluble in pure ^{i}PrOH**.** However, when KOH is added the solution turns dark purple and the complex is solubilized. Figure 30 shows the structure of the catalyst under basic catalytic conditions. Although proton signals are not possible to integrate due to the low concentration of the sample (low solubility) a general assignation can be proposed. Signals between 9 and 6.5 ppm correspond to the pyridine and imidazole hydrogens present in the NHC ligand. Other protons of the ligand can be assigned to the multiplets at 4.17 ppm and those between 1 and 2.5 ppm. The Cp* moiety gives rise to the more intense signal at 1.93 ppm.

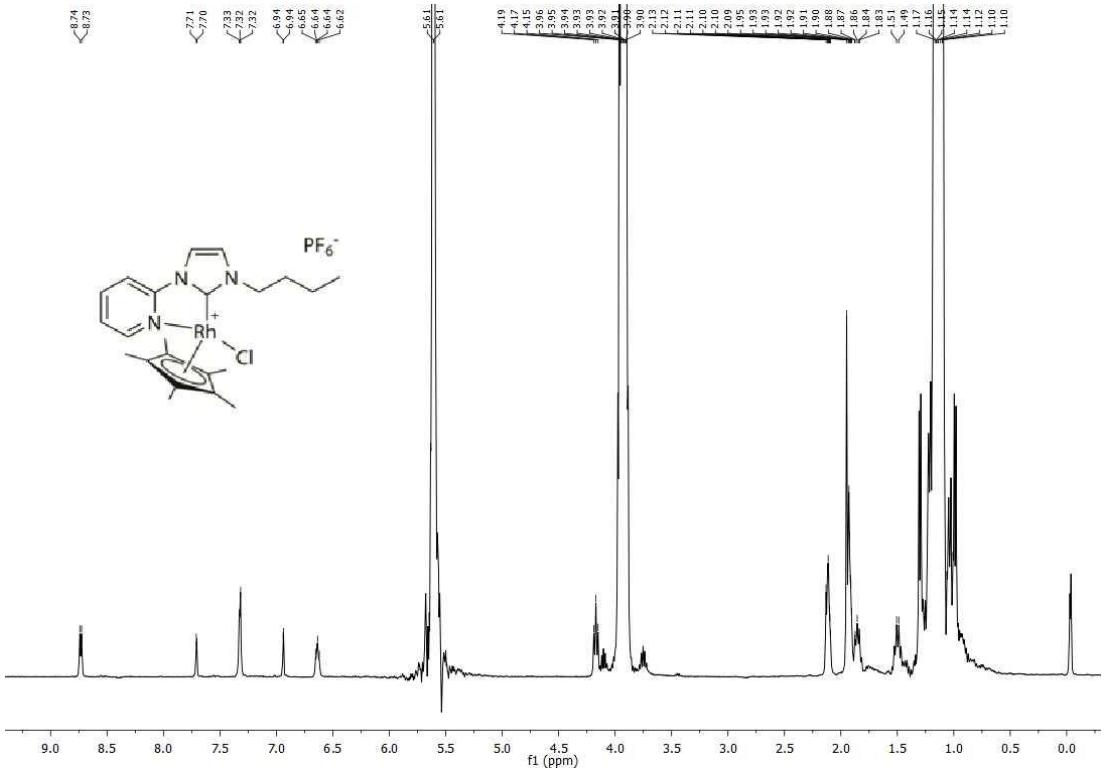

Figure 30. ^{1}H NMR spectrum **19a** in the mixture KOH/^{i}PrOD.

The solubility of catalyst **20a** in isopropanol too changes when KOH is added. Initially the iridium complex is not soluble in pure isopropanol. However, when KOH is present (under the same conditions as in the catalysis) the solution turns from pale yellow to dark purple suggesting a change in the structure of the catalyst. ^{1}H NMR spectrum of **20a** in isopropanol and KOH mixture corroborates this structural change. A new series of peaks appears, although the intensity is too low for a feasible integration and assignment of the signals.

In contrast to these samples, the osmium complex (**18a**) is partially soluble in isopropanol. A ^{1}H NMR spectrum was recorded in ^{i}PrOD and the proton signals could be assigned. Hydrogens of the pyridine can be found at 9.28(d), 8.24(d), 8.11(t) and 7.41(t) ppm; imidazole hydrogens appear at 8.29(d) and 7.69(d) ppm respectively. The aliphatic chain of the imidazole ligand

appears as multiplets at 1.95, 1.40 and 0.97 ppm respectively. The aromatic protons of the p-cymene ligand appear as four different signals between 6.4 and 5.6 ppm, the methyl group at 2.28 ppm, the C*H* proton at 2.32 ppm and the two terminal CH_3 groups of the ligand appear at 0.88 ppm (Figure 31). However, when KOH is introduced in the isopropanol solution of the catalyst, the color changes drastically to dark brown. A ^{1}H NMR spectra of this solution was recorded immediately after the addition of KOH without any variation of the hydrogen signals. However, when the sample is measured after 12 h either at room temperature or at 80°C, no peaks can be detected in ^{1}H NMR, suggesting the decomposition of the catalyst.

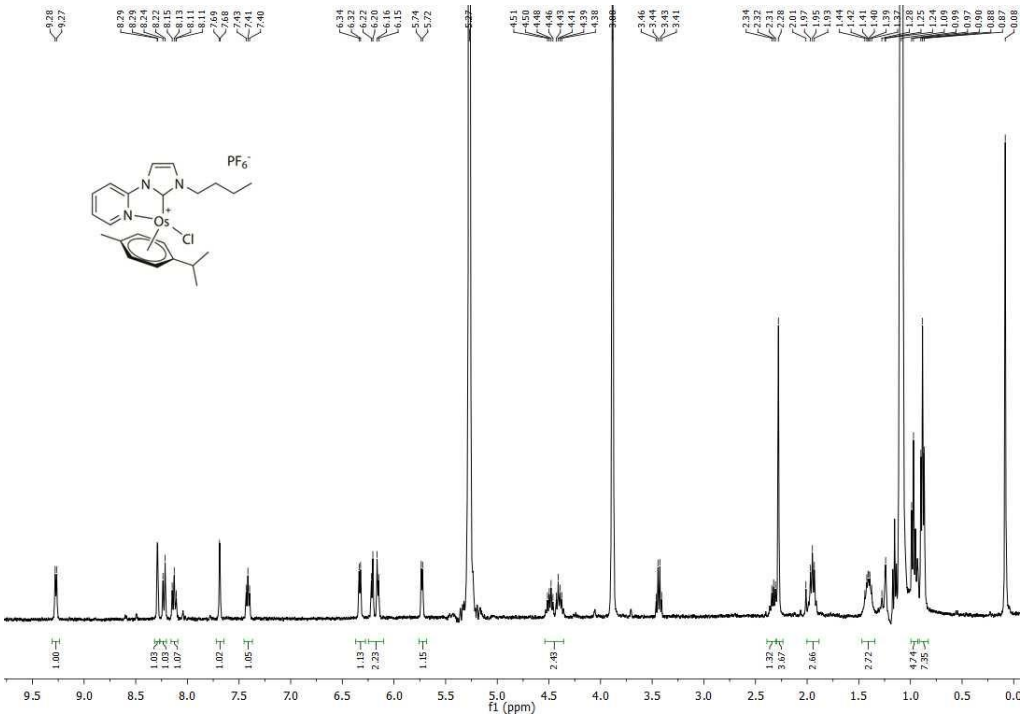

Figure 31. ^{1}H NMR spectrum of **18a** in neat ^{i}PrOD.

These stability analyses are in agreement with the different catalytic behavior. Ruthenium (**17a**) and rhodium (**19a**) catalysts which are the most stable ones among the here examined, have been found to be the most active. Followed by iridium complex (**20a**) and lastly the osmium compound (**18a**) which is the least stable in solution, obtaining also only 60% yield in the catalytic runs. A mechanism for the transfer hydrogenation catalytic reaction is proposed (*vide infra*) based on the most active catalyst (**17a**) and considering previous studies of Xiufang Xu *et al*.[118].

3.1.2 Proposed mechanism

Being a mild reaction route for the reduction of polar double bonds, homogeneous TH reactions have been widely studied[119–122]. Two general pathways have been suggested for the transfer hydrogenation of ketones. The "direct hydrogen transfer route" which is usually catalyzed by main group metals without involvement of a metal hydride intermediate, and the "hydridic route" which implies the transition metal catalysts involving a metal hydride intermediate. For this "hydridic route" there are two different hydrogen transfer mechanisms: an *inner-sphere* (concerted or stepwise) and an *outer-sphere* mechanism. By means of density functional theory calculations and the topological analysis method Xiufang Xu *et al.*[118] investigated whether the "direct hydrogen transfer" or the "hydridic route" is favored for similar TH reactions.

Functionalized NHC ligands containing a hemilabile group which can reversibly dissociate and coordinate to the metal center have been used to synthesize various homogeneous catalysts[108,123,124] among which particularly, the N-functionalized NHC ligands have received significant attention.[36,125,126] The hemilability of picolyl-NHC ligands in metal alkoxides has an influence on the mechanism. The reaction proceeds via the concerted mechanism when the picoly group coordinates to the metallic center (to form an $18e^-$ catalyst) and can follow the stepwise inner-sphere or the direct hydrogen transfer route when the picolyl group decoordinates from the metal to give a $16e^-$ metal alkoxide catalyst. The authors conclude that from an energetic point of view the transfer hydrogenation reaction should work through a stepwise *inner-sphere* mechanism due to the lower overall energy barrier as compared to a concerted *inner-sphere* mechanism and a "direct hydrogen transfer route". Furthermore, topological analyses confirmed that the agostic interactions can facilitate the β-*H* elimination and ketone insertion processes in the stepwise *inner-sphere* mechanism.[118]

Based on this analysis a stepwise *inner-sphere* mechanism for the transfer hydrogenation of acetophenone with 1-(2-pyridinyl)-3-*n*-butyl)imidazol-2-ylidene metal complexes is proposed (Scheme 22), although we have not enough data to confirm it. The first step is the pre-catalyst activation. Under basic conditions (KOH/^{i}PrOH), a solvent molecule (^{i}PrOH) loses a proton to generate the ^{i}PrO$^-$ anion, which can coordinate to the metal center of **A** to yield the metal alkoxide **B**. The picolyl group decoordinates from the metal to give a $16e^-$ metal alkoxide catalyst (**B**). This catalyst generates the hydride intermediate **C** and releases acetone by β-hydrogen elimination. At this point, acetophenone attacks the metal hydride intermediate to form a new alkoxide intermediate (**D**). A proton transfer process regenerates species **B** and leads to the formation of the product.

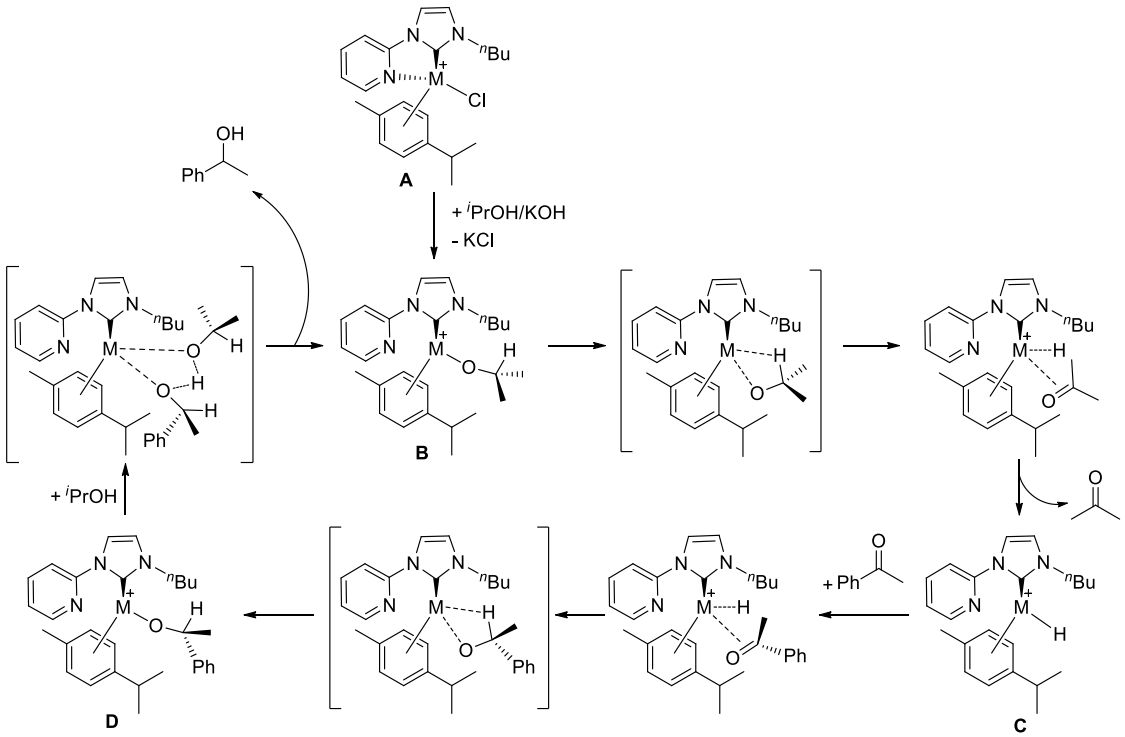

Scheme 22. Proposed mechanism for the transfer hydrogenation of acetophenone with 1-(2-pyridinyl)-3-*n*-butyl)imidazol-2-ylidene metal complexes.

3.2 Catalytic transfer hydrogenation of acetophenone with water-soluble 1-(2-pyridinyl)-3-(sulfonatepropyl)imidazol-2-ylidene metal complexes

3.2.1 Experimental

Catalysts **17b**-**20b** were applied as catalysts in TH reactions in aqueous solution using HCO_2Na/HCO_2H as hydrogen source and acetophenone as model substrate (Table 3). Complex **19b** was used as model substrate to determine optimal reaction conditions. Catalytic runs were performed without either air exclusion, degassing and/or inert gas protection. Blank experiments were performed without adding catalyst by heating the substrate in an aqueous buffer solution, showing no conversion of substrate. The best catalytic activities are obtained when using 1 mol% catalyst at 80°C, at a pH value of 2.75 in a 6M HCO_2Na/HCO_2H aqueous buffer solution (entry 12, Table 3). Temperature apparently has a strong influence on the reaction, as temperature decrease correlates with activity reduction. The pH value of the solution is also crucial as an increase to 3.75 leads to a decrease in activity.

Table 3. Catalytic transfer hydrogenation with water-soluble catalysts **17b**-**20b**

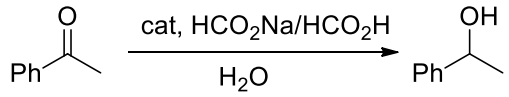

Entry	Catalyst	Cat (mol %)	T (°C)	pH	Buffer (M)	Time (min)	Yield (%)[b]
1	19b	1	RT	2,75	2	30	33
2	19b	1	RT	3,75	2	30	9
3	19b	1	40	2,75	2	30	55
4	19b	1	60	2,75	2	30	90
5	19b	1	80	2,75	2	30	93
6	19b	1	80	3,75	2	30	46
7	19b	1	80	2,75	1	10	47
8	19b	1	80	2,75	2	10	68
9	19b	1	80	2,75	3	10	80
10	19b	1	80	2,75	4	10	87
11	19b	1	80	2,75	5	10	95
12	19b	1	80	2,75	6	10	96
13	19b	1	80	2,75	7	10	90
14	19b	0,5	80	2,75	6	10	70
15	17b	1	80	2,75	6	10	3
16	18b	1	80	2,75	6	10	0
17	20b	1	80	2,75	6	10	6
18	17b	1	80	2,75	6	420	87
19	18b	1	80	2,75	6	420	3
20	20b	1	80	2,75	6	420	92

[a] Acetophenone and catalyst were mixed into a HCOONa/ HCOOH buffer solution (500 µL) with the desired concentrations. [b] yields were determined by ^{1}H NMR and GC-MS using nitrobenzene as standard.

Comparable results have been reported in literature in the last years with monotosylated diamine rhodium and iridium complexes, which were found to catalyze the transfer hydrogenation of acetophenone in air with full conversions in 15 min at 40°C. Other transfer hydrogenation reaction catalysts in water require the presence of inert atmosphere and/or methanol/water or HCO_2H-NEt_3 azeotropic mixtures to facilitate high conversions[109]. The present system, examined in this work, offers several advantages in comparison to previously described catalyst systems: It uses air-stable catalysts, displaying NHC ligands, also enhancing the thermal stability of the catalysts[109].

In order to further analyze the catalytic activities of complexes **17b**, **18b** and **20b**, the conditions, optimized for complex **19b** were applied (Entries 15-17, Table 3). Surprisingly, their activities after 10 min were much lower yielding only 3% and 6% with compounds **17b** and **20b** respectively, and no conversion is observed in case of **18b**. Catalysts **17b** and **20b** are able to hydrogenate the ketone obtaining 87% and 92% yield respectively in 7 h (Entries 18 and 20, Table 3). In contrast, the osmium catalyst reaches only 3% yield in 7 h (Entry 19, Table 3). The rhodium (**19b**) catalyst appears to be the most active one, followed by iridium (**20b**), ruthenium (**17b**) and osmium (**18b**). This confirms the results of similar studies suggesting that rhodium catalysts outperform ruthenium and iridium complexes in terms of catalytic activity[109].

Different stability of compounds **17b**-**20b** in neat water and in the presence of the buffer solution is studied to understand their different behavior in the catalysis. ^{1}H NMR spectra of all catalysts were recorded in D_2O at room temperature and after heating the solution to 80°C. Rhodium (**19b**) and iridium (**20b**) complexes proved to be stable under both conditions. No color changes were observed in the solutions and ^{1}H NMR spectra show no differences between room temperature and heated samples. Their high stability in water is in agreement with the fact that both compounds crystallize after some hours in water at room temperature (as previously described). Ruthenium (**17b**) and osmium (**18b**) compounds were not stable for longer time periods in water. ^{1}H NMR spectra of **17b** and **18b** in D_2O were recorded at room temperature. The solutions were orange but after 24 h they turned darker. In both cases ^{1}H NMR spectra show the presence of two different species in solution (Figure 32 and Figure 33). However, in other solvents such as methanol and DMSO, the complexes are stable. When the solutions are heated to 80°C, the color turns from orange to dark green although there are no significate changes observable in the ^{1}H NMR spectra. It can be concluded that rhodium and iridium catalysts are completely stable in neat water while ruthenium and osmium catalysts are not. This behavior is in agreement with the experimental results being **19b** and **20b** the most active catalysts. However, these analyses do not explain the big difference between the activities of rhodium and iridium compounds. Consequently, ^{1}H NMR experiments of each catalyst were recorded in D_2O containing a HCO_2Na/HCO_2H buffer solution, the same as previously employed in the catalytic runs.

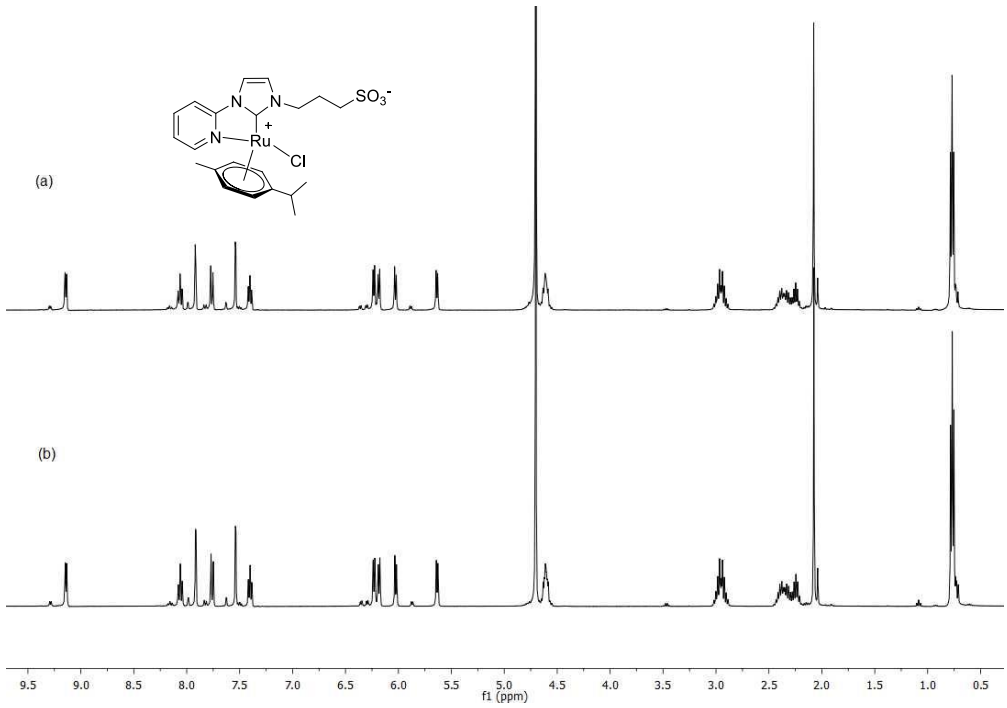

Figure 32. ^{1}H NMR spectra of **17b** measured after stirring the samples in D_2O at RT (a) and at 80°C (b).

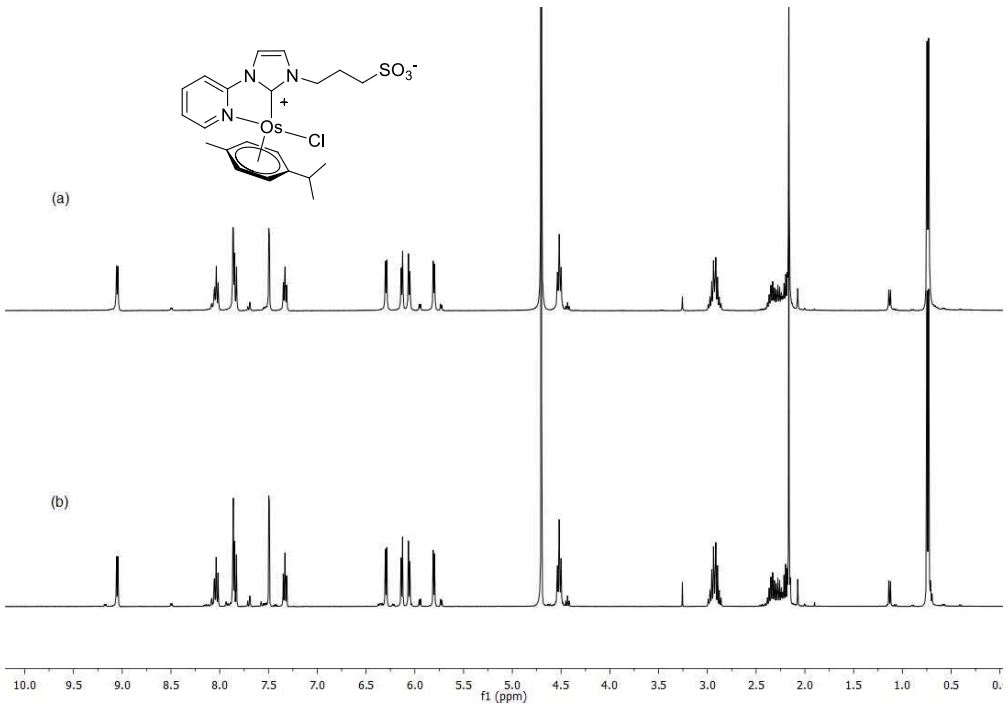

Figure 33. ^{1}H NMR spectra of **18b** measured after stirring the samples in D_2O at RT (a) and at 80°C (b).

In order to check the stability of compounds **17b**-**20b** in the catalytic reaction mixture the desired amount of the catalyst was dissolved in a solution of deuterated water containing the formate/formic acid combination, which had been used in the catalytic studies. Ruthenium (**17b**) and osmium (**18b**) catalysts have been found to be not stable under catalytic conditions (80°C), as expected. At room temperature both samples are orange and ^{1}H NMR spectra do not indicate any difference in the catalyst signals as compared to the ^{1}H NMR spectra recorded in neat D_2O, even after 20 h. This indicates the absence of formate coordination to the metallic center. Nevertheless, after keeping the solution at 80°C during 20 h the samples turned black. ^{1}H NMR experiments with **17b** and **18b** confirm the decomposition of the catalysts (Figure 34 and Figure 35).

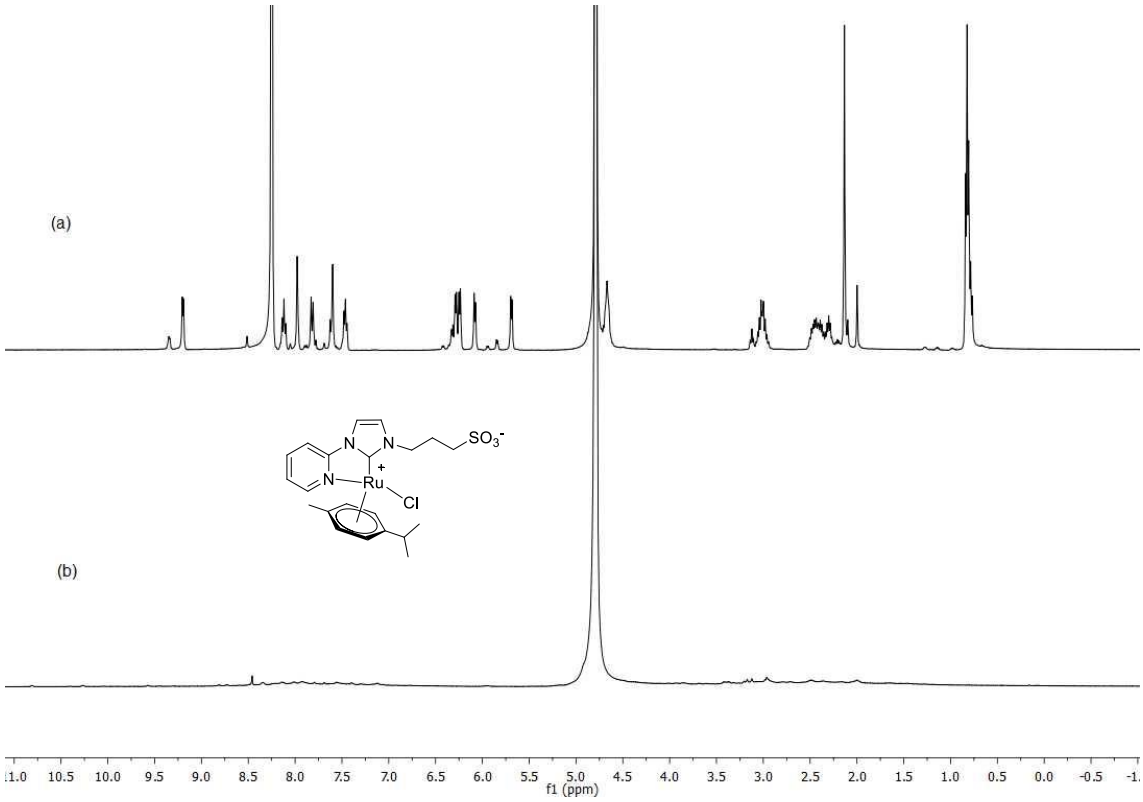

Figure 34. ^{1}H NMR spectra of **17b** measured after stirring the sample in HCO_2Na/HCO_2H aqueous solution at RT (a) and 80°C (b) for 20 h.

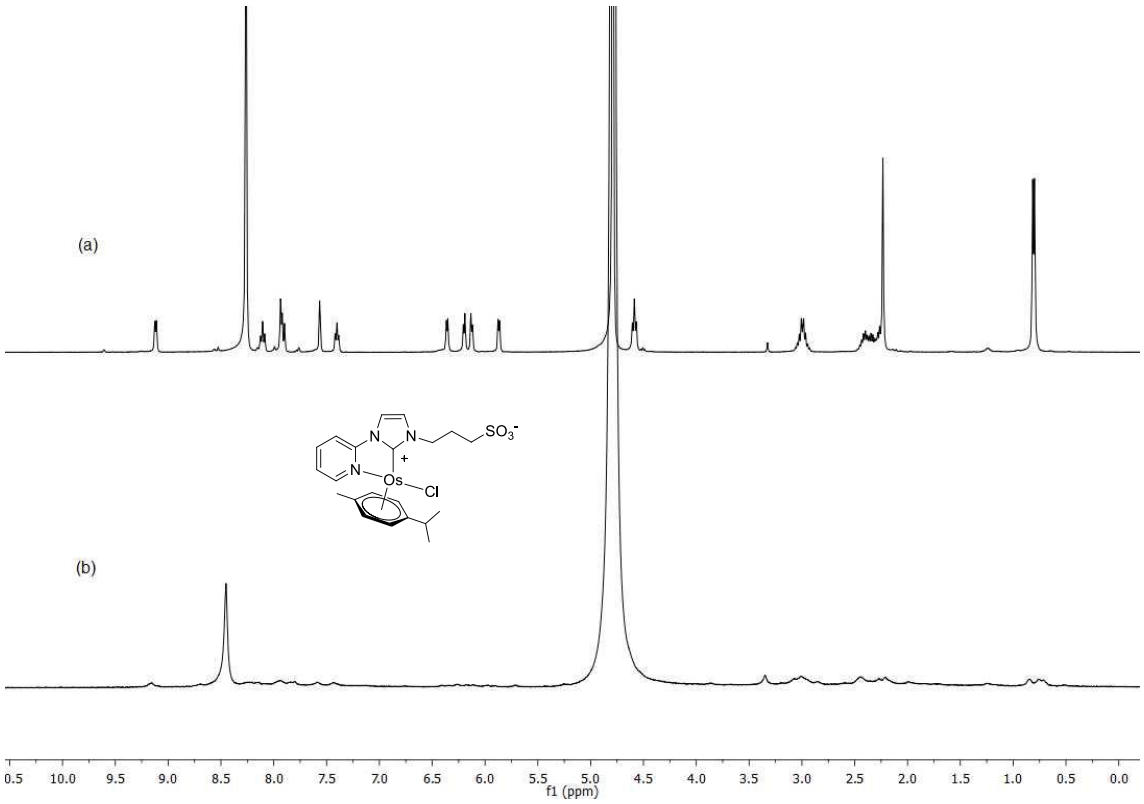

Figure 35. ^{1}H NMR spectra of **18b** measured after stirring the sample in HCO_2Na/HCO_2H aqueous solution at RT (a) and 80°C (b) for 20 h.

When **20b** is dissolved in the deuterated aqueous buffer solution at room temperature (yellow solution), more than one species can be detected by ^{1}H NMR. It shows the HCO_2H peak (at 8.25 ppm) and proton signals of the catalyst. Additionally, some new peaks suggest the formation of new species in the solution. These are very similar to those that correspond to **20b** but shifted to higher fields. When the sample is heated up to 80°C the solution did not undergo any color changes. ^{1}H NMR spectra reveal different species in the solution as those detected at room temperature and the HCO_2H peak disappears (Figure 36). This suggests that **20b** is active and it is able to decompose formic acid to H_2(g) and CO_2(g).

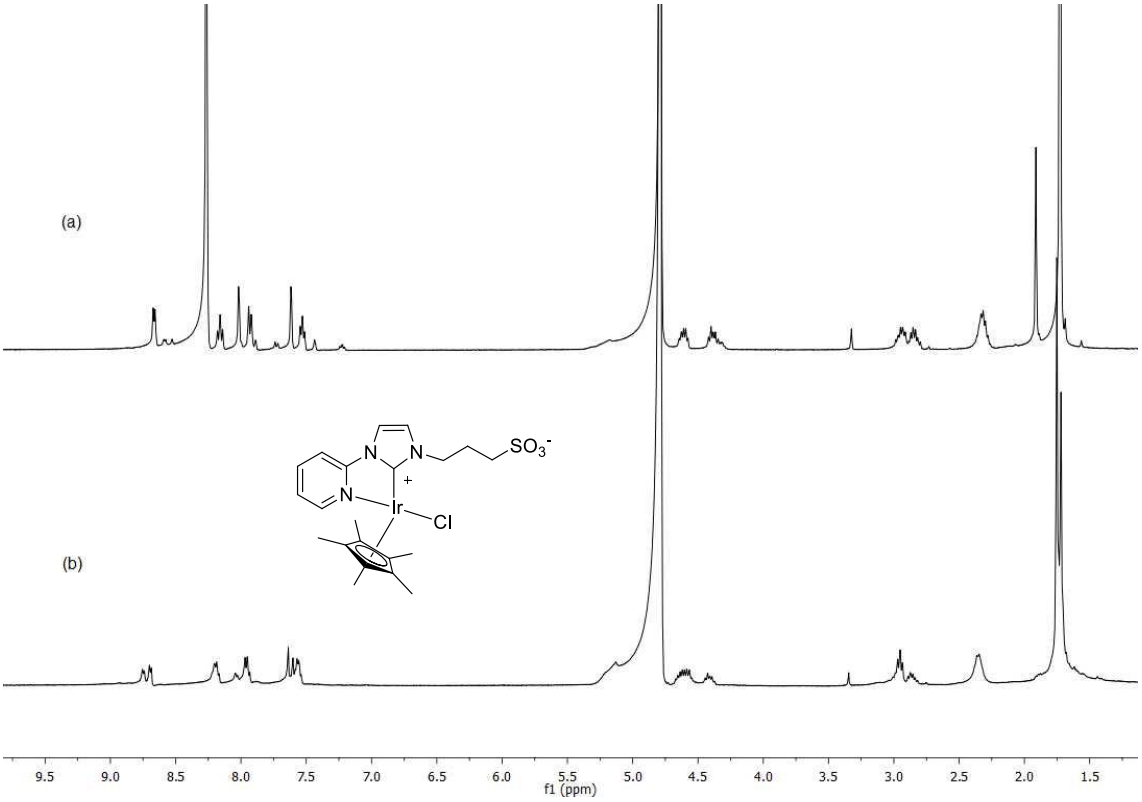

Figure 36. ^{1}H NMR spectra of **20b** measured after stirring the sample in HCO_2Na/HCO_2H aqueous solution at RT (a) and 80°C (b) for 7 h.

When the rhodium compound **19b**, which showed the highest catalytic activity is dissolved in aqueous buffer solution, its color changes from yellow to dark red and gas bubbles appear in the sample, suggesting that some modifications have taken place at the metallic center reacting HCO_2H with the catalyst. ^{1}H NMR spectra were recorded after stirring the sample, which contained complex **19b** and formate/formic acid buffer solution in D_2O, with 1:10 ratio (as in previous experiments) for 15 min at room temperature and at 80°C. At room temperature the HCO_2H peak appears with high intensity but the catalyst signals broaden, suggesting a different behavior in the reaction medium. When the sample is heated to 80°C the HCO_2H peak almost vanishes and the catalyst signals broaden even more, indicating that a paramagnetic species is formed (Figure 37). A series of ^{1}H NMR kinetic studies was executed in order to get a more detailed insight in in the catalytic process and involved active species.

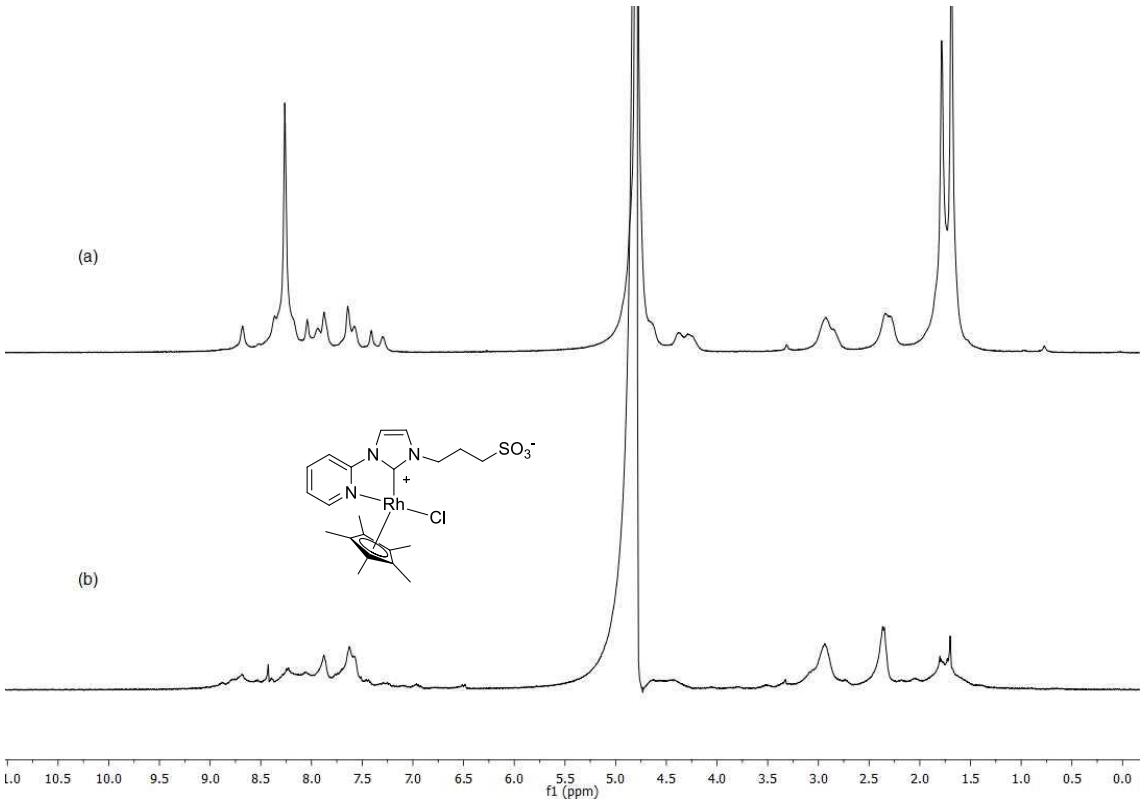

Figure 37. 1H NMR spectra of **19b** measured after stirring the sample in HCO_2Na/HCO_2H aqueous solution at RT (a) and 80°C (b) for 15 min.

A NMR tube containing the sample as described above was analyzed with ^1H NMR at 5°C in order to reduce the reaction rate. ^1H NMR spectra were recorded each 1.7 min (Figure 38). First measurements showed the characteristic peaks of HCO_2H and catalysts, but also new signals corresponding to the presence of different species in solution (as previously observed for room temperature experiments) appear (Figure 38 (a)). After 30 min, the NMR spectrum shows broad and poorly defined peaks which may be attributed to the new paramagnetic nature of the sample (Figure 38 (b)). During the next 30 min the sample appears to display more paramagnetism and the HCO_2H peak intensity decreases (Figure 38 (c)). At this point more buffer solution was added to the sample and the reaction was further monitored. As expected, the intensity of the formic acid peak increases and the sample gets diamagnetic again (proton peaks more defined) (Figure 38 (d)). Other proton signals could be detected with lower intensity, probably due to other species formed in solution. Nevertheless, with time the signals broaden again (Figure 38 (e)). This behavior of the catalyst agrees with the proposed mechanism (vide infra). According to this mechanism the paramagnetic species decomposes in the presence of formic acid yielding a diamagnetic intermediate catalyst (see next section).

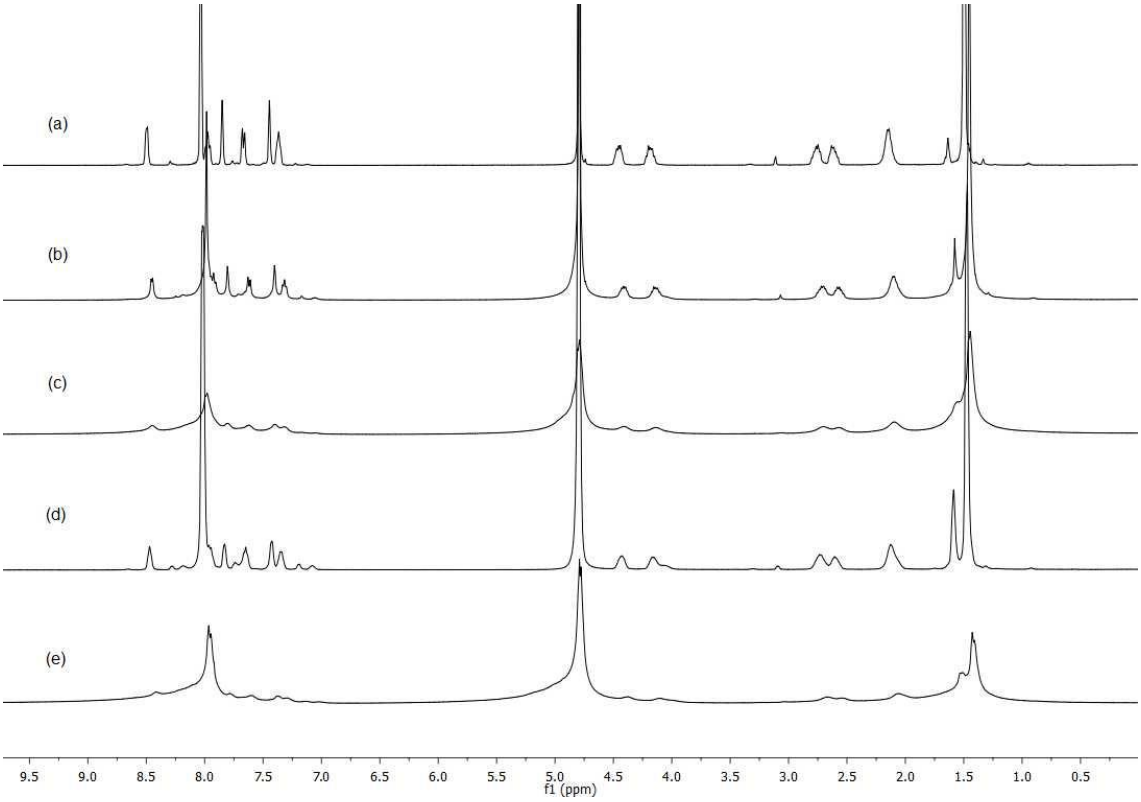

Figure 38. ^{1}H NMR spectra of **19b** measured at 5°C in HCO_2Na/HCO_2H aqueous solution after (a) 1.7 min, (b) 30 min, (c) 1 h, (d) addition of more HCO_2Na/HCO_2H solution, (e) 30 min after the latter addition.

3.2.2 Proposed mechanism

To the best of our knowledge, no detailed theoretical study of the transfer hydrogenation of ketones catalyzed by sulfonated NHC catalysts in aqueous solution has been published. For this reason, an *inner-sphere* mechanism (Scheme 23) for the transfer hydrogenation of acetophenone with the rhodium complex **19b** based on the above presented kinetic ^{1}H NMR experiments is proposed.

The Rhodium carbene catalyst **19b** catalyzes transfer hydrogenation reaction of acetophenone involving several elementary steps. Starting from the metal chloride complex **A** the first step consists of the displacement of the chloride by a formate molecule to form the metal alkoxide **B** and the picolyl group decoordinating from the metallic center to give a 16 e^- catalyst. Therefore, **B** generates the hydride intermediate **C** and release a CO_2(g) molecule by β-hydrogen elimination. At this point acetophenone attacks on the metal hydride intermediate **C** to form a new alkoxi intermediate (**D**), which regenerates species **B** by a proton transfer process leading to the formation of the desired hydrogenated product.

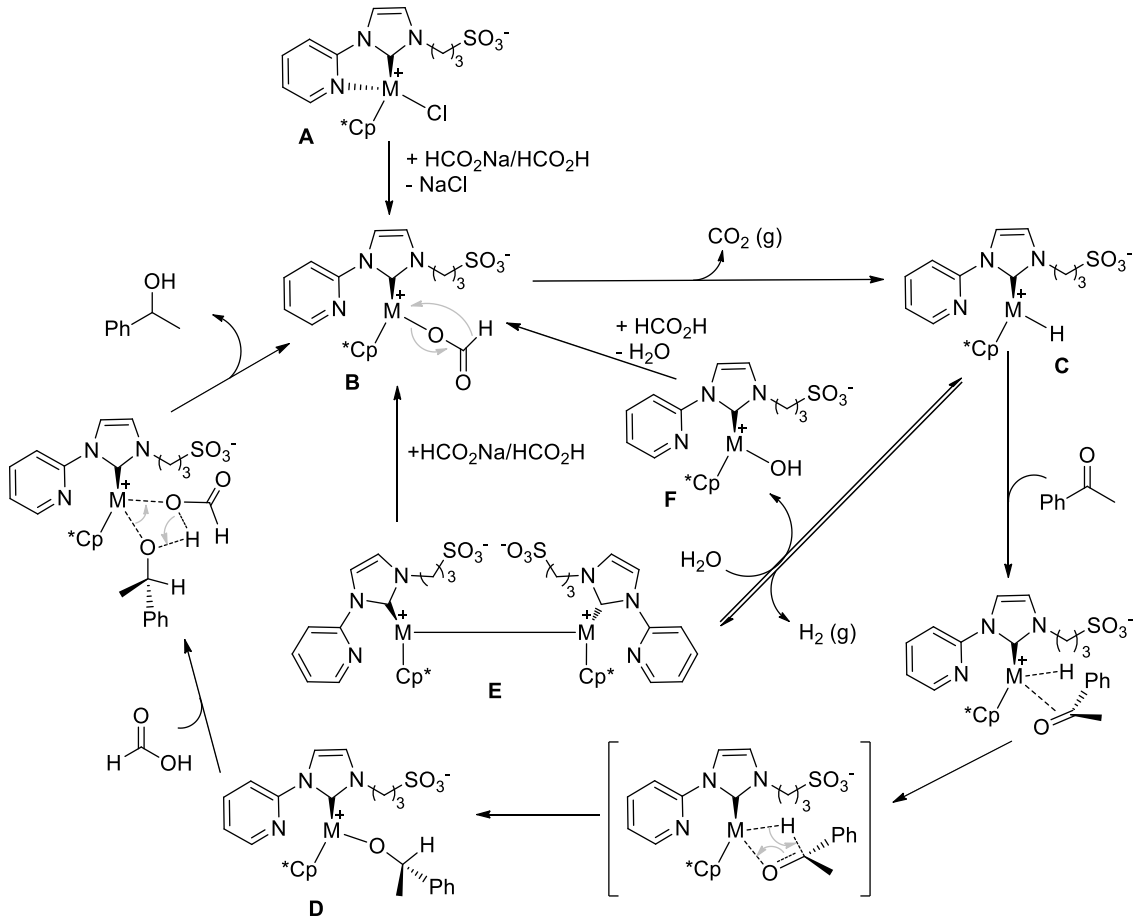

Scheme 23. Proposed inner-sphere mechanism for the transfer hydrogenation of acetophenone with Rhodium complex **19b**.

Although it appears that the hydrogenation transfer mechanism in water is similar to this in organic solvents, various studies have shown that water is not an innocent spectator. It may react with intermediates, transition states and hydrides or dihydrogen species, as well as it may participate in an acid base equilibrium with the catalyst[127]. In hydrogenation reactions water can act as a proton carrier facilitating protonation of substrates and catalysts or it can use its conjugate base to affect deprotonation[109]. A significant consequence of acid-base equilibrium is the pH effect on the rate of hydrogenation as already observed in the catalytic experiments described above (see Table 3). At very low pH, the hydride species can be protonated releasing H_2(g), and at high pH values, potential aqua complexes can be deprotonated resulting in an inactive hydroxo species as it has already been observed for other iridium catalysts[128].

Due to this reason and the observation of paramagnetic species in the reaction mixture, a parallel catalytic cycle, competing with the main catalytic route can be suggested. The already mentioned hydride species **C** can dimerize to form the dinuclear paramagnetic compound **E** by loss of H_2(g). **E** can also react further with formate molecules in solution to regenerate **B** species

or it can react with water molecules to form the hydroxy intermediate **F**. The formation of hydroxy species can slow down the catalysis by inhibiting the coordination of reactants, such as formate. However, a buffer solution with low pH maintains the pH value and facilitates the hydroxy group protonation due to the presence of an excess of protons in solution. Therefore, this new **F** species evolves to the active species **B** when HCO_2H molecules protonates the hydroxy ligand and further displaces the water molecule, which was formed by formate coordination to the rhodium metallic center.

3.3 Complete hydrogenation of acetophenone in water

Based on these literature studies and already having proved the reactivity in transfer hydrogenation reactions, the use of water-soluble 1-(2-pyridinyl)-3- sulfonatepropyl)imidazol-2-ylidene metal complexes has been tested for the complete hydrogenation of acetophenone in aqueous media.

3.3.1 First experiments in an autoclave system

Due to the observed activity of the above described water-soluble catalysts in transfer hydrogenation reactions it was decided to explore their potential for the complete hydrogenation of acetophenone. In order to hydrogenate the aromatic ring, more rigorous reaction conditions are required. The reactions were therefore carried out in an autoclave system using H_2(g) as hydrogen source. It is noteworthy that hydrogen has a lower solubility in water (0.81 mM at 20°C) than in common organic solvents and implies diffusion control if the reaction occurs in the organic phase.[109] The catalytic studies were restricted to complexes **17b**-**20b** since catalysts **17a**-**20a** display very low solubility in water (namely 1.55 mg/ml for complex **17a**). Acetophenone was used as model substrate to examine the activity in hydrogenation reactions in aqueous media. It is well known that colloidal transition metal nanoparticles hydrogenate aromatic compounds in aqueous and organic solvents as well as under biphasic conditions[113], although there are not so many examples for homogeneous hydrogenation of oxygen-functionalized arenes utilizing monometallic complexes in aqueous phase.

First experiments were carried out by stirring an aliquot of a freshly prepared catalyst in basic solution (500 µL of 2 mM catalyst in 0.1 M KOH aqueous solution) with variable amounts of acetophenone. Samples were introduced in an autoclave system and purged three times with hydrogen. Different hydrogen pressures, temperatures and catalyst amounts were examined in order to optimize the catalytic reaction conditions (Table 4). After the catalytic run the organic compounds were extracted with $CDCl_3$ and further analyzed by ^{1}H NMR spectroscopy and gas chromatography.

Table 4. Optimization of reaction conditions for the hydrogenation of acetophenone with catalysts **17b**-**20b**.

Entry	Cat.	T (°C)	P (bar)	t (h)	Cat. (mol%)	Conversion (%)[a]	Yield (%)[a] B1	B2	C
1	19b	80	40	1	1	99	91	0	8
2	19b	80	40	2	1	100	9	0	91
3	19b	80	40	3	1	100	0	0	100
4	19b	80	20	3	1	99	21	0	78
5	19b	60	40	3	1	79	79	0	0
6	19b	80	40	3	0,4	100	19	0	81
7	17b	80	40	1	1	0	0	0	0
8	17b	80	40	2	1	5	4	0	1
9	17b	80	40	3	1	100	0	0	100
10	17b	80	20	3	1	100	19	0	81
11	17b	60	40	3	1	1	1	0	0
12	17b	80	40	3	0,4	2	2	0	0
13	20b	80	40	3	1	4	4	0	0
14	20b	80	40	4	1	10	10	0	0
15	20b	80	40	16	1	26	26	0	0
16	20b	80	40	24	1	100	100	0	0
17	18b	80	40	3	1	0	0	0	0
18	18b	80	40	4	1	0	0	0	0
19	18b	80	40	16	1	1	1	0	0
20	18b	80	40	24	1	100	100	0	0

[a] Yields and conversions are determined by using ^{1}H NMR and GC-MS measurements

According to literature[37] there are two different pathways for the hydrogenation of acetophenone to 1-cyclohexyl ethanol (Scheme 24). In the first pathway, the ketone can be initially reduced to 1-phenylethanol (**B1**) and then be further converted to **C** after addition of three molecules of hydrogen. The second possibility is that the aromatic ring is hydrogenated

and cyclohexyl methyl ketone (**B2**) can be identified as an intermediate whereas the ketone is further reduced to form the desired product (**C**).

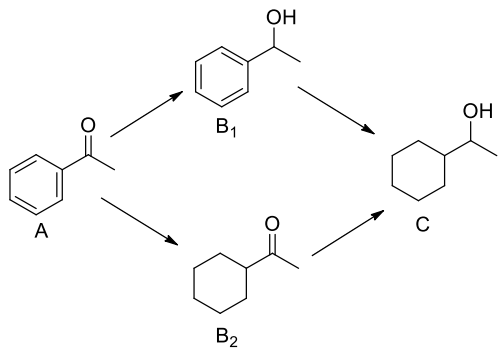

Scheme 24. Possible pathways in the hydrogenation of acetophenone.

Catalytic studies show no formation of species **B2** in the course of the hydrogenation process indicating that catalysts **17b**-**20b** are selectively reacting to 1-phenylethanol as implied by the first pathway. This result shows a distinct advantage of the presented catalyst as -compared to analogous water-soluble catalysts previously described in the literature – one pathway is clearly favored.[37]

A comparison of the catalytic performance with catalysts **17b**-**20b** in the hydrogenation of acetophenone is presented (Table 4). Ideal conditions utilizing 1 mol% of catalysts **17b** and **19b** were found by stirring the samples at 80°C and 40 bar H_2 pressure for 3 h (entries 3 and 9 in Table 4). However, the iridium **20b** and osmium **18b** complexes were found to be less active than catalysts **17b** and **19b**. When catalysis is executed under the same reaction conditions, these compounds need 24 h to completely hydrogenate the acetophenone. Therefore, the present study further focused on the hydrogenation reaction using Rhodium and Ruthenium catalysts. For both, **17b** and **19b**, when time, hydrogen pressure, temperature or amount of catalysts is decreased, the amount of the desired product also decreases. Both behave differently under identical catalytic conditions and the main differences can be observed when temperatures and times are varied. For both catalysts, an induction period is observed, lasting longer for the ruthenium compound indicating that the formation of the active species in the course of the catalytic reaction takes at least 2 h (Figure 39). Moreover, after catalysis and extraction of the organic compounds with chloroform, a black suspension was observed remaining in the aqueous phase (Figure 40). Therefore, reaction solutions were prepared (without the substrate) to activate the (pre-)catalysts. Thereby, exact catalytic reaction conditions were applied. The only difference was that no substrate was added.

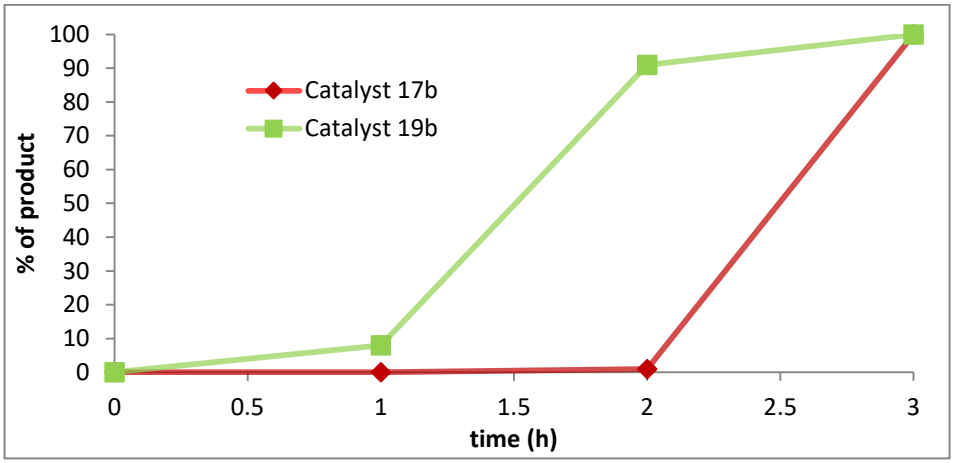

Figure 39. Plot of the conversion of acetophenone vs. time using catalysts **17b** and **19b**.

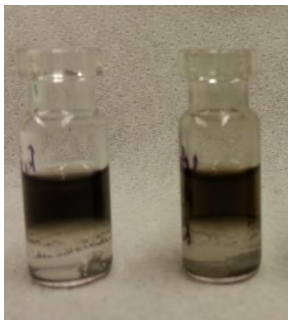

Figure 40. Black suspension observed after catalysis for **17b** (right) and **19b** (left).

3.3.2 Optimization of the catalysis for ruthenium and rhodium catalysts

After activation (3 h), the substrate was added to the solution containing the (activated) catalyst. The catalytic results obtained using these freshly prepared catalytic solutions (**17b** and **19b**) are presented in Table 5. When the activated catalysts are used, no induction period for the hydrogenation of acetophenone is observed supporting the assumption that the active species is already present in solution. When catalysis is carried out under the previously optimized conditions (40 bar H_2 pressure, 80°C and 1 mol% of catalyst), a quantitative yield of 1-cyclohexyl ethanol is detected in both cases after 2 h (entries 2 and 8 in Table 5). When catalyst **5b** is applied, the decrease of the catalyst concentration had a big influence on product formation (entry 5 in Table 5), followed by the influence of temperature (entry 4 in Table 5) obtaining only 69% and 78% of the product respectively. On the other hand, H_2 pressure appeared to have no major influence obtaining 95% of the desired product (entry 3 in Table 5). Nevertheless, it is observed that the Ruthenium catalyst is more active than its rhodium analogous. When time,

pressure and temperature are modified, a quantitative conversion of acetophenone is observed (entries 9, 10 and 14 in Table 5). In order to be able to compare both catalysts, the applied amount of catalyst is decreased to generate optimized conditions for Rh (80°C, 40 bar H_2 pressure and 2 h) to 0.4 mol% of catalyst. In this case too, complete conversion of the acetophenone to 1-cyclohexylethanol is observed (entry 11 in Table 5). However, when the load of catalyst is further decreased to 0.03 mol% of catalyst, the conversion drops to 60% (entries 15-18).

Table 5. Optimization of reaction conditions for the hydrogenation of acetophenone by **17b** and **19b** with previous preparation of the active NPs solution.

Entry	Cat.	T (°C)	P (bar)	t (h)	Cat. (mol%)	Conversion (%)[a]	Yield (%)[a] B1	B2	C
1	19b	80	40	1	1	100	3	5	92
2	19b	80	40	2	1	100	0	0	100
3	19b	80	20	2	1	100	1	3	95
4	19b	60	40	2	1	97	13	5	78
5	19b	80	40	2	0,4	94	23	2	69
6	19b	80	20	2	0,4	98	18	24	56
7	19b	60	40	2	0,4	94	40	25	29
8	17b	80	40	2	1	100	0	0	100
9	17b	60	40	2	1	100	0	0	100
10	17b	80	20	2	1	100	0	0	100
11	17b	80	40	2	0,4	100	0	0	100
12	17b	80	20	2	0,4	100	0	0	100
13	17b	60	40	2	0,4	100	0	0	100
14	17b	80	40	1	1	100	0	0	100
15	17b	80	40	2	0,2	100	1	1	98
16	17b	80	40	2	0,1	100	7	17	75
17	17b	80	40	2	0,05	90	41	31	19
18	17b	80	40	2	0,03	59	31	21	7

[a] Yields and conversions are determined by using ^{1}H NMR and GC-MS measurements.

3.3.3 Characterization of the active species in catalysis

In order to determine the nature of the catalytically active species two 2 mM basic solutions of complexes **17b** and **19b** were hydrogenated under the above-mentioned conditions (80°C, 40 bar H_2 pressure) for 3 h (see experimental section). The potential formation of rhodium and ruthenium nanoparticles was examined by means of TEM measurements. For this propose the obtained black suspensions were centrifuged and washed with bidistilled water in order to avoid the presence of base in the suspension. Figure 41 confirms the formation of ruthenium and rhodium nanoparticles with sizes between 2.6-2.9 nm in case of Ru and 2.2 - 2.5 nm for Rh.

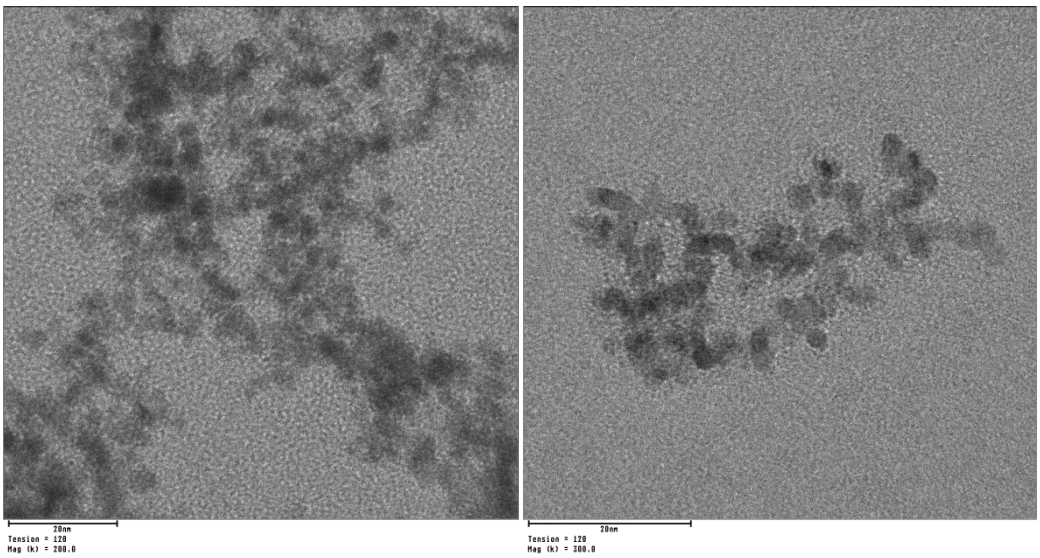

Figure 41. TEM micrographs of the active Ru (left) and Rh (right) solution after 3 h reaction time.

Based on these observations it can be concluded that complexes **17b** and **19b** are able to completely hydrogenate acetophenone in short reaction times (2 h) by activating the pre-catalyst for 3 h. It must be emphasized that this catalytic system provides higher yields and shorter reaction times as previously published studies. Our research group[37] had presented the hydrogenation of acetophenone with a ruthenium complex bearing a bidentate chelating sulfonated NHC-ligand before. This system is also able to hydrogenate acetophenone in 2 h. However, a distinct drawback was that the conversion of acetophenone was not complete. The maximal conversion to the desired hydrogenated product (77% yield) was obtained using 1 mol% of the catalyst at 40 bar H_2 pressure, 60°C and 16 h under the same conditions to prepare the pre-formed catalyst solution. The best catalyst presented in this study shows some significant advantages, namely shorter time periods for both preparation of the active species in catalysis and the catalysis itself. Additionally, lower catalyst loadings are possible (only 0.4 mol% of catalyst necessary in the case of **17b**). On the other hand, a molecular mechanism

for the catalysis was suggested, while in the case described in this work, nanoparticles are clearly the active species for both, Ru and Rh. In contrast to the non-activated compounds (Table 4), **B2** can be observed as intermediate (Table 5), for some catalysts. This fact raises the question if the mechanism is always taking the road over intermediate **B1**. Further detailed investigations of the mechanism for different metals and ligands are necessary to explain the formation of **B2** and **B1** in the course of the catalytic reaction.

4 Conclusion and outlook

In this research work a description of different ligands and metal precursors is given, based on previously reported synthetic procedures with the exception of sulfonated imidazolium ligands. They present slightly modified procedures, which exhibits some advantages to the already published, like reduced reaction time and reduced amounts of hazardous reagents.

With some of these new ligands and metal precursors, a series of silver, ruthenium, osmium, rhodium and iridium, with chelating, functionalized NHC ligands (Figure 42), have been synthesized and characterized by NMR spectroscopy, X-ray diffraction crystallography, mass spectrometry and elemental analysis. The X-ray crystal structures of seven novel complexes (**16a/b**, **18b**, **19a/b** and **20a/b**) have been determined, among them the first osmium, rhodium and iridium monocarbene complexes bearing sulfonated groups.

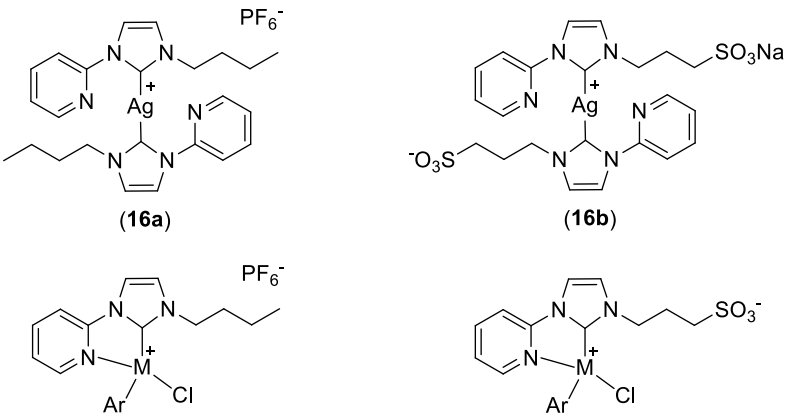

Figure 42. New synthesized pyridine-functionalized NHC complexes.

The non-sulfonated compounds (**17a**–**20a**) exhibit very good solubility in organic solvents, but not in water. The sulfonated derivatives (**17b**–**20b**) are highly soluble in water, but insoluble in most organic solvents, making them ideal candidates for a rather simple work-up in two-phase catalysis. All complexes are active in the catalytic hydrogenation of acetophenone as a model substrate. The water-insoluble compounds (**17a**–**20a**) catalyze this reaction under inert conditions in isopropanol, while their water-soluble analogous (**17b**–**20b**) are able to hydrogenate the substrate in a HCOONa/HCOOH aqueous solution in air. The rhodium-based compound **19b** shows the highest activity. Additionally, complexes **17b** (Ru) and **19b** (Rh) were also able to hydrogenate the aromatic ring of acetophenone. Both compounds display an induction period of 3 h. However, this period can be avoided by activating the pre-catalysts in

aqueous solution. In this reaction, the ruthenium complex is more active than its rhodium analogue. For both catalytic reactions, higher conversions with lower catalyst loadings are obtained as compared to literature-known complexes.

In this work, the importance and advantages of the development of aqueous hydrogenation reactions when compared to the analogous systems developed in organic systems is presented. These advantages are not only related to the intrinsic convenience of using water as solvent (abundant, cheap, non-toxic, easy to handle without health hazards, etc.), or because of the contribution to a more sustainable and "greener" chemistry. The opportunity of working in a biphasic system offers big facilitations in experimental workup.

With respect to catalytic transfer hydrogenation of ketones, huge improvements have been achieved in this work. For example, when water-soluble catalyst **19b** is applied under the optimized conditions, 96% yield of the hydrogenated product is obtained after only 10 min reaction time. This means an enormous performance improvement when comparing to the Rh water-insoluble analogous catalyst, which achieved only 89% after 3 h reaction time in transfer hydrogenation.

An extension of the designed new presented catalysts to other metals, such as cobalt, palladium, iron or nickel should be investigated. Other synthetic routes to access a broader range of ligands are also of interest. This could be of great significance for further studies of the catalytic possibilities with these complexes and further application in industry. More specifically, a detailed study of the catalytically active species in solution, e.g. using DFT calculations, for transfer hydrogenation reactions should be explored. In case of aqueous hydrogenation reactions, it would be quite important to learn more about formation and recyclability possibilities of the synthesized NPs, since they are the active species in the catalysis. That involves a more precise study of the morphology, size, surface characteristics, possible agglomeration and, in that case, their stabilization.

Hydrogenation reactions are widely used in industry, as for example in electronic industry, metallurgical applications, fertilizer production, oil and fat hydrogenation, petroleum processing and petrochemical production. Focusing on, e.g. a greener way of energy production, the use of lignin has become a more sustainable alternative to petrochemical fossil resources. It is the major aromatic resource of the bio-based economy where a wide variety of bulk and fine chemicals can potentially be obtained. Having in mind such applications, the extension of the presented study would definitely yield to significant advances for the improvement of homogeneous or "semi-heterogeneous" catalysis in industry.

A. Annex

A.1 Experimental methods

A.1.1 General remarks

All reactions were performed under argon atmosphere using standard Schlenk techniques. Unless stated otherwise, reagents and solvents were used as received from commercial sources. Methanol was distilled under argon atmosphere over magnesium turnings.

A.1.2 Analytical methods

- **NMR spectroscopy**

NMR spectra were recorded with a Bruker Avance DPX-400 NMR spectrometer at the following mesearument frequencies: ^{1}H 400.13 MHz, ^{13}C 100.61 MHz. Chemical shifts are reported in ppm and were referenced to the residual solvent signals: $CDCl_3$ (δH = 7.26 ppm, δC = 77.16 ppm), D_2O (δH = 4.79 ppm), MeOD-*d*4 (δH = 3.31 ppm, δC = 49.00 ppm) and DMSO-d_6 (δH = 2.50 ppm, δC = 39.52 ppm) and using as internal standard MeOH (δH = 3.34 ppm, δC = 49.50 ppm) in D_2O. Signal multiplicities are given as s (singlet), d (doublet), dd(doublet of doublets), ddd(doublet of doublet of doublets), t (triplet), dt (doublet of triplets), q (quartet), p (pentet), br (broad signal), m (multiplet). Assignments of proton and carbon signals were confirmed by two-dimensional NMR spectroscopy (COSY and HMQC).

- **GC-MS measurements**

Catalytic runs were monitored by using GC methods on a Hewlett-Packard HP 6890 Series GC System equipped with a FID and using Standard ChemStation G1701AA Version A.03.00 as software.

- **Mass spectrometry**

FAB mass spectra were recorded on a MAT 90 mass spectrometer from Finnigan MAT, 3-nitrobenzylalcohol was used as the matrix substance and xenon was used as the ionization gas with ionization energy of 70 eV.

- **Elemental analysis**

Elemental analyses were performed in the Technische Universität München Microanalytical laboratory.

- **TEM measurements**

Freshly prepared analyte solutions were adsorbed for 5 min on previously hydrophilized plasma sample carrier (Quantifoil Multi A holey films plus 2 nm carbon). Excess solution was removed with a cloth. Electron micrographs were then taken at a magnification of 100,000 with a JEOL JEM 100CX at a voltage of 100 kV. The images were digitized at a resolution of 3000 dpi using a FlexTight Precision II scanner from Hassleblad. The pixel size was determined to be 0.85*. The recordings were then edited with the Macbiophotonics ImageJ Paket.

- **X-Ray analysis**

Crystallographic measurements and structural refinements were carried out by Dr. Alexander Pöthig and Marlene Kaposi.

A.1.3 Synthesis of catalysts

Ligand precursors

2-(imidazole-1-yl)pyridine (**1**) (MW = 145.16 g/mol)[59]

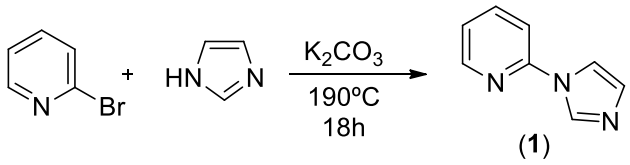

A mixture of H-imidazole (10.61 g, 155.8 mmol, 3.0 equiv.), 2-bromopyridine (5.0 mL, 8.20 g, 51.9 mmol, 1.0 equiv.) and K_2CO_3 (14.35 g, 103.8 mmol, 2.0 equiv.) is degassed, put under Argon, heated neat at 190°C and stirred at the desired temperature for 18 h. After cooling to room temperature the solid is dissolved in 40 mL H_2O and the aqueous solution is extracted with $CHCl_3$ (4x, 30 mL). The combined organic phases are washed with water (2x, 30 mL) and saturated aqueous Na_2CO_3-solution (1x, 30 mL). After removing the solvent under reduced pressure and drying under vacuum the product is obtained as an off-white solid (7.08 g, 49.78 mmol, 94%).

^{1}H NMR (400MHz, $CDCl_3$): δ (ppm) = 8.50 – 8.47 (m, 2H, NC*H*N, $C_{Py,ortho}H$), 7.83 (m, 1H, $N_{Py}CHC_{Py,meta}H$), 7.67 (s, 1H, $C_{im}H$), 7.41 (d, 1H, J = 8.2 Hz, $N_{im}CC_{Py,meta}H$), 7.26 – 7.22 (m, 1H, $C_{Py,para}H$), 7.21 (s, 1H, $C_{im}H$).

^{13}C NMR (101 MHz, $CDCl_3$): δ (ppm) = 149.31 ($C_{Py,ortho}$H), 149.06 ($N_{Py}C_{Py,ortho}N_{im}$), 139.02 ($N_{Py}CHC_{Py,meta}$H), 135.04 (N*C*HN),130.15(C_{im}), 122.31($C_{Py,para}$), 116.37(C_{im}), 112.59($N_{im}CC_{Py,meta}$H).

Bis(imidazol-1-yl)methane (**2**) (MW = 148.17 g/mol)[60,61]

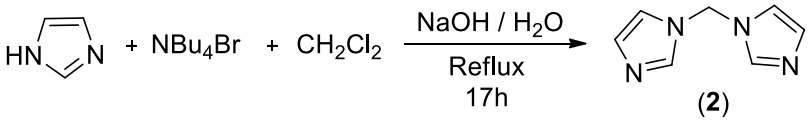

H-Imidazole (6.06 g, 89.0 mmol, 1 equiv.) and NBu_4Br (0.85 g, 2.64 mmol, 0.03 equiv.) are dissolved in 120 mL CH_2Cl_2 and 120 mL of NaOH-aqueous solution (45%). The resulting two-phase mixture is stirred and heated under reflux for 17 h. After cooling the sample to room temperature, the phases are separated and the aqueous phase is extracted with CH_2Cl_2. The combined organic phases are dried with $MgSO_4$ and filtered. The product (dried under vacuum) is obtained as a white solid (2.03 g, 13.71 mmol, 31%).

^{1}H NMR (400 MHz, DMSO-d_6): δ (ppm) = 7.91 (s, 2H, NC*H*N), 7.31 (s, 2H, C_{im}*H*), 6.91 (s, 2H, C_{im}*H*), 6.17 (s, 2H, NCH_2N).

^{13}C NMR (101 MHz, DMSO-d_6)**:** δ (ppm) = 138.24 (N*C*HN), 129.95 (C_{im}), 120.39 (C_{im}), 56.19 (N*C*H_2N).

Bis(1,2,4-triazol-1-yl)methan (**3**) (MW = 150.14 g/mol)[62]

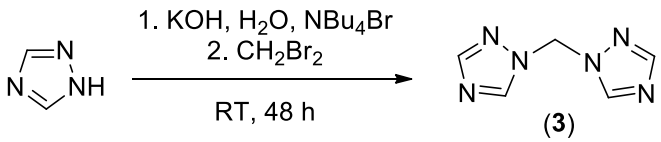

1,2,4-triazole (2.76 g, 40.0 mmol, 1equiv.), NBu_4Br (0.39 g, 1.20 mmol, 0.03 equiv.) and KOH (4.52 g, 80.0 mmol, 2 equiv.) are added to 0.3 mL of H_2O. The resulting mixture is stirred at room temperature for 1 h. Then, CH_2Br_2 is added and the resulting mixture is stirred at room temperature for 48 h. Afterwards, the mixture is extracted with CH_2Cl_2 (4x, 15 mL). The combined organic phases are dried with $MgSO_4$, filtered and dried under vacuum. The product is obtained as a white solid (1.05 g, 7 mmol, 35%).

^{1}H NMR (400 MHz, DMSO-d_6): δ (ppm) = 8.86 (s, 2H, C_{Tr}*H*), 8.04 (s, 2 H, C_{Tr}*H*), 6.67 (s, 2 H, NCH_2N).

^{13}C NMR (101 MHz, DMSO-d_6)**:** δ (ppm) = 152.43 (C_{Tr}), 145.24 (C_{Tr}), 59.06 (N*C*H_2N).

2,6-Bis(imidazol-1-yl)pyridine (**4**) (MW = 211.22 g/mol)[59]

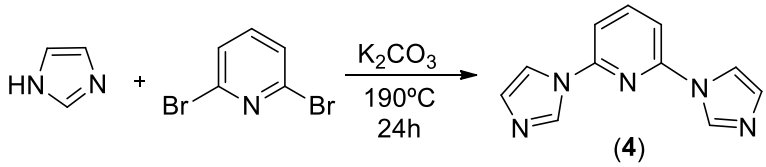

A mixture of H-imidazole (4.08 g, 60.0 mmol, 6.0 equiv.), 2,6-bromopyridine (2.37 g, 10.0 mmol, 1.0 equiv.) and K_2CO_3 (5.53 g, 40.0 mmol, 4.0 equiv.) are put under vacuum. The neat mixture is heated at 190°C for 24 h. After cooling to room temperature the solid was suspended in 150 mL $CHCl_3$. The organic phase was extracted with saturated aqueous $NaHCO_3$-solution (3x, 80 mL) and the combined aqueous phases are extracted with $CHCl_3$ (2x, 40 mL). The combined organic phases were dried with $MgSO_4$. After removing the solvent under reduced pressure and drying under vacuum, the produc is obtained as an off-white solid (2.05 g, 9.7 mmol, 97%).

^{1}H NMR (400 MHz, $CDCl_3$): δ (ppm) = 8.39 (s, 2H, NC*H*N), 7.98 (t, 1H, *J* = 8.0 Hz, $C_{Py,para}H$), 7.68 (t, 2H, *J* = 1.2 Hz, $C_{im}H$), 7.30 (d, 2H, *J* = 8 Hz, $C_{Py,meta}H$), 7.24 (s, 2H, $C_{im}H$).

^{13}C NMR (101 MHz, $CDCl_3$): δ (ppm) = 148.55 ($C_{Py,ortho}$), 142.26 ($C_{Py,para}$), 135.14 (NCHN), 131.30 (C_{im}), 116.26 (C_{im}), 109.79 ($C_{Py,meta}$).

Non-sulfonated imidazolium salts

2-(Imidazole-1-yl-3-n-butyl)pyridine (**5**) (MW = 282.19 g/mol)[46]

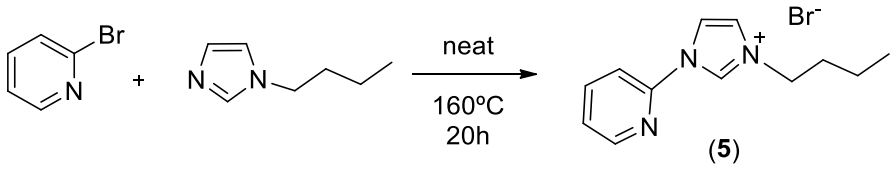

A mixture of 1-butylimidazole (3.18 mL, 3.00 g, 24.16 mmol, 1.0 equiv.) and 2-bromopyridine (2.36 mL, 3.82 g, 24.16 mmol, 1.0 equiv.) are heated at 160°C for 20 h. After cooling to room temperature the mixture is dissolved in 20 mL of CH_2Cl_2 and Et_2O is added to precipitate a brown solid. The liquid is decanted and the solid re-dissolved in CH_2Cl_2 and re-precipitated and washed with pentane. After drying under vacuum the product is isolated as a brown solid (0.68 g, 2.4 mmol, 10%).

^{1}H NMR (400 MHz, $CDCl_3$): δ (ppm) = 11.88 (s, 1H, NC*H*N), 8.63 (d, 1H, *J* = 8.3 Hz, $C_{Py,ortho}H$), 8.52 – 8.48 (m, 1H, $N_{im}CC_{Py,meta}H$), 8.32 (t, 1H, *J* = 1.7 Hz, $C_{im}H$), 8.05 (td, 1H, *J* = 8.1, 1.8 Hz, $N_{py}CHC_{Py,meta}H$), 7.47 (t, 1H, *J* = 1.7 Hz, $C_{im}H$), 7.45 (dd, 1H, *J* = 7.5, 4.9 Hz, $C_{Py,para}H$), 4.57 (t, 2H, *J* = 7.4 Hz, NCH_2CH_2), 2.05 – 1.97 (m, 2H, $NCH_2CH_2CH_2$), 1.50 – 1.40 (m, 2H, $CH_2CH_2CH_3$), 0.99 (t, 3H, *J* = 7.4 Hz, $CH_2CH_2CH_3$).

^{13}C NMR (101 MHz, $CDCl_3$): δ (ppm) = 149.99 ($N_{Py}CC_{Py,meta}H$), 146.06 ($N_{Py}C_{Py,ortho}N_{im}$), 140.86 ($N_{Py}CHC_{Py,meta}H$), 136.26 (N*C*HN), 125.28 ($C_{Py,para}$), 121.97 (C_{im}), 118.91 (C_{im}), 115.35 ($C_{Py,ortho}H$), 50.57 (NCH_2CH_2), 32.30 ($NCH_2CH_2CH_2$), 19.63 ($CH_2CH_2CH_3$), 13.61 ($CH_2CH_2CH_3$).

2,6-Bis(imidazol-1-yl-3-n-butyl)pyridine (**6**) (MW = 485.27 g/mol)[46]

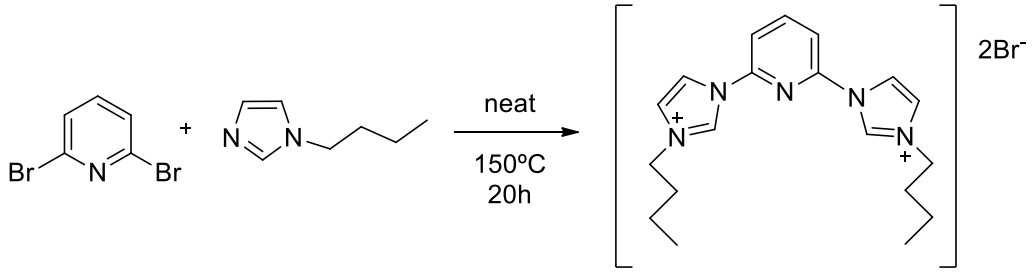

(**6**)

A mixture of 1-butylimidazole (3.55 mL, 3.36 g, 27.0 mmol, 4.0 equiv.) and 2,6-dibromopyridine (1.60 g, 6.75 mmol, 1.0 equiv.) is heated neat at 150°C for 20 h. After cooling to room temperature the mixture is dissolved in 25 mL $CHCl_3$ and Et_2O is added to precipitate a grey solid. The liquid is decanted and the solid re-dissolved in $CHCl_3$ and re-precipitated with Et_2O. The liquid is again decanted and the solid is now dissolved in MeOH and precipitated with Et_2O. After drying under vacuum the product is isolated as a grey solid (2.28 g, 4.7 mmol, 70%).

^{1}H NMR (400 MHz, $CDCl_3$): δ (ppm) = 12.01 (s, 2H, NC*H*N), 9.30 (s, 2H, $C_{im}H$), 8.81 (d, 2H, *J* = 7.9 Hz, $C_{Py,meta}H$), 8.27 (t, 1H, *J* = 8.1 Hz, $C_{Py,para}H$), 7.49 (s, 2H, $C_{im}H$), 4.61 (t, 4H, *J* = 7.2 Hz, NCH_2CH_2), 2.00 (p, 4H, *J* = 7.5 Hz, $NCH_2CH_2CH_2$), 1.46 (h, 4H, *J* = 7.7 Hz, $CH_2CH_2CH_3$), 1.00 (t, 6H, *J* = 7.4 Hz, $CH_2CH_2CH_3$).

^{13}C NMR (101 MHz, $CDCl_3$): δ (ppm) = 145.42 ($C_{Py,para}$), 145.36 ($C_{Py,ortho}$), 136.89 (N*C*HN), 123.07 (C_{im}), 121.04 (C_{im}), 115.60 ($C_{Py,meta}$), 50.70 (NCH_2CH_2), 32.33 ($NCH_2CH_2CH_2$), 19.59 ($CH_2CH_2CH_3$), 13.60 ($H_2CH_2CH_3$).

Bis(imidazol-1-yl-3-butyl)methane dibromide (**7**) (MW = 422.21 g/mol)[129, 63]

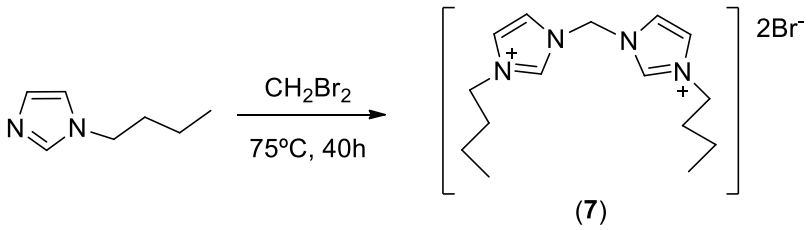

(**7**)

1-butylimidazole (3 mL, 2.83 g, 22.8 mmol, 1.0 equiv.) is dissolved in dibromomethane (10 mL, 24.8 g, 142.5 mmol, 6.24 equiv.). The mixture is stirred at 75°C for 40 h. After cooling to room temperature, the solvent is removed and the resulting solid is washed with THF. The obtained white solid is dried under vacuum (4.53 g, 10.7 mmol, 94%).

^{1}H NMR (400 MHz, DMSO-d_6): δ (ppm) = 9.75 (s, 2H, NC*H*N), 8.18 (s, 2H, $C_{im}H$), 7.95 (s, 2H, $C_{im}H$), 6.78 (s, 2H, NCH_2N), 4.24 (t, 4H, *J* = 7.2 Hz, NCH_2CH$_2$), 1.79 (p, 4H, *J* = 7.5 Hz, NCH$_2$CH_2CH$_2$), 1.28 (h, 4H, *J* = 7.4 Hz, CH$_2$CH_2CH$_3$), 0.90 (t, 6H, *J* = 7.4 Hz, CH$_2$CH$_2$CH_3).

^{13}C NMR (101 MHz, DMSO-d_6): δ (ppm) = 137.51 (N*C*HN), 123.08 (C_{im}), 122.13 (C_{im}), 57.93 (N*C*H$_2$N), 49.02 (N*C*H$_2$CH$_2$), 31.03 (NCH$_2$*C*H$_2$CH$_2$), 18.75 (CH$_2$*C*H$_2$CH$_3$), 13.31 (CH$_2$*C*H$_3$).

Sulfonated imidazolium salts

1-Methylimidazolium-3-propylsulfonate (**8**) (MW = 204.25 g/mol)[33, 35]

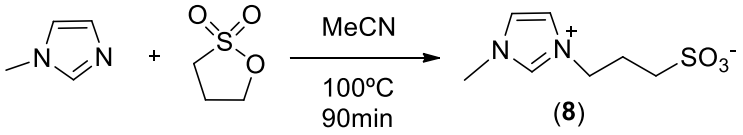

1-Methylimidazole (0.50 g, 6.09 mmol, 1.0 equiv.) and 1,3-Propansultone are dissolved in 10 mL MeCN in a pressure tube for 90 min at 100°C. After the solution is cooled to room temperature, a white precipitate is formed. The solid is decanted and washed with MeCN (2x, 20 mL) and Et$_2$O (2x, 20 mL) and dried under vacuum. The product is obtained as a white solid (1.053 g, 5.15 mmol, 85%).

^{1}H NMR (400 MHz, D$_2$O): δ (ppm) = 8.76 (s, 1H, NC*H*N), 7.50 (s, 1H, CH_{Im}), 7.45 (s, 1H, CH_{Im}), 4.37 (t, 2H, *J* = 7.1 Hz, CH$_2$CH_2SO$_3$), 3.90 (s, 3H, NCH_3), 2.93 (m, 2H, NCH_2CH$_2$), 2.32 (m, 2H, CH$_2$CH_2CH$_2$).

2-(imidazole-1-yl-3-propylsulfonate)pyridine (**9**) (MW = 267.30 g/mol)[34]

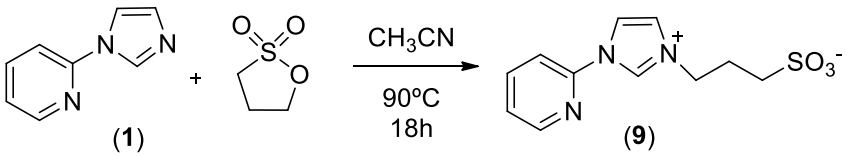

2-(imidazole-1-yl)pyridine (**1**) (1.79 g, 12.33 mmol, 1.0 equiv.) and 1,3-propanesultone (2.16 mL, 3.01 g, 24.66 mmol, 2.0 equiv.) are dissolved in 20 mL acetonitrile and heated at 90°C for 18 h in a pressure tube. After cooling to room temperature the solvent is decanted and the solid is washed with MeCN (2x, 20 mL) and Et$_2$O (6x, 20 mL). The product is dried under vacuum and isolated as a white solid (3.22 g, 12.04 mmol, 98%).

^{1}H NMR (400 MHz, D$_2$O): δ (ppm) = 9.63 (s, 1H, NC*H*N), 8.58 (d, 1H, *J* = 4.4 Hz, $C_{Py,ortho}H$), 8.20 – 8.09 (m, 2H, $C_{im}H$, $N_{Py}CHC_{Py,meta}H$), 7.83 – 7.76 (m, 2H, $N_{im}CC_{Py,meta}H$, $C_{im}H$), 7.62 (dd, 1H, *J* = 7.5, 5.0 Hz, $C_{Py,para}H$), 4.53 (t, 2H, *J* = 7.1 Hz, NCH_2CH$_2$), 3.00 (t, 2H, *J* = 7.3 Hz, CH$_2$CH_2SO$_3$), 2.42 (p, 2H, *J* = 7.2 Hz, CH$_2$CH_2CH$_2$).

^{13}C NMR (101 MHz, D_2O): δ 149.25 ($C_{Py,ortho}H$), 146.25 ($N_{Py}C_{Py,ortho}N_{im}$), 140.96 ($C_{Py,para}$), 125.55 ($N_{Py}CHC_{Py,meta}H$), 123.26 (C_{im}), 120.01 (C_{im}), 114.99 ($N_{im}CC_{Py,meta}H$), 48.52 (NCH_2CH_2), 47.22 ($CH_2CH_2SO_3$), 25.00 ($CH_2CH_2CH_2$).

Bis(imidazol-1-yl-3-propylsulfonate)methane (**10**) (MW = 392.45 g/mol)[33, 64]

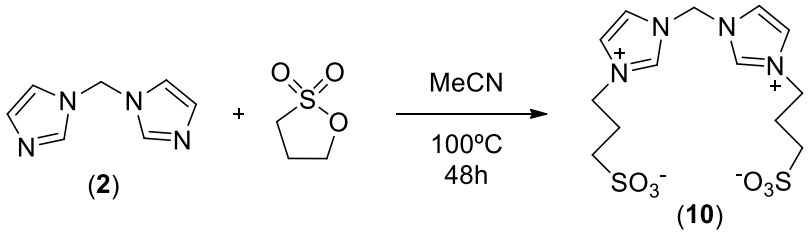

Bis(imidazol-1-yl)methane (**2**) (1.55 g, 10.5 mmol, 1 equiv.) and 1,3-propanesultone (6 mL, 8.35 g, 68.4 mmol, 6.5 equiv.) are disolved in 10 mL MeCN. The resulting mixture is stirred at 100°C in a pressure tube for 48 h. After cooling to room temperature, the solvent is removed and the resulting white solid is washed with MeCN (2x, 10 mL) and Et2O (3x, 10 mL) and dried under vacuum (3.68 g, 9.38 mmol, 89%).

^{1}H NMR (400 MHz, D_2O): δ (ppm) = 7.82 (s, 2H, $C_{im}H$), 7.72 (s, 2H, $C_{im}H$), 6.72 (s, 2H, NCH_2N), 4.45 (t, 4H, J = 7.1 Hz, NCH_2CH_2), 2.96 (t, 4H, J = 7.2 Hz, $CH_2CH_2SO_3$), 2.36 (p, 4H, J = 7.2 Hz, $CH_2CH_2CH_2$).

^{13}C NMR (101 MHz, D_2O): δ (ppm) = 124.01 (C_{im}), 122.47 (C_{im}), 59.17 (NCH_2N), 48.74 (NCH_2CH_2), 47.41 ($CH_2CH_2SO_3$), 25.02 ($CH_2CH_2CH_2$).

2,6-Bis(imidazol-1-yl-3-propylsulfonate)pyridine (**11**) (MW = 455.51 g/mol)[33]

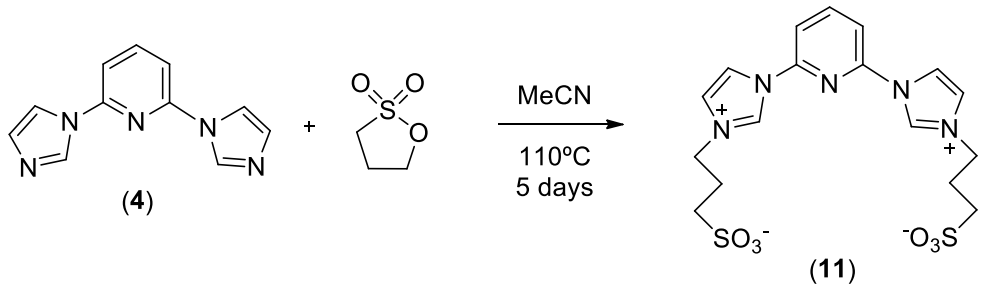

2,6-Bis(imidazole-1-yl)pyridine (**4**) (0.50 g, 2.37 mmol, 1.0 equiv.) and 1,3-propanesultone (1.25 mL, 1.74 g, 14.2 mmol, 6.0 equiv.) are dissolved in 25 mL MeCN and heated to 110°C for 5 days in a pressure tube. After cooling to room temperature the solvent is decanted and the formed solid is washed with MeCN (3x, 25 mL) and Et_2O (3x, 25 mL). After drying under vacuum the product is isolated as a white solid (1.03 g, 2.25 mmol, 95%).

^{1}H NMR (400 MHz, D_2O): δ (ppm) = 9.88 (t, 2H, J = 1.6 Hz, $NCHN$), 8.42 (t, 1H, J = 8.1 Hz, $C_{Py,para}H$), 8.35 (t, 2H, J = 1.9 Hz, $C_{im}H$), 8.00 (d, 2H, J = 8.2 Hz, $C_{Py,meta}H$), 7.83 (t, 2H, J = 1.8 Hz, $C_{im}H$), 4.55

(t, 4H, J = 7.1 Hz, NCH_2CH$_2$), 3.01 (t, 4H, J = 7.1 Hz, CH$_2$CH_2SO$_3$), 2.44 (p, 4H, J = 7.2 Hz, CH$_2$$CH_2CH_2$).

^{13}C NMR (101 MHz, D$_2$O): δ 145.85 ($C_{Py,ortho}$), 145.00 ($C_{Py, para}$), 135.35 (NCHN), 123.83 (C_{im}), 120.07 (C_{im}), 115.05 ($C_{Py,meta}$), 48.97 (NCH$_2$CH$_2$), 47.44 (CH$_2$$CH_2SO_3$), 25.17 (CH$_2$$CH_2CH_2$).

Metal precursors

[(η^6-*p*-Cymene)RuCl$_2$]$_2$ (12) (MW = 612.39 g/mol)[65]

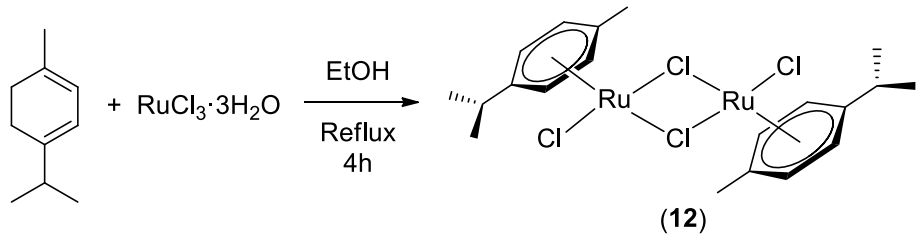

RuCl3·3H2O (1.77 g, 6.77 mmol, 1.0 equiv.) and α-terpinene (15.00 mL, 12.56 g, 92.19 mmol, 13.6 equiv.) are disolved in 100 mL absolute EtOH and the solution is heated under reflux for 4 h. After cooling the solution to room temperature the solvent is removed under reduced pressure and the rest of the liquid is decanted. The obtained solid is washed with ice cold MeOH (10 mL) and ice cold Et$_2$O (3x, 10 mL). After drying under vacuum the product is isolated as a red solid (1.63 g, 2.67 mmol, 79%).

^{1}H NMR (400 MHz, DMSO-d_6): δ (ppm) = 5.82 (d, 4H, J = 6.4 Hz, C$_{arom}$$H$), 5.78 (d, 4H, J = 6.3 Hz, C$_{arom}$$H$), 2.83 (hept, 2H, J = 6.9 Hz, CH(CH$_3$)$_2$), 2.08 (s, 6H, CH_3), 1.19 (d, 12H, J = 6.9 Hz, CH(CH_3)$_2$).

^{13}C NMR (101 MHz, DMSO-d_6): δ (ppm) = 106.33 ($C_{arom,quat}$), 100.05 ($C_{arom,quat}$), 86.35 (C_{arom}H), 85.49 (C_{arom}H), 29.96 (CH(CH$_3$)$_2$), 21.49 (CH(CH$_3$)$_2$), 17.87 (CH$_3$).

[(η6-*p*-Cymene)OsCl2]2 (13) (MW = 612.39 g/mol)[66]

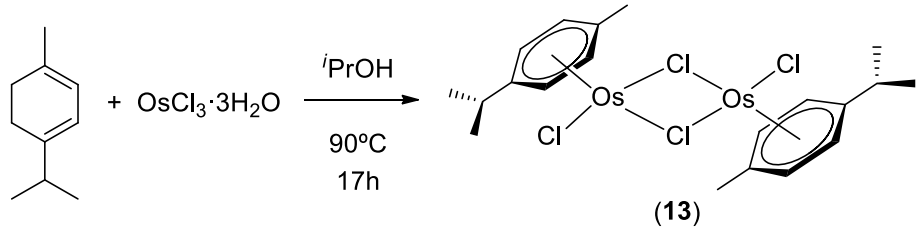

OsCl$_3$·3H$_2$O (1.00 g, 2.85 mmol, 1.0 equiv.) and α-terpinene (4.00 mL, 3.37 g, 24.70 mmol, 8.67 equiv.) are dissolved in 15 mL of ^{i}PrOH. The resulting mixture is heated at 90°C and stirred at that temperature for 17 h. After cooling to room temperature, the solvent was removed under reduced pressure and the resulting solid was washed with ^{i}PrOH (3x, 10 mL), Et$_2$O (5x, 10 mL) and hexane (1x, 10 mL). The solid is re-dissolved in DCM and filtered over celite. The DCM volume is reduced and Et$_2$O is added to precipitate an orange solid. The liquid is decanted and

the solid is washed with Et_2O (3x, 10 mL). After drying under vacuum the solid is isolated as an orange solid (479.10 mg, 0.61 mmol, 43%).

^{1}H NMR (400 MHz, $CDCl_3$): δ (ppm) = 6.18 (d, 4H, *J* = 5.7 Hz, $C_{arom}H$), 6.02 (d, 4H, *J* = 5.7 Hz, $C_{arom}H$), 2.78 (hept, 2H, *J* = 6.8 Hz, $CH(CH_3)_2$), 2.21 (s, 6H, CH_3), 1.29 (d, 12H, *J* = 6.9 Hz, $CH(CH_3)_2$).

^{13}C NMR (101 MHz, $CDCl_3$): δ (ppm) = 92.59 ($C_{arom,quat}$), 89.27 ($C_{arom,quat}$), 74.16 (C_{arom}H), 72.59 (C_{arom}H), 31.45 ($CH(CH_3)_2$), 22.62 ($CH(CH_3)_2$), 19.59 (CH_3).

[(*η*^{5}-Cp*)RhCl$_2$]$_2$ (**14**) (MW = 618.07 g/mol)[67]

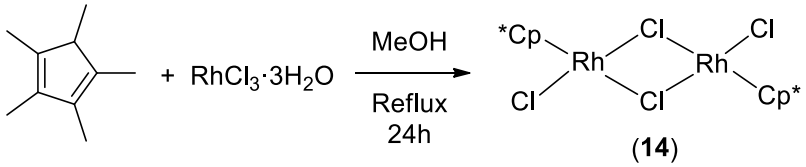

$RhCl_3 \cdot 3H_2O$ (0.20 g, 0.76 mmol, 1.0 equiv.) and 1,2,3,4,5-pentamethylcyclopentadiene (0.43 mL, 0.37 g, 2.73 mmol, 3.60 equiv.) are disolved in 12 mL of dry and degassed MeOH and heated under reflux for 24 h. The solution is cooled at room temperature and into a refrigerator and the solvent is decanted. The solid is washed with ice cold Et_2O (4x, 5 mL) and after drying under vacuum the product is isolated as a red solid (182.0 mg, 0.29 mmol, 78%).

^{1}H NMR (400 MHz, DMSO-d_6): δ (ppm) = 1.62 (s, 30H, CH_3).

^{13}C NMR (101 MHz, DMSO-d_6): δ (ppm) = 98.74 (C_{Cp*}), 8.59 (CH_3).

[(*η5*-Cp*)IrCl$_2$]$_2$ (**15**) (MW = 796.71 g/mol)[67]

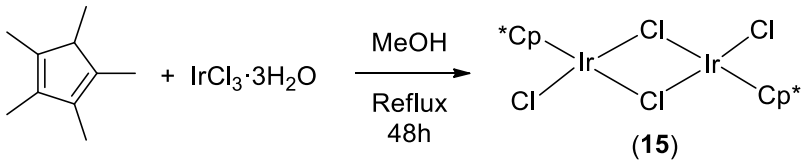

$IrCl_3 \cdot 3H_2O$ (1.00 g, 2.84 mmol, 1.0 equiv.) and 1,2,3,4,5-pentamethylcyclopentadiene (0.89 mL, 772.8 mg, 5.67 mmol, 2.0 equiv.) are dissolved in 30 mL of dry and degassed MeOH and heated under reflux for 48 h. The solution is cooled at room temperature and into a refrigerator and the solvent is decanted. The solid is washed with ice cold MeOH (2x, 15 mL) and after drying under vacuum the product is isolated as an orange solid (0.81 g, 1.01 mmol, 71%).

^{1}H NMR (400 MHz, DMSO-d_6): δ (ppm) = 1.63 (s, 30H, CH_3).

^{13}C NMR (101 MHz, DMSO-d_6): δ (ppm) = 92.08 (C_{Cp*}), 8.25 (CH_3).

Metal complexes

Silver complexes

Bis-(1-(2-pyridinyl)-3-n-butyl)imidazol-2-ylidene) argentate (I) Hexafluorophosphate (**16a**)
(MW = 655.37 g/mol)

A solution of 2-(imidazole-1-yl-3-n-butyl)pyridine (**5**) (120.2 mg, 0.426 mmol, 1.0 equiv.) and Ag_2O (98.9 mg, 0.427 mmol, 1.0 equiv.) is stirred in dichloromethane for 2 h at room temperature, then $AgPF_6$ is added (109.1 mg, 0.427 mmol, 1.0 equiv.) and the mixture is stirred for 30 min at room temperature. The solvent is removed under reduced pressure and the resulting oil is dissolved in methanol and filtered over Celite. A beige solid is obtained by addition of Et_2O. The powder is washed with Et_2O (3x10 mL) and dried under vacuum.

Yield: 91.3 mg, 65%.

^{1}H NMR (400MHz, MeOD-d_4): δ (ppm) = 8.38 – 8.24 (m, 2H, H_{Py}), 8.18 – 8.02 (m, 2H, H_{Py}), 7.98 (d, J = 2.0 Hz, 2H, H_{im}), 7.87 (d, J = 8.1 Hz, 2H, H_{Py}), 7.60 (d, J = 2.0 Hz, 2H, H_{im}), 7.56 – 7.48 (m, 2H, H_{Py}), 4.19 (t, J = 7.3 Hz, 4H, NCH_2), 1.82 (p, J = 7.3 Hz, 4H, NCH_2CH_2), 1.31 (hept, J = 7.4 Hz, 4H, $NCH_2CH_2CH_2$), 0.90(t, J = 7.4 Hz, 6H, CH_3).

^{13}C NMR (100 MHz, MeOD-d_4): δ (ppm) = 152.07 (s, C_{quat}), 150.32, 141.86, 125.53 (3 x s, C_{Py}), 124.34, 121.60 (2 x s, C_{Im}), 117.37 (C_{Py}), 53.063 (s, NCH_2), 34.46 (s, NCH_2CH_2), 20.72 (s, $CH_2CH_2CH_2$), 13.96 (s, CH_3).

FAB-MS (positive ion) calcd. for $[C_{22}H_{25}AgN_6O_6S_2]^+$ m/z 509.16, 511.16, 510.16, 512.16; found 508.9, 510.9, 509.9, 511.9.

FAB-MS (negative ion) calcd. for $[PF_6]^-$ m/z 144.96; found 145.3.

Anal. calcd. for $C_{24}H_{30}AgF_6N_6P \cdot 0.55AgPF_6$: C, 36.28; H, 3.81; N, 10.58; F, 22.24. Found: C, 36.48; H, 3.71; N, 10.58;F, 22.24.

Sodium bis-(1-(2-pyridinyl)-3-sulfonatepropyl)imidazol-2-ylidene)argentate (I) (**16b**)

(MW = 663.45 g/mol)

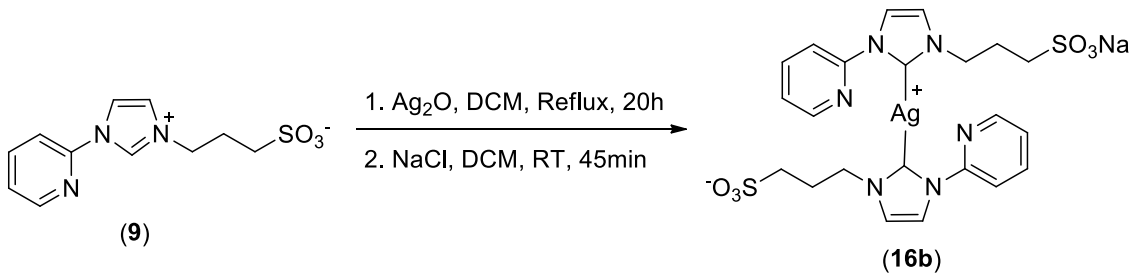

2-(imidazole-1-yl-3-propylsulfonate)pyridine (**9**) (1.00 g, 3.76 mmol, 1.0 equiv.) and Ag_2O (1.74 g, 7.52 mmol, 2.0 equiv.) are refluxed in CH_2Cl_2 (20 mL) for 20 h in the dark. Then, NaCl (0.22 g, 3.76 mmol, 1.0 equiv.) is added to the solution and stirred for 45 min. The solvent is removed under reduce pressure. The solid is dissolved in methanol and filtered over Celite. The silver complex is precipitated, washed with Et_2O (3x10 mL) and dried under vacuum. Complex **16b** is isolated as a white solid.

Yield: 1.14 g, 91%.

^{1}H NMR (400MHz, DMSO-d_6): δ (ppm) = 8.43 – 8.39 (m, 2H, H_{Py}), 8.16 (d, J = 1.9 Hz, 2H, H_{im}), 8.11 - 8.02 (m, 4H, H_{Py}), 7.82 (d, J = 1.9 Hz, 2H, H_{im}), 7.47 (ddd, J = 6.7, 4.9, 2.3 Hz, 2H, H_{Py}), 4.37 (t, J = 6.9 Hz, 4H, $CH_2SO_3^-$), 2.45 (dd, J = 8.7, 6.2 Hz, 4H, NCH_2), 2.25 – 2.07 (m, 4H, NCH_2CH_2).

^{13}C NMR (100 MHz, DMSO-d_6): δ (ppm) = 150.52 (s, C_{quat}), 148.76, 139.98, 123.91 (3 x s, C_{Py}), 123.42, 120.20 (2 x s, C_{im}), 115.56 (s, C_{Py}), 51.09 (s, $CH_2SO_3^-$), 47.99 (s, NCH_2), 27.55 (s, $CH_2CH_2CH_2$).

FAB-MS (positive ion) calcd. for $[C_{22}H_{25}AgN_6NaO_6S_2]^+$ m/z 665.02, 663.02, 664.03, 666.03; found. 664.50, 662.40, 663.40, 665.40.

FAB-MS (negative ion) calcd. for $[C_{22}H_{24}AgN_6O_6S_2]^-$ m/z 641.02, 639.03, 640.03; found. 641.3, 639.4, 640.3.

Anal. calcd. for $C_{22}H_{24}AgN_6NaO_6S_2 \cdot H_2O$: C, 38.77; H, 3.85; N, 12.33; S, 9.41. Found: C, 38.97; H, 3.67; N, 11.95; S, 8.75.

1-(2-pyridinyl)-3-n-butyl)imidazol-2-ylidene metal complexes (Water-insoluble metal complexes)

Chloro(p-cymene)(1-(2-pyridinyl)-3-n-butyl)imidazol-2-ylidene)ruthenium (II) Hexafluorophosphate (**17a**) (MW = 616.97 g/mol)

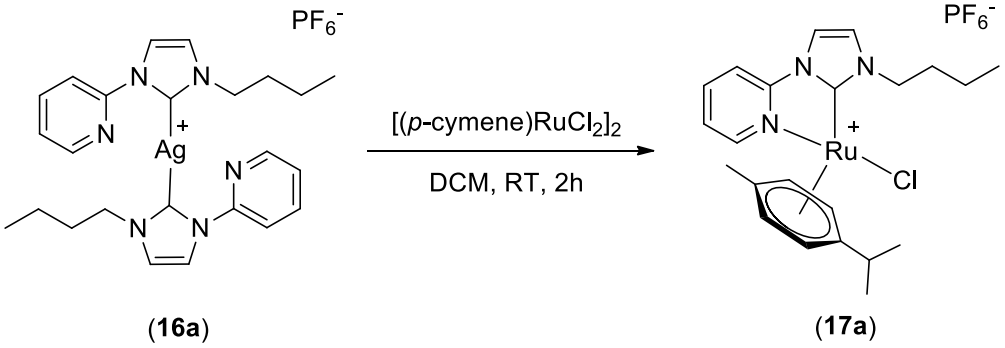

Transmetallation reaction is carried out by stirring a solution of **16a** (66.4 mg, 0.101 mmol, 1 equiv.) and $[RuCl_2(p\text{-cymene})]_2$ (62.1 mg, 0.101 mmol, 1 equiv.) in 15 mL of CH_2Cl_2 at room temperature in the dark for 2 h. The solvent is removed under reduced pressure and the resulting solid dissolved in MeCN and filtered through Celite and neutral Al_2O_3. The MeCN is removed under reduced pressure and the resulting oil is dissolved in CH_2Cl_2. Complex **17a** is isolated as an air stable orange solid by addition of Et_2O. The solid is washed with Et_2O (3x10 mL) and dried under vacuum.

Yield: 62.5 mg, 50%.

^{1}H NMR (400MHz, MeOD-d_4): δ (ppm) = 9.40 – 9.18 (m, 1H, H_{Py}), 8.31 – 8.08 (m, 2H, H_{Py}, H_{im}), 7.99 (d, J = 8.3Hz, 1H, H_{Py}), 7.69 (d, J = 2.3 Hz, 1H, H_{im}), 7.60 – 7.44 (m, 1H, H_{Py}), 6.27 (d, J = 8.0 Hz, 1H, CH_{arom}), 6.24 (d, J = 8.0 Hz, 1H, CH_{arom}), 6.09 (d, J = 8.0 Hz, 1H, CH_{arom}), 5.60 (d, J = 8.0 Hz, 1H, CH_{arom}), 4.59 (dt, J = 14.3, 7.3 Hz, 1H, NCH_2), 4.44 (dt, J = 13.6, 7.5 Hz, 1H, NCH_2), 2.39 (p, J = 6.9 Hz, 1H, CH(CH_3)$_2$), 2.21, (s, 3H, Ar-CH_3), 2.07 – 1.95 (m, 2H, NCH_2CH_2), 1.46 (m, 2H, $NCH_2CH_2CH_2$), 1.02 (t, J = 7.4 Hz, 3H, $NCH_2CH_2CH_2CH_3$), 0.94 (dd, J = 11.6, 6.9 Hz, 6H, CH(CH_3)$_2$).

^{13}C NMR (100 MHz, MeOD-d_4): δ (ppm) = 184.63 (s, $C_{carbene}$), 156.81 (s, C_{Py}), 153.20 (s, C_{quat}), 142.77(s, C_{Py}), 126.17 (s, C_{Im}), 124.40 (s, C_{Py}), 117.76 (s, C_{im}), 113.40 (s, C_{Py}),109.79, 105.61(2 x s, C_{quat}), 92.65, 92.60, 87.73, 83.41 (4 x s, C_{arom}), 52.53 (s, NCH_2), 33.53 (s, NCH_2CH_2), 32.34 (s, CH(CH_3)$_2$), 22.82, 22.25 (2 x s, CH(CH_3)$_2$), 20.85 (s, $NCH_2CH_2CH_2$), 19.22 (s, Ar-CH_3), 14.10 (s, $NCH_2CH_2CH_2CH_3$).

FAB-MS (positive ion) calcd. for $[C_{22}H_{29}ClN_3Ru]^+$ m/z 472.1, 474.11, 471.11, 470.1, 473.1; found 471.9, 473.9, 470.9, 469.9, 472.9.

Anal. calcd. for $C_{22}H_{29}ClF_6N_3PRu$: C, 42.83; H, 4.74; N, 6.81; P, 5.02. Found: C, 42.65; H, 4.70; N, 6.89; P, 5.17.

Chloro(*p*-cymene)(1-(2-pyridinyl)-3-n-butyl)imidazol-2-ylidene)osmium (II) Hexafluorophosphate (**18a**). (MW = 706.13 g/mol)

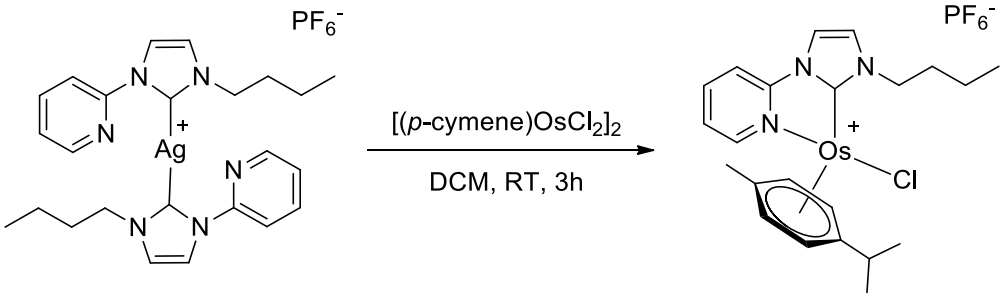

(**16a**) (**18a**)

A mixture of **16a** (73.2 mg, 0.112 mmol, 1 equiv.) and [Os(*p*-cymene)Cl_2]$_2$ (88.4 mg, 0.112 mmol, 1 equiv.) is stirred in CH_2Cl_2 (15 mL) at room temperature in the dark for 3 h. The solvent is removed under reduced pressure and the resulting solid dissolved in MeCN and filtered through Celite and neutral Al_2O_3. The MeCN is removed under reduced pressure and the resulting oil is dissolved in CH_2Cl_2. Complex **18a** is isolated as a yellow air stable solid by addition of Et_2O. The solid is washed with Et_2O (3x10 mL) and dried under vacuum.

Yield: 73.5 mg, 46.6%.

^{1}H NMR (400 MHz, MeOD-d_4): δ (ppm) = 9.26 – 9.15 (m, 1H, H_{Py}), 8.15 (ddd, J = 8.7, 7.4, 1.5 Hz, 1H, H_{Py}), 8.10 (d, J = 2.3 Hz, 1H, H_{im}), 8.05 (d, J = 8.3Hz, 1H, H_{Py}), 7.63 (d, J = 2.3 Hz, 1H, H_{im}), 7.42 (ddd, J = 7.4, 5.9, 1.3 Hz, 1H, H_{Py}), 6.32, 6.17, 6.10, 5.73 (4 x dd, J = 5.9, 1.3 Hz, 4H, CH_{arom}), 4.49 (dt, J = 14.0, 7.5 Hz, 1H, NCH_2), 4.37 (dt, J = 14.0, 7.5 Hz, 1H, NCH_2), 2.36 – 2.29 (m, 1H, CH(CH_3)$_2$), 2.28 (s, 3H, Ar-CH_3), 1.95 (p, J = 7.5 Hz, 2H, NCH_2CH_2), 1.42 (ddd, J = 14.9, 7.5, 3.3 Hz, 2H, $NCH_2CH_2CH_2$), 0.99 (t, J = 7.5 Hz, 3H, $NCH_2CH_2CH_2CH_3$), 0.90 (dd, J = 6.9, 3.3 Hz, 6H, CH(CH_3)$_2$).

^{13}C NMR (100 MHz, MeOD-d_4): δ (ppm) = 170.80 (s, $C_{carbene}$), 157.16 (s, C_{Py}), 154.06 (s, C_{quat}), 142.89 (s, C_{Py}), 125.62 (s, C_{im}), 124.86 (s, C_{Py}), 117.38 (s, C_{im}), 112.94 (s, C_{Py}), 84.07, 83.26, 78.73, 73.21 (4 x s, C_{arom}), 52.45 (s, NCH_2), 33.63 (s, NCH_2CH_2), 32.52 (s, CH(CH_3)$_2$), 23.00 (s, CH(CH_3)$_2$), 22.75 (s, CH(CH_3)$_2$), 20.82 (s, $NCH_2CH_2CH_2$), 18.91 (s, Ar-CH_3), 14.09 (s, $NCH_2CH_2CH_2CH_3$).

FAB-MS (positive ion) calcd. for [$C_{22}H_{29}ClN_3Os$]$^+$ m/z; 562.17, 560.16, 559.16, 558.16; found 561.7, 559.7, 558.7, 557.7.

Anal. calcd. for $C_{22}H_{29}ClF_6N_3POs$: C, 37.42; H, 4.14; N, 5.95; P, 4.39. Found: C, 37.15; H, 4.13; N, 5.89; P, 4.21.

Chloro(pentamethylcyclopentadienyl) (1-(2-pyridinyl)-3-n-butyl)imidazol-2-ylidene) rhodium (III) Hexafluorophosphate (**19a**). (MW = 619.82 g/mol)

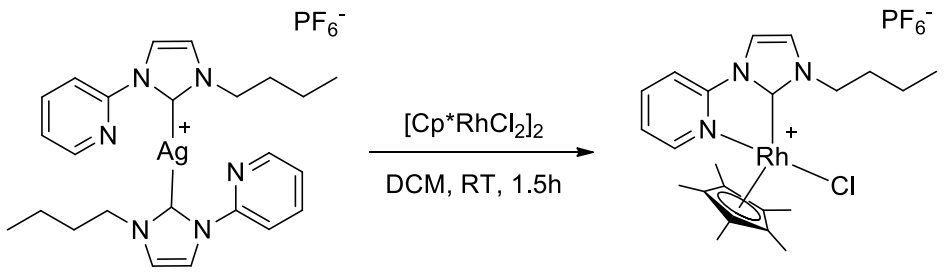

(**16a**) (**19a**)

A mixture of **16a** (43.9 mg, 0.067 mmol, 1 equiv.) and $[Cp^*RhCl_2]_2$ (41.2 mg, 0.066 mmol, 1 equiv.) is stirred in CH_2Cl_2 (15 mL) at room temperature in the dark for 1.5 h. The solvent is removed under reduced pressure and the resulting solid dissolved in acetone and filtered through Celite and neutral Al_2O_3. Complex **19a** is isolated as an air stable orange powder by addition of Et_2O. The solid is washed with Et_2O (3x10 mL) and dried under vacuum.

Yield: 40.1 mg, 49%.

^{1}H NMR (400 MHz, DMSO-d_6): δ (ppm) = 8.79 – 8.72 (m, 1H, H_{Py}), 8.54 (d, J = 2.3 Hz, 1H, H_{im}), 8.40 - 8.30 (m, 1H, H_{Py}), 8.24 (d, J = 8.2 Hz, 1H, H_{Py}), 7.95 (d, J = 2.3 Hz, 1H, H_{im}), 7.70 - 7.60 (m, 1H, H_{Py}), 4.38, 4.21 (2 x ddd, J = 13.1, 8.4, 6.3 Hz, 2H, NCH_2), 1.93 – 1.80 (m, 2H, NCH_2CH_2), 1.72 (s, 15H, Cp*), 1.40 – 1.25 (m, 2H, $NCH_2CH_2CH_2$), 0.92 (t, J = 7.3 Hz, 3H, $NCH_2CH_2CH_2CH_3$).

^{13}C NMR (100 MHz, DMSO-d_6): δ (ppm) = 179.22 (s, $C_{carbene}$), 178.80, 151.16 (2 x s, C_{quat}), 150.85, 142.16 (2 x s, C_{Py}), 125.10 (s, C_{im}), 124.07 (s, C_{Py}), 117.97 (s, C_{im}), 112.55 (s, C_{Py}), 98.88, 98.82 (2 x s, $C_{Cp,*quat}$), 50.28 (s, NCH_2), 32.03 (s, NCH_2CH_2), 19.19 (s, $NCH_2CH_2CH_2$), 13.70 (s, $NCH_2CH_2CH_2CH_3$), 9.15 (s, C_{Cp*}).

FAB-MS (positive ion) calcd. for $[C_{22}H_{30}ClN_3Rh]^+$ m/z 474.12, 476.12, 475.12, 477.12; found. 473.9, 475.9, 474.9, 476.9.

Anal. calcd. for $C_{22}H_{30}ClF_6N_3PRh$: C, 42.63; H, 4.88; N, 6.78; P, 5.00. Found: C, 42.94; H, 4.61; N, 6.87; P, 5.07.

Chloro(pentamethylcyclopentadienyl) (1-(2-pyridinyl)-3-n-butyl)imidazol-2-ylidene)iridium (III) Hexafluorophosphate (**20a**). (M = 709.13 g/mol)

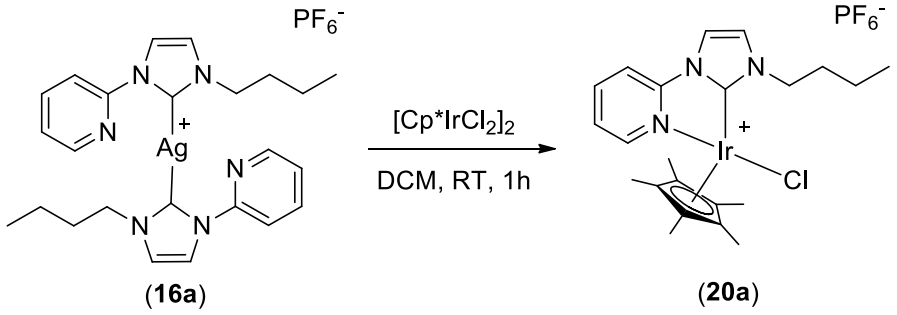

Complex **20a** is prepared as described for **19a** stirring a solution of **16a** (91.3 mg) and $[Cp^*IrCl_2]_2$ (41.2 mg, 0.066 mmol) for 1 h in CH_2Cl_2 (15 mL). Complex **20a** is obtained as an air stable light yellow solid.

Yield: 98.8 mg, 50%.

^{1}H NMR (400 MHz, DMSO-d_6): δ (ppm) = 8.73 (d, J = 8.0 Hz, 1H, H_{Py}), 8.50 (d, J = 2.3 Hz, 1H, H_{im}), 8.37 – 8.26 (m, 2H, H_{Py}), 7.91 (d, J = 2.3 Hz, 1H, H_{im}), 7.65 – 7.55 (m, 1H, H_{Py}), 4.35, 4.20 (2 x s, dt, J = 13.7, 7.5 Hz, 2H, NCH_2), 1.88 – 1.78 (m, 2H, NCH_2CH_2), 1.75 (s, 15H, Cp*), 1.29 (hept, J = 7.5 Hz, 2H, $NCH_2CH_2CH_2$), 0.90 (t, J = 7.4 Hz, 3H, $NCH_2CH_2CH_2CH_3$).

^{13}C NMR (100 MHz, DMSO-d_6): δ (ppm) = 165.63 (s, $C_{carbene}$), 151.84 (s, C_{quat}), 151.27, 142.29 (2 x s, C_{Py}), 124.52 (s, C_{im}), 124.25 (s, C_{Py}), 117.50 (s, C_{im}), 112.08 (s, C_{Py}), 91.89 (s, $C_{Cp^*,quat}$), 50.09 (s, NCH_2), 32.10 (s, NCH_2CH_2), 19.13 (s, $NCH_2CH_2CH_2$), 13.71 (s, $NCH_2CH_2CH_2CH_3$), 8.91 (s, C_{Cp^*}).

FAB-MS (positive ion) calcd. for $[C_{22}H_{30}ClIrN_3]^+$ m/z 564.18, 562.17, 566.17, 565.18; found. 564.20, 562.20, 566.2, 565.2.

Anal. calcd. for $C_{22}H_{30}ClF_6IrN_3P$: C, 37.26; H, 4.26; N, 5.93; P, 4.37. Found: C, 37.32; H, 4.40; N, 5.92; P, 4.05.

1-(2-pyridinyl)-3-sulfonatepropyl)imidazol-2-ylidene metal complexes (water-soluble metal complexes)

Chloro(p-cymene)(1-(2-pyridinyl)-3-sulfonatepropyl)imidazol-2-ylidene)ruthenium (II) (**17b**). (MW = 537.05 g/mol)

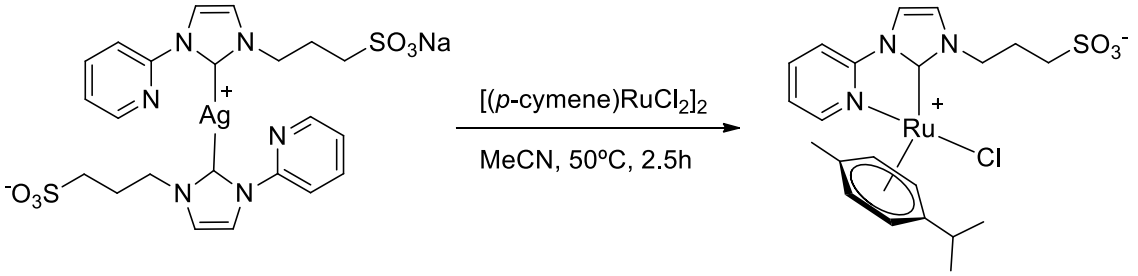

(**16b**) (**17b**)

A solution of **16b** (103 mg, 0.155 mmol, 1.0 equiv.) and $[Ru(p\text{-cymene})Cl_2]_2$ (94.7 mg, 0.155 mmol, 1.0 equiv.) is stirred at 50°C in acetonitrile for 2.5 h in the dark. The solution is filtered over Celite. The solvent is removed under reduced pressure and the resulting oil is dissolved in methanol and filtered over neutral Al_2O_3. An air stable orange solid is obtained by addition of Et_2O. The powder is washed with Et_2O (3x10 mL) and dried under vacuum.

Yield: 100.2 mg, 60%.

^{1}H NMR (400 MHz, MeOD-d_4): δ (ppm) = 9.29 (d, J = 8.0 Hz, 1H, H_{Py}), 8.20 – 8.14 (m, 2H, H_{Py}, H_{im}), 7.99 (d, J = 8.2Hz, 1H, H_{Py}), 7.75 (d, J = 2.2Hz, 1H, H_{im}), 7.53 – 7.43 (m, 1H, H_{Py}), 6.43, 6.27, 6.10, 5.84 (4 x ddd, J = 6.2, 1.3 Hz, 4H, CH_{arom}), 4.84 – 4.73, 4.72 – 4.62 (2 x m, 2H, $CH_2SO_3^-$), 3.10 – 2.95 (m, 2H, NCH_2), 2.65 – 2.50 (m, 1H, NCH_2CH_2), 2.45 – 2.32 (m, 2H, NCH_2CH_2, $CH(CH_3)_2$), 2.24 (s, 3H, Ar-CH_3), 0.94 (dd, J = 6.9, 4.0 Hz, 6H, $CH(CH_3)_2$).

^{13}C NMR (100 MHz, MeOD-d_4): δ (ppm) = 185.28 (s, $C_{carbene}$), 156.75 (s, C_{Py}), 142.67, 126.20 (2 x s, C_{im}), 124.25, 118.07, 113.51 (3 x s, C_{Py}), 101.39(s, C_{quat}), 92.39, 88.32, 82.55 (3 x s, C_{arom}), 51.34 (s, $CH_2SO_3^-$), 48.98 (s, NCH_2), 32.49 (s, $CH(CH_3)_2$), 27.77 (s, NCH_2CH_2), 22.90, 22.52 (2 x s, $CH(CH_3)_2$), 19.33 (s, Ar-CH_3).

FAB-MS (positive ion) calcd. for $[C_{21}H_{26}ClN_3O_3RuS+H]^+$ m/z 538.05, 540.05, 537.05, 539.05; found 537.8, 539.8, 536.8, 538.8.

Anal. calcd. for $C_{21}H_{26}ClN_3O_3RuS \cdot 0.1AgCl$: C, 45.66; H, 4.98; N, 6.90; S, 7.60; Cl, 5.44. Found: C, 45.75; H, 4.75; N, 7.07; S, 7.62; Cl, 5.81.

Chloro(p-cymene)(1-(2-pyridinyl)-3-sulfonatepropyl)imidazol-2-ylidene)osmium (II) (**18b**).
(MW = 626.20 g/mol)

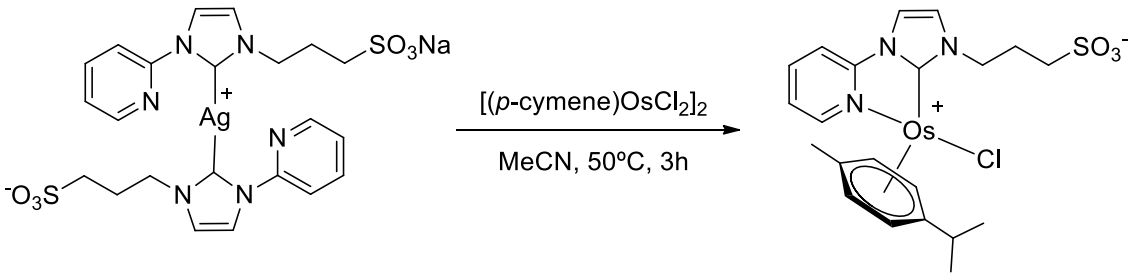

(**16b**) (**18b**)

A solution of **16b** (100 mg, 0.150 mmol, 1.0 equiv.) and [Os(*p*-cymene)Cl_2]$_2$ (118.7 mg, 0.150 mmol, 1.0 equiv.) is stirred in acetonitrile for 3 h at 50°C in the dark. The solution is filtered over Celite. The solvent is then removed under reduced pressure and the resulting oil is dissolved in methanol and filtered over neutral Al_2O_3.The resulting solid after methanol is removed under reduced pressure was washed with Et_2O (3x10 mL). The yellow air stable compound is dried under vacuum. Yield: 143 mg, 76%.

^{1}H NMR (400 MHz, MeOD-d_4): δ (ppm) = 9.22 (d, J = 8.2 Hz, 1H, H_{Py}), 8.19 – 8.12 (m, 2H, H_{Py}, H_{im}), 8.08 (d, J = 8.2 Hz, 1H, H_{Py}), 7.71 (d, J = 2.3Hz, 1H, H_{im}), 7.42 (m, 1H, H_{Py}), 6.49 (d, J = 5.7 Hz, 1H, CH_{arom}), 6.19, 6.15 (2 x d, J = 6.0 Hz, 2H, CH_{arom}), 6.01 (d, J = 5.7 Hz, 1H, CH_{arom}), 4.75 – 4.65, 4.65 – 4.55 (2 x m, 2H, $CH_2SO_3^-$), 3.07 - 2.92 (m, 2H, NCH_2), 2.58 – 2.46 (m, 1H, NCH_2CH_2), 2.38 – 2.31 (m, 2H, NCH_2CH_2, $CH(CH_3)_2$), 2.30 (s, 3H, Ar-CH_3), 0.91 (dd, J = 8.0, 6.9 Hz, 6H, $CH(CH_3)_2$).

^{13}C NMR (100 MHz, MeOD-d_4): δ (ppm) = 171.37 (s, $C_{carbene}$), 157.17 (s, C_{Py}), 154.18 (s, C_{quat}), 142.82(s, C_{Py}), 125.63 (s, C_{im}), 124.81(s, C_{Py}), 117.71(s, C_{im}), 113.07(s, C_{Py}), 84.21, 83.15, 79.31, 72.50 (4 x s, C_{arom}),70.58(s, C_{quat}), 51.31 (s, $CH_2SO_3^-$), 49.04 (s, NCH_2), 32.66 (s, $CH(CH_3)_2$), 27.56 (s, NCH_2CH_2), 23.12, 22.97 (2 x s, $CH(CH_3)_2$), 19.01 (s, Ar-CH_3).

FAB-MS (positive ion) calcd. for $[C_{21}H_{26}ClN_3O_3OsS+H]^+$ m/z 628.1, 626.1, 625.1; found 627.8, 625.9, 624.9.

Anal. calcd. for $C_{21}H_{26}ClN_3O_3OsS \cdot 0.2AgCl$: C, 38.52; H, 4.00; N, 6.42; S, 4.90; Cl, 6.50. Found: C, 38.56; H, 4.13; N, 6.34; S, 4.67; Cl, 6.80.

Chloro(pentamethylcyclopentadienyl) (1-(2-pyridinyl)-3-sulfonatepropyl)imidazol-2-ylidene)rhodium (III) (**19b**) (MW = 539.88 g/mol)

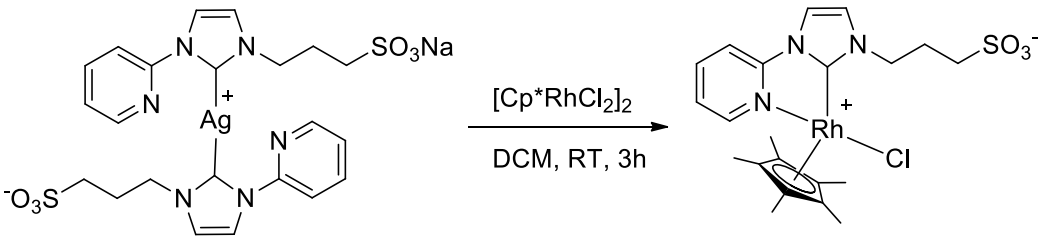

(**16b**) (**19b**)

A solution of **16b** (75 mg, 0.113 mmol, 1.0 equiv.) and $[Cp^*RhCl_2]_2$ (70.0 mg, 0.113 mmol, 1.0 equiv.) is stirred in CH_2Cl_2 (10 mL) for 3 h at room temperature in the dark. The solvent is removed under reduced pressure and the resulting solid is dissolved in methanol and filtered over neutral Al_2O_3. The methanol is removed and the solid dissolved in water and filtered over Celite. Complex **19b** is obtained as an orange solid by addition of Et_2O. The powder is then washed with Et_2O (3x10 mL) and dried under vacuum.

Yield: 90.2 mg, 74%.

^{1}H NMR (400 MHz, D_2O): δ (ppm) = 8.75 – 8.66 (m, *J* = 5.4 Hz, 1H, H_{Py}), 8.29 – 8.14 (m, 1H, H_{Py}), 8.07 (d, *J* = 2.1 Hz, 1H, H_{im}), 7.90 (d, *J* = 8.3Hz, 1H, H_{Py}), 7.68 (d, *J* = 2.2 Hz, 1H, H_{im}), 7.64 – 7.55 (m, *J* = 6.4 Hz, 1H, H_{Py}), 4.75 – 4.50, 4.47 - 4.36 (2 x m, 2H, $CH_2SO_3^-$), 3.10 – 2.94, 2.92 – 2.80 (2 x m, 2H, NCH_2), 2.47 – 2.30 (m, 2H, NCH_2CH_2), 1.72 (s, 15H, Cp*).

^{13}C NMR (100 MHz, D_2O): δ (ppm) = 180.97 (s, $C_{carbene}$), 180.45, 152.62 (2 x s, C_{quat}), 152.02, 143.86 (2 x s, C_{Py}), 125.98 (s, C_{im}), 125.86 (s, C_{Py}), 119.65 (s, C_{im}), 114.21 (s, C_{Py}), 101.50, 101.47, 101.43 (3 x s, $C_{Cp^*,quat}$), 51.16 (s, $CH_2SO_3^-$), 49.50 (s, NCH_2, MeOH), 26.99 (s, NCH_2CH_2), 10.21 (s, C_{Cp^*}).

FAB-MS (positive ion) calcd. for $[C_{21}H_{27}ClN_3O_3RhS+H]^+$ m/z 540.1, 542.1, 541.1; found. 540.0, 542.1, 541.0.

Anal. calcd. for $C_{21}H_{27}ClN_3O_3RhS \cdot 0.35AgCl$: C, 42.75; H, 4.61; N, 7.12; S, 5.43; Cl, 8.11. Found: C, 42.70; H, 4.38; N, 6.84; S, 5.10; Cl, 8.11.

Chloro(pentamethylcyclopentadienyl) (1-(2-pyridinyl)-3-sulfonatepropyl)imidazol-2-ylidene) iridium (III) (**20b**) (MW = 629.19 g/mol)

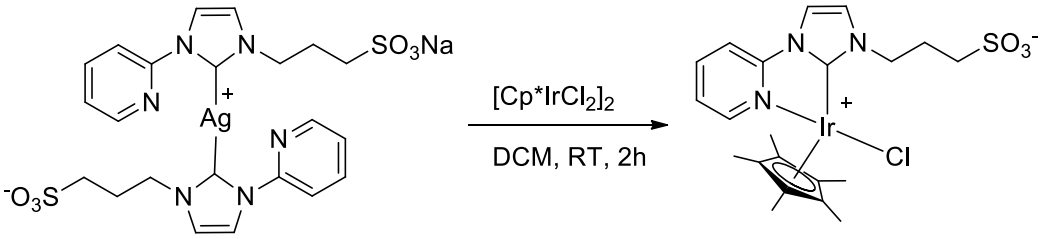

(**16b**) (**20b**)

A solution of **16b** (121.1 mg, 0.182 mmol, 1.0 equiv.) and $[Cp^*RhCl_2]_2$ (145.2 mg, 0.182 mmol, 1.0 equiv.) is stirred in CH_2Cl_2 for 2 h at room temperature in the dark. The solvent is removed under reduced pressure and the resulting solid is dissolved in methanol and filtered over Celite and neutral Al_2O_3. Complex **20b** is obtained as a yellow solid by addition of Et_2O. The powder is then washed with Et_2O (3x10 mL) and dried under vacuum.

Yield: 161.4 mg, 70%.

^{1}H NMR (400 MHz, D_2O): δ (ppm) = 8.80 - 8.60 (m, 1H, H_{Py}), 8.25 – 8.15 (m, 1H, H_{Py}), 8.05 (d, J = 2.4 Hz, 1H, H_{im}), 8.00 - 7.90 (m, 1H, H_{Py}), 7.65 (d, J = 2.4 Hz, 1H, H_{im}), 7.65 - 7.50 (m, 1H, H_{Py}), 4.70 – 4.55, 4.50 - 4.30 (2 x m, 1H, $CH_2SO_3^-$), 3.00 - 2.92 (m, 1H, NCH_2), 2.92 – 2.80 (m, 2H, NCH_2), 2.40 – 2.30 (m, 2H, NCH_2CH_2), 1.76 (s, 15H, Cp*).

^{13}C NMR (100 MHz, D_2O): δ (ppm) = 167.2 (s, $C_{carbene}$), 152.82 (s, C_{quat}), 151.31, 143.11, 125.08 (3 x s, C_{Py}), 124.51, 118.35 (2 x s, C_{im}), 112.91 (s, C_{Py}), 93.48 (s, $C_{Cp^*,quat}$), 50.14 (s, $CH_2SO_3^-$), 48.61 (s, NCH_2), 26.18 (s, NCH_2CH_2), 9.08 (s, C_{Cp^*}).

FAB-MS (positive ion) calcd. for $[C_{21}H_{27}ClIrN_3O_3S+H]^+$ m/z 630.1, 628.1, 632.1, 631.1, 629.1; found. 629.8, 627.8, 631.8, 630.8, 628.8.

Anal. calcd. for $C_{21}H_{27}ClIrN_3O_3S$: C, 40.09; H, 4.33; N, 6.68; S, 5.10. Found: C, 9.73; H, 4.43; N, 6.53; S, 4.98; Cl, 5.84.

A.1.4 Representative procedure for catalytic experiments

Representative Procedure for Transfer Hydrogenation of Acetophenone with 1-(2-pyridinyl)-3-n-butyl)imidazol-2-ylidene metal complexes

Acetophenone (2.00 mmol), KOH (0.2 mmol), catalyst (0.020 mmol) and and 1,3,5-trimethoxybenzene (used as an internal standard) are added into a dried Schlenk flask. Dry ^{i}PrOH (3.0 mL) is added to the flask, and the mixture is refluxed for the specified time under argon. An aliquot is transferred to another dried schlenk flask where the solvent is evacuated, the resulting residue re-dissolved in $CDCl_3$ and further analyzed by ^{1}H NMR.

Representative Procedure for Transfer Hydrogenation of Acetophenone with 1-(2-pyridinyl)-3-sulfonatepropyl)imidazol-2-ylidene metal complexes

Acetophenone and catalyst are mixed into a HCOONa/ HCOOH buffer solution (500 µL) with the desired concentrations and added into a GC vial equipped with a magnetic stirring bar. The mixture is heated at the specified temperature and time on air. After the reaction, the solutions are cooled to room temperature, directly extracted with $CDCl_3$ (500 µL) and subjected to ^{1}H NMR and GC-MS analysis (using nitrobenzene as external standard).

Representative Procedure for Hydrogenation of Aromatic Compounds in Autoclave

An alicuot of freshly prepared catalyst solution (500 µL) is added to a GC vial equipped with a magnetic stirring bar containing the substrate, directly transferred to a steel autoclave system and flushed three times with hydrogen gas. After the reaction, the solutions are cooled to room temperature, directly extracted with $CDCl_3$ (500 µL) and subjected to ^{1}H NMR and GC-MS analysis (using nitrobenzene as internal standard).

Representative Procedure for the synthesis of Ru and Rh nanoparticles

A 2 mM solution of Ru or Rh complex (in 0.1 M KOH/H_2O solution) in a glass vial is transferred into a steel autoclave system, flushed three times with hydrogen, heated to 80°C and then pressurized with 40 bar hydrogen gas. After 3 h at the desired temperature, the solution is cooled to RT and the hydrogen is released. The solution is directly used for analytic measurements or catalytic reactions.

A.3 Supporting information

A.3.1 ^{1}H and ^{13}C NMR spectra

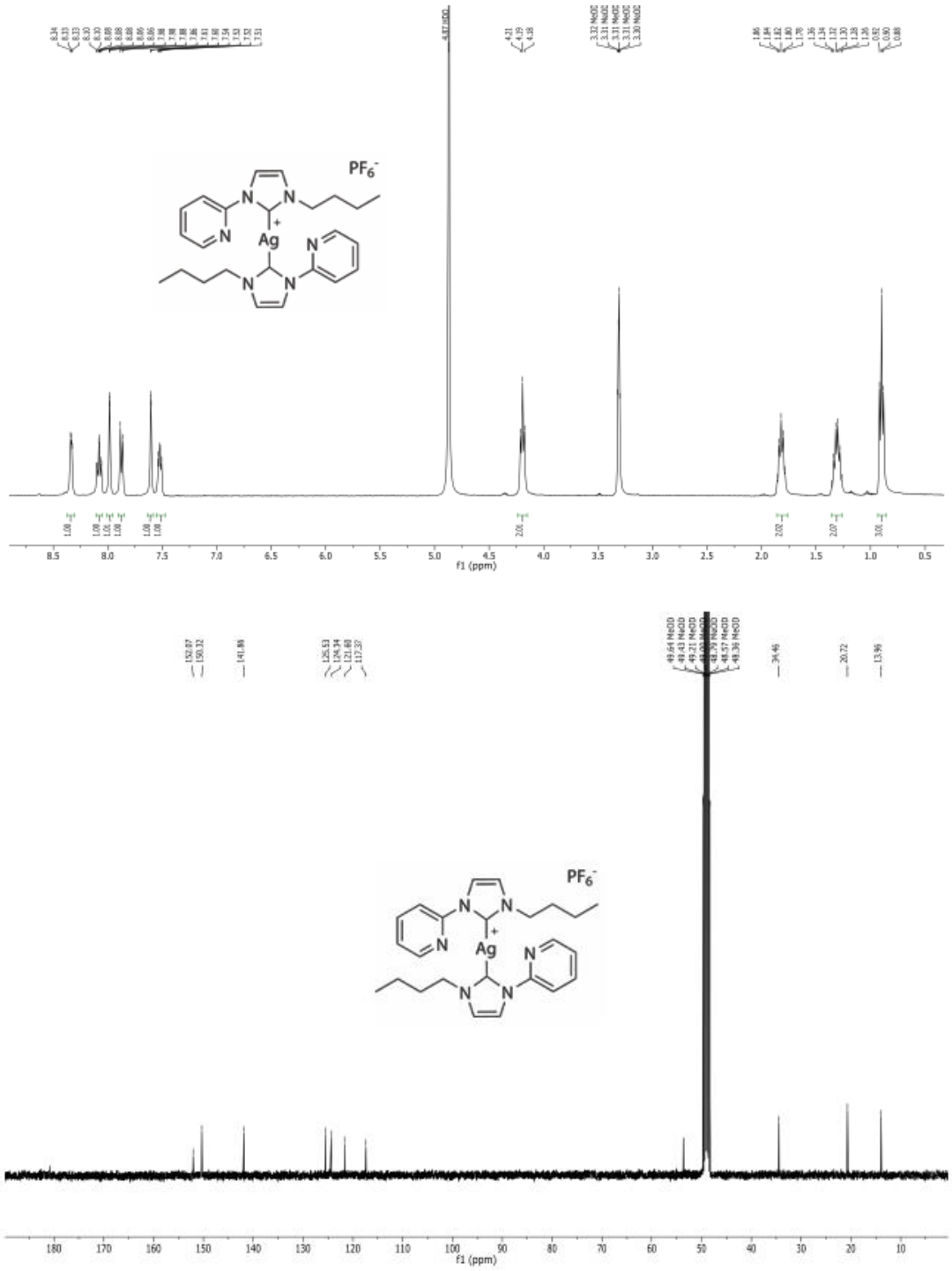

Figure 43. ^{1}H (MeOD-d_4, 400 MHz) and ^{13}C (MeOD-d_4, 100 MHz) NMR spectra of **16a**.

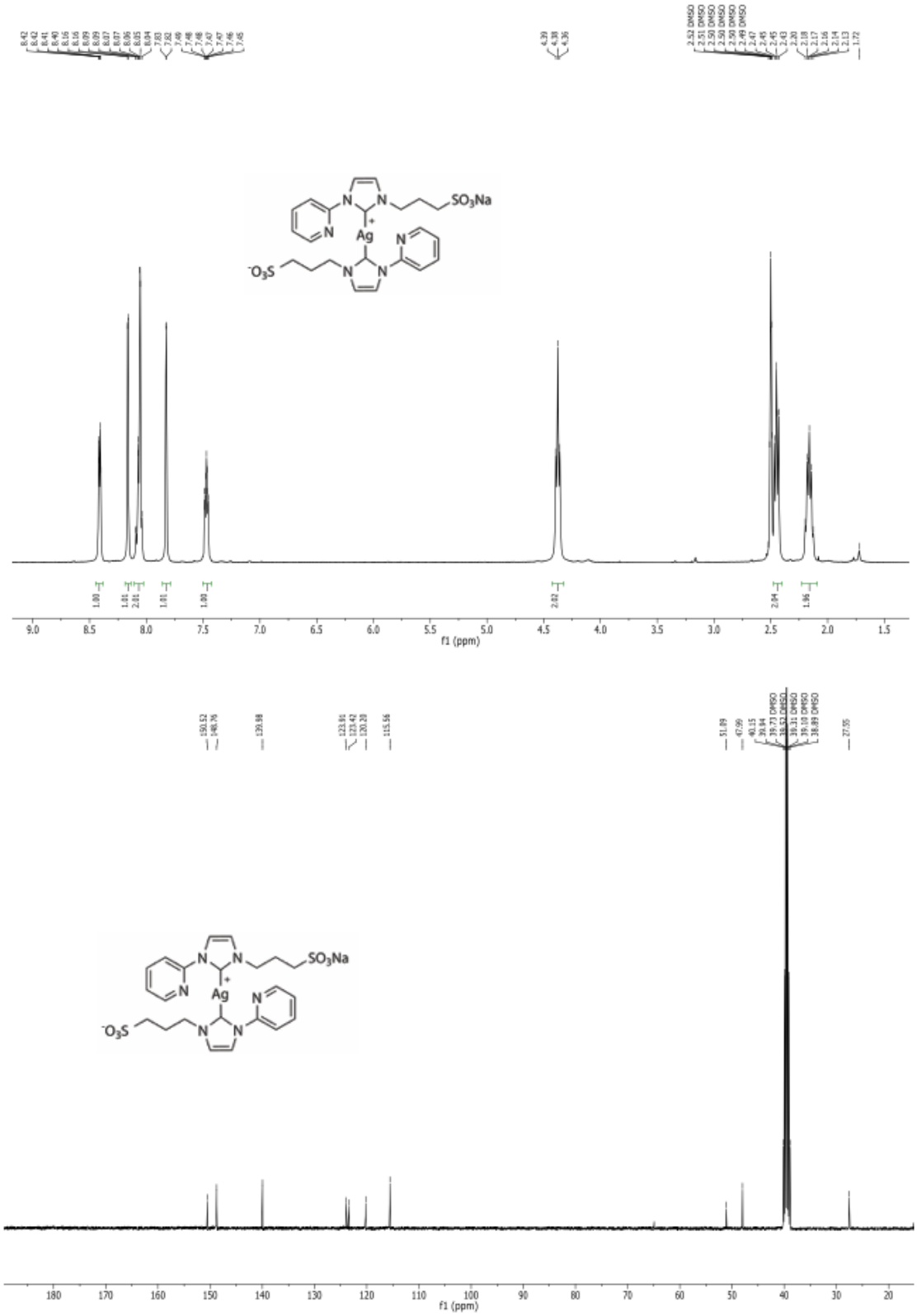

Figure 44. ^{1}H (DMSO-d_6, 400 MHz) and ^{13}C (DMSO-d_6, 100 MHz) NMR spectra of **16b**.

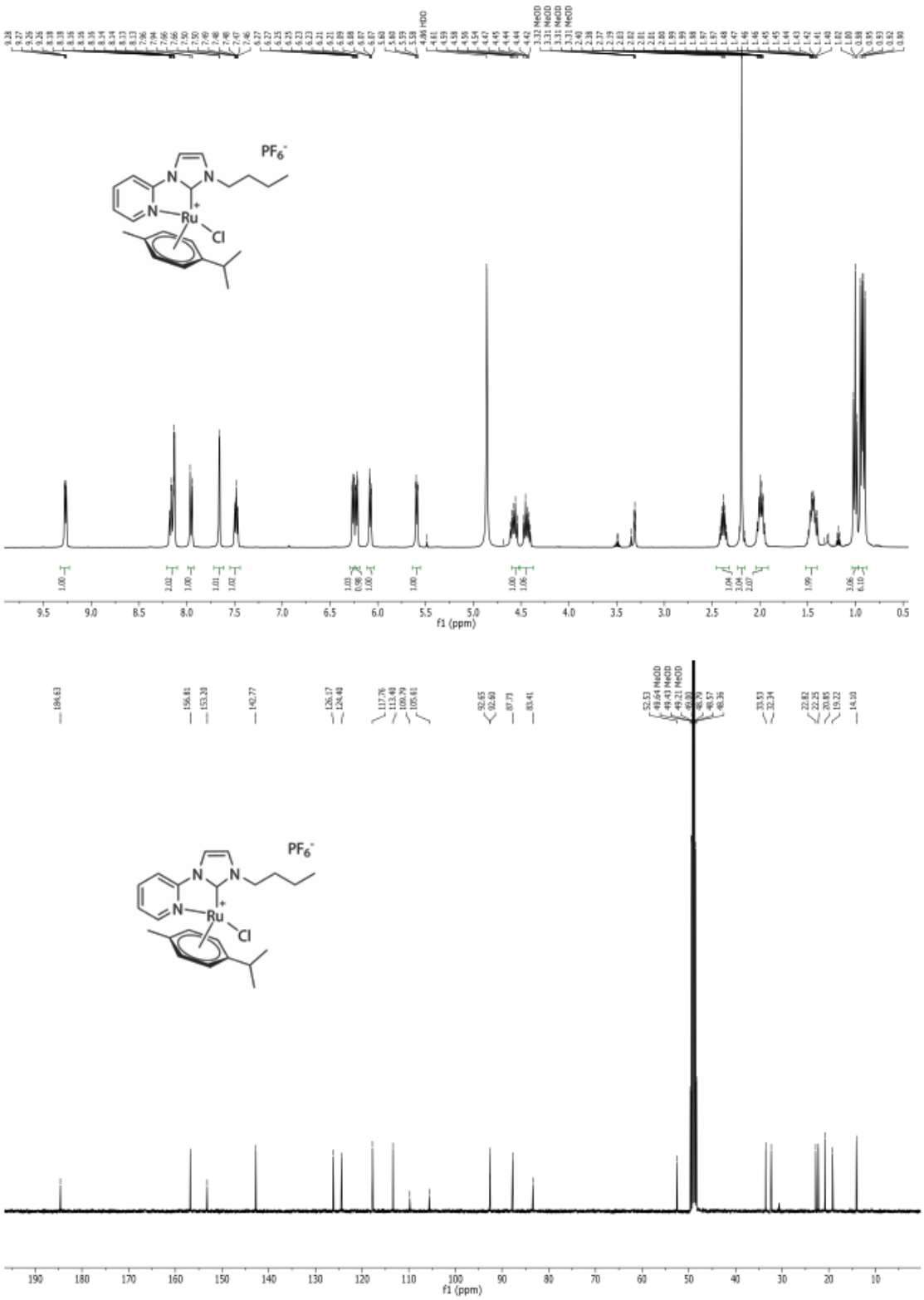

Figure 45. ^{1}H (MeOD-d_4, 400 MHz) and ^{13}C (MeOD-d_4, 100 MHz) NMR spectra of **17a**.

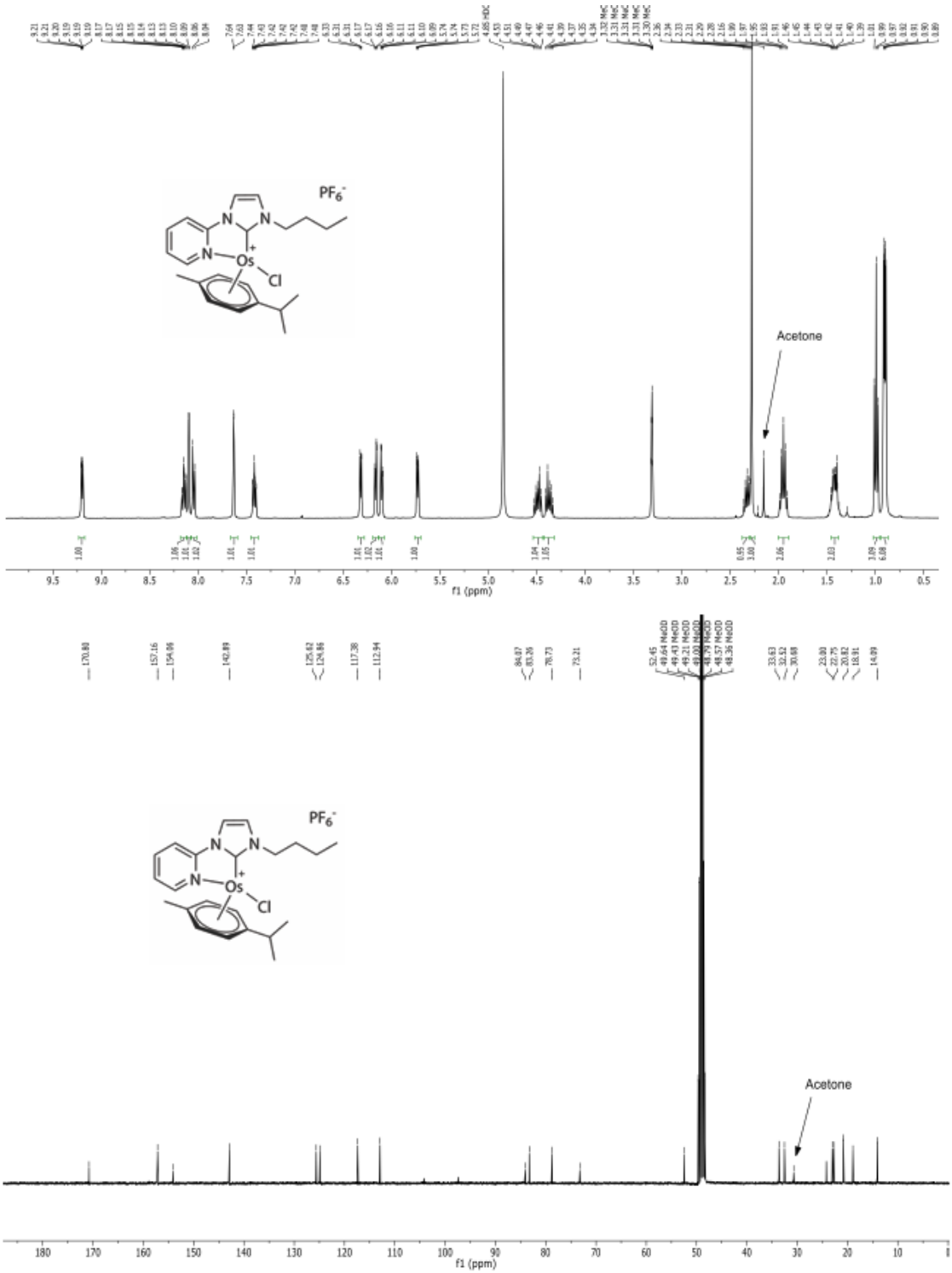

Figure 46. ^{1}H (MeOD-d_4 , 400 MHz) and ^{13}C (MeOD-d_4 , 100 MHz) NMR spectra of **18a**.

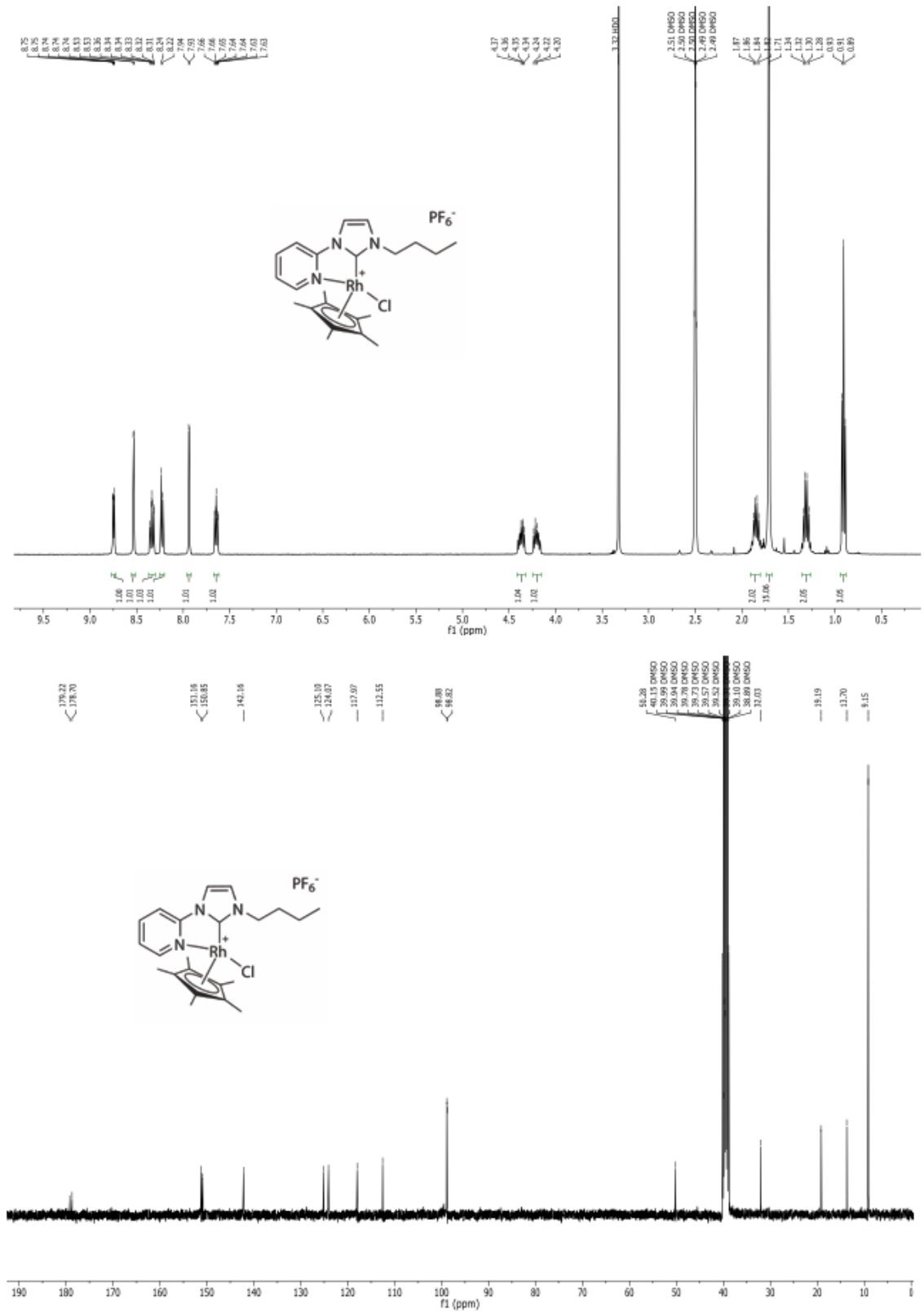

Figure 47. ^{1}H (DMSO-d_6, 400 MHz) and ^{13}C (DMSO-d_6, 100 MHz) NMR spectra of **19a**.

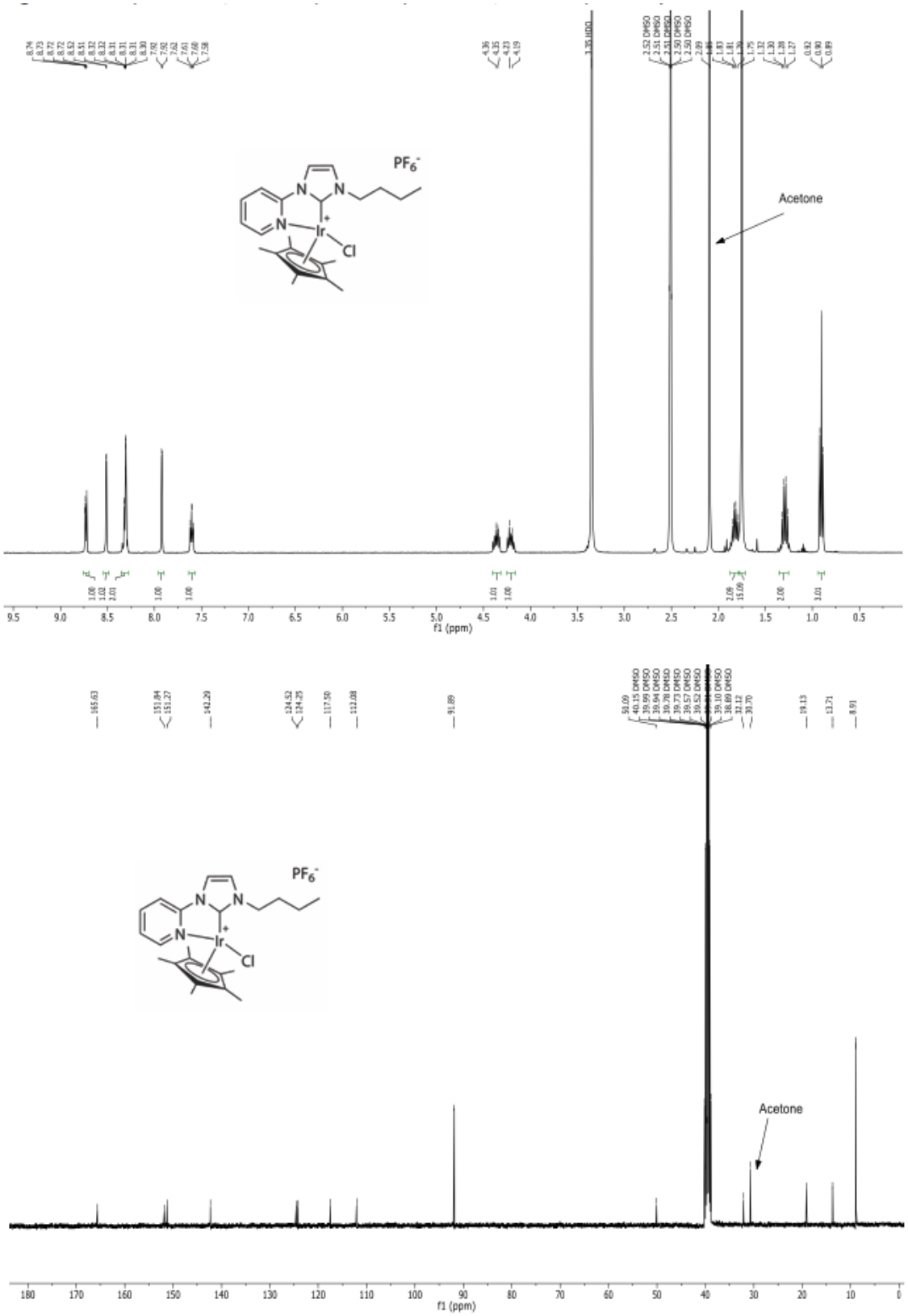

Figure 48. ^{1}H (DMSO-d_6, 400 MHz) and ^{13}C (DMSO-d_6, 100 MHz) NMR spectra of **20a**.

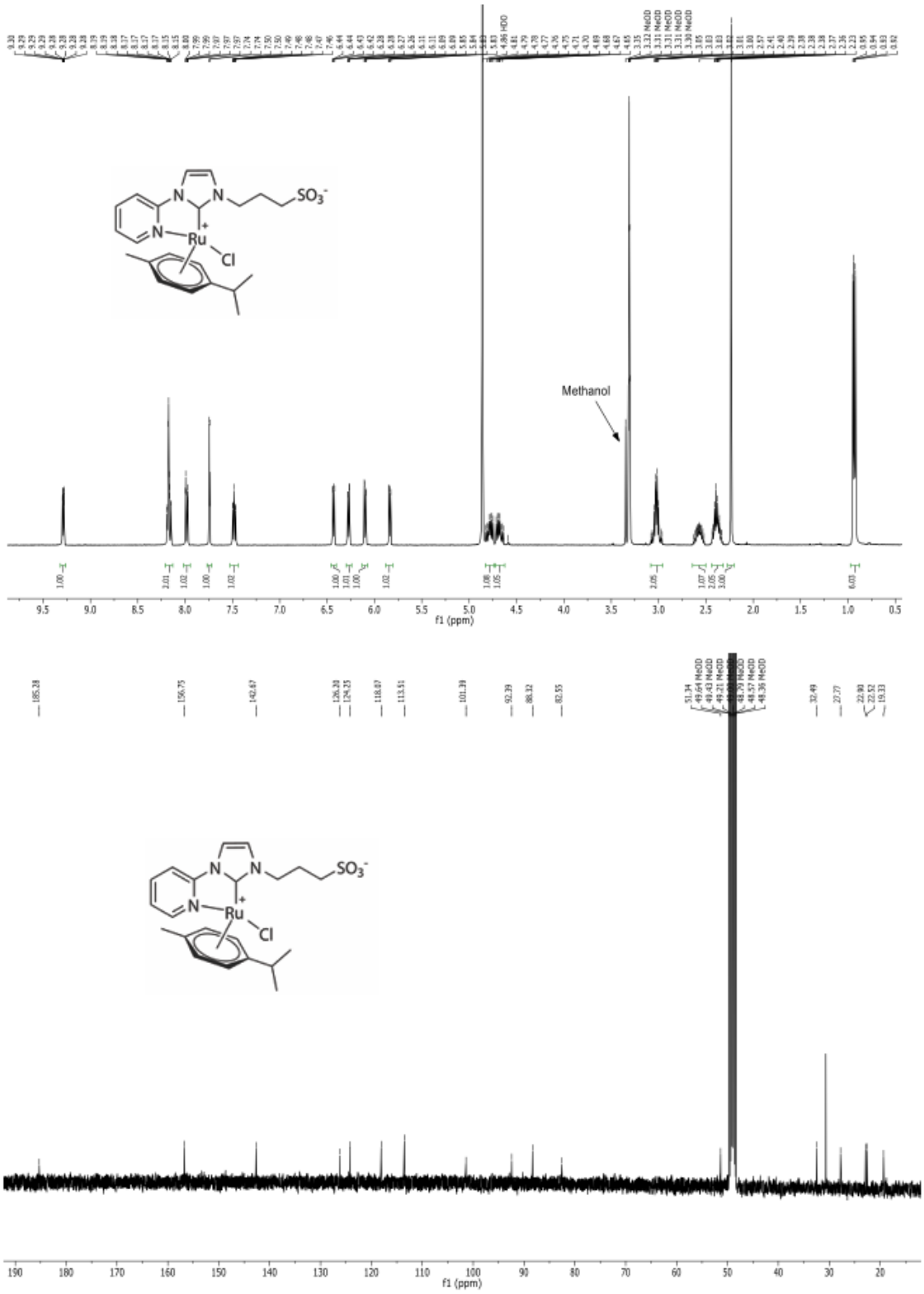

Figure 49. ^{1}H (MeOD-d_4, 400 MHz) and ^{13}C (MeOD-d_4, 100 MHz) NMR spectra of **17b**.

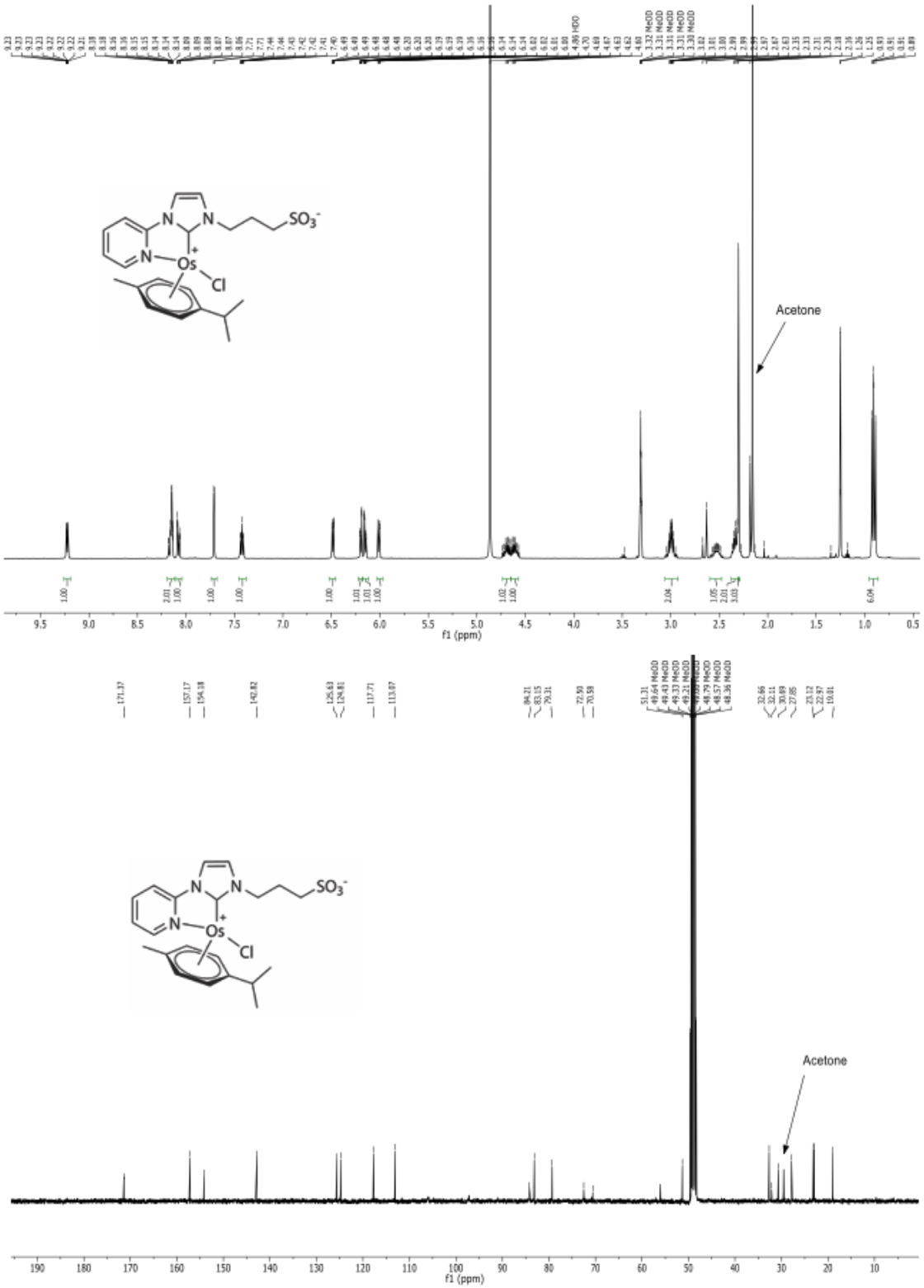

Figure 50. ^{1}H (MeOD-d_4, 400 MHz) and ^{13}C (MeOD-d_4, 100 MHz) NMR spectra of **18b**.

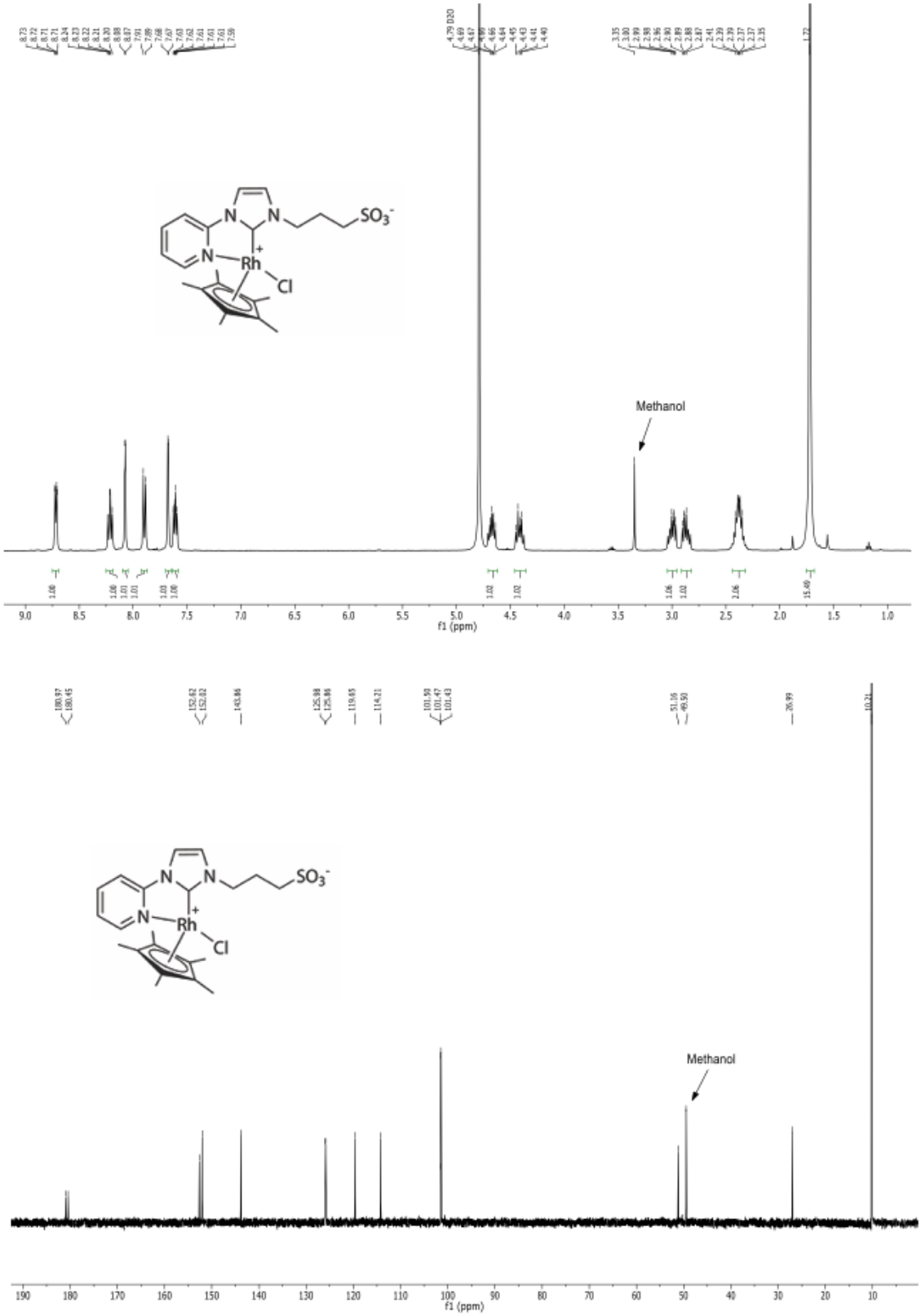

Figure 51. ^{1}H (D_2O, 400 MHz) and ^{13}C (D_2O, 100 MHz) NMR spectra of **19b**.

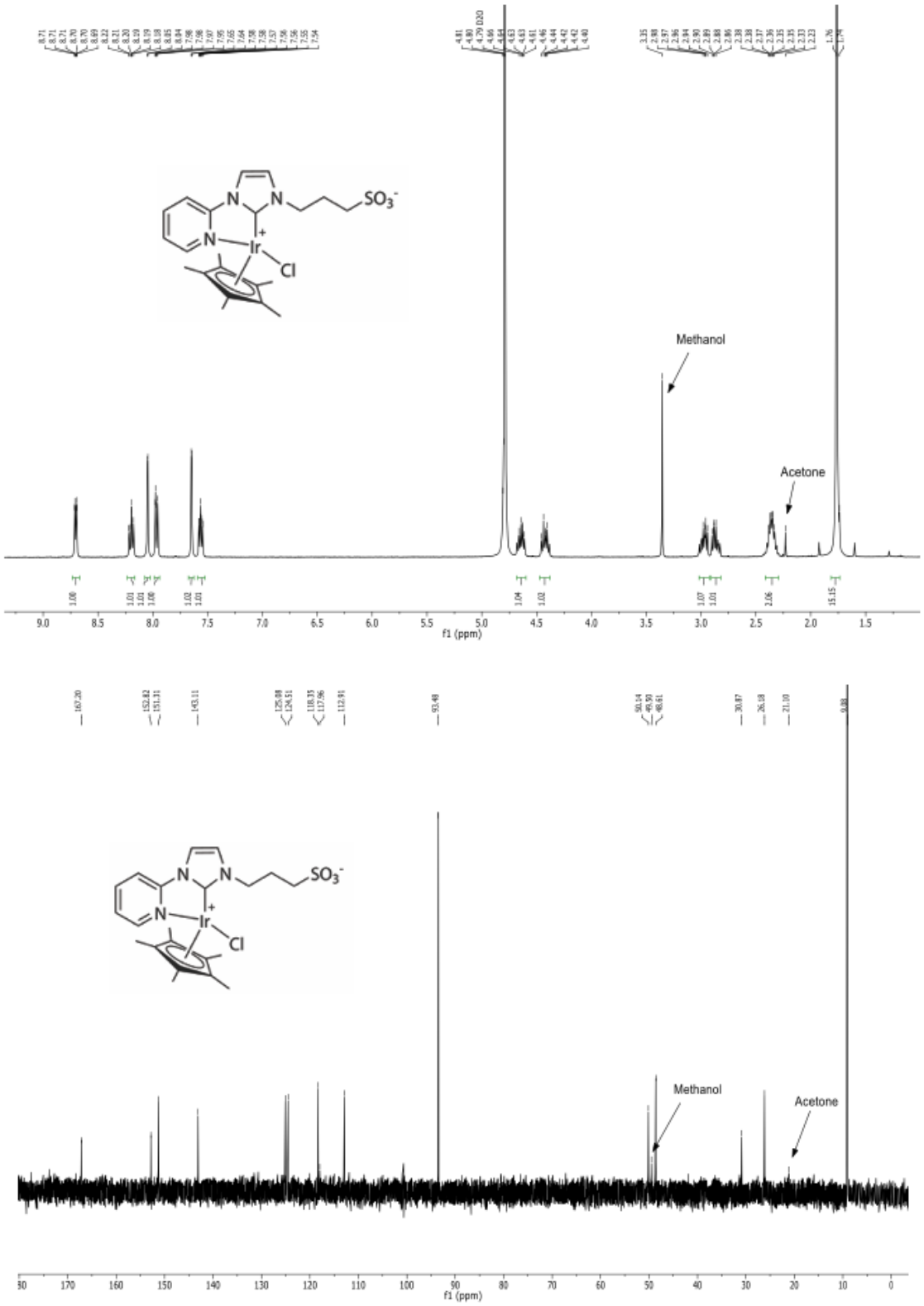

Figure 52. ^{1}H (D_2O, 400 MHz) and ^{13}C (D_2O, 100 MHz) NMR spectra of **20b**.

A.3.2 X-Ray crystallographic data

Data were collected on an X-ray single crystal diffractometer equipped with a CCD detector (APEX II, κ-CCD), a rotating anode FR591 equipped with a Montel mirror optic (**19a**, **19b**, **20a**, **20b**) or a fine focused sealed tube equipped with a graphite monochromator (**16a**, **16b**, **18b**) by using the APEXII software package.[S1] The measurements were performed on single crystals coated with perfluorinated ether. The crystals were fixed on the top of a glass fiber and transferred to the diffractometer. Crystals were frozen under a stream of cold nitrogen. A matrix scan was used to determine the initial lattice parameters. Reflections were merged and corrected for Lorenz and polarization effects, scan speed, and background using SAINT.[S2] Absorption corrections, including odd and even ordered spherical harmonics were performed using SADABS.[S2] Space group assignments were based upon systematic absences, *E* statistics, and successful refinement of the structures. Structures were solved by direct methods with the aid of successive difference Fourier maps,[S3] and were refined against all data using the APEX 2 software[S1] in conjunction with SHELXL-97[S4] and SHELXLE.[S5] Methyl hydrogen atoms were refined as part of rigid rotating groups, with a C–H distance of 0.98 Å and $U_{iso(H)} = 1.5 \cdot U_{eq(C)}$. Other H atoms were placed in calculated positions and refined using a riding model, with methylene and aromatic C–H distances of 0.99 and 0.95 Å, respectively, and $U_{iso(H)} = 1.2 \cdot U_{eq(C)}$. Non-hydrogen atoms were refined with anisotropic displacement parameters. Full-matrix least-squares refinements were carried out by minimizing $\Sigma w(F_o^2-F_c^2)^2$ with SHELXL-97 weighting scheme.[S4] Neutral atom scattering factors for all atoms and anomalous dispersion corrections for the non-hydrogen atoms were taken from *International Tables for Crystallography*.[S6] Images of the crystal structures were generated by Mercury.[S7] Crystallographic data (excluding structure factors) for the structures reported in this paper have been deposited with the Cambridge Crystallographic Data Centre as supplementary publication No.'s 1404189-1404195. Copies of the data can be obtained free of charge on application to CCDC, 12 Union Road, Cambridge CB2 1EZ, UK (fax: (+44)1223-336-033; e-mail: deposit@ccdc.cam.ac.uk.).

References:

S1 APEX suite of crystallographic software. APEX 2 Version 2008.4. Bruker AXS Inc., Madison, Wisconsin, USA, 2008.

S2 SAINT, Version 7.56a and SADABS Version 2008/1. Bruker AXS Inc., Madison, Wisconsin, USA, 2008.

S3 G. M. Sheldrick, "**SHELXS-97**", Program for Crystal Structure Solution, Göttingen, 1997.

S4 G. M. Sheldrick, "SHELXL-97", University of Göttingen, Göttingen, Germany, 1998, *or* Sheldrick, G. M. "SHELXL-2014", University of Göttingen, Göttingen, Germany, 2014.

S5 C. B. Huebschle, G. M. Sheldrick and B. Dittrich, "SHELXLE", *J. Appl. Cryst.,* 2011, **44,** 1281.

S6 A. J. C. Wilson, (Ed.), International Tables for Crystallography, Vol. C, Tables 6.1.1.4 (pp. 500-502), 4.2.6.8 (pp. 219-222), and 4.2.4.2 (pp. 193-199), Kluwer Academic Publishers, Dordrecht, The Netherlands, 1992.

S7 Mercury: visualization and analysis of crystal structures C.F. Macrae, P.R. Edgington, P McCabe, E. Pidcock, G.P. Shields, R. Taylor, M. Towler, J. van de Streek, *J. Appl. Cryst.* (2006), 39-3, 453-457.

Table 6. Crystallographic data for compounds **16a**, **16b**, **19a**, **20a**, **18b**, **19b** and **20b**.

20b	**19b**	**18b**	**20a**	**19a**	**16b**	**16a**	
$C_{21}H_{31}ClIrN_3O_{5.09}S$	$C_{21}H_{31}ClN_3O_{5.1}RhS$	$C_{22}H_{30}ClN_3O_4OsS$	$C_{22}H_{30}ClF_6IrN_3P$	$C_{22}H_{30}ClF_6N_3PRh$	$C_{23}H_{28}AgN_6NaO_7S_2$	$C_{36}H_{45}Ag_2F_{12}N_9P_2$	**Formula**
666.72	577.55	658.24	709.13	619.82	695.51	1109.49	**fw**
yellow plate	orange block	yellow block	yellow plate	orange fragment	colourless fragment	brown fragment	**Colour/habit**
0.164 x 0.378 x 0.445	0.227 x 0.231 x 0.279	0.186 x 0.230 x 0.370	0.090 x 0.179 x 0.290	0.134 x 0.232 x 0.277	0.080 x 0.250 x 0.310	0.090 x 0.120 x 0.260	**Cryst. dimensions (mm^3)**
monoclinic	monoclinic	monoclinic	orthorhombic	orthorhombic	triclinic	triclinic	**Crystal system**
$P\ 2_1/n$	*$P\ 2_1/n$*	*$P\ 2_1/c$*	*P bca*	*P bca*	*P -1*	*P -1*	**Space group**
11.3664(6)	11.3895(3)	10.5278(2)	15.0548(6)	14.9552(4)	9.0008(3)	12.6948(6)	***a*, Å**
12.2127(6)	12.1721(3)	17.4635(4)	14.9891(6)	15.0093(4)	12.2235(4)	13.5073(6)	***b*, Å**
17.5641(9)	17.5563(5)	13.6800(3)	21.8205(9)	21.7963(6)	13.4457(5)	14.4562(7)	***c*, Å**
90	90	90	90	90	71.899(2)	94.699(2)	**α, deg**
93.028(2)	93.134(1)	93.009(1)	90	90	82.767(2)	105.537(2)	**β, deg**
90	90	90	90	90	76.054(2)	112.654(2)	**γ, deg**
2434.8(2)	2430.26(11)	2511.63(9)	4924.0(3)	4892.6(2)	1362.57(8)	2155.71(18)	***V*, $Å^3$**
4	4	4	8	8	2	2	***Z***

Continuation Table 6. Crystallographic data for compounds **16a**, **16b**, **19a**, **20a**, **18b**, **19b** and **20b**.

19b	**18b**	**20a**	**19a**	**16b**	**16a**	
123	123	123	123	123	123	***T*, K**
1.579	1.741	1.913	1.683	1.695	1.709	**D_{calcd}, g cm^{-3}**
0.936	5.299	5.658	0.935	0.964	1.074	**μ, mm^{-1}**
1187.3	1296	2768	2512	708	1112	***F*(000)**
2.04 – 33.14	1.89 – 26.37	1.87 – 26.02	1.87 – 25.35	2.02 – 25.35	1.84 – 26.87	**ϑ range, deg**
-17 – 16, ±18, -24 – 27	±13, ±21, ±17	±18, -16 – 18, ±26	±18, ±18, ±26	±10, ±14, ±16	±16, ±17, ±18	**Index ranges (*h*, *k*, *l*)**
51535	92387	92223	82866	50061	65786	**No. of rflns collected**
9255/0.0494	5125/0.0589	4859/0.0476	4466/0.0649	4965/0.0748	9239/0.0717	**No. of independent rflns/R_{int}**
8308	4445	4133	3634	3948	6537	**No. of observed rflns (I>2σ(I))**
9255/6/311	5125/0/294	4859/0/313	4466/0/313	4965/0/363	9239/0/ 553	**No. of data/restraints/parameters**
0.0237/0.0595	0.0227/0.0491	0.0179/0.0360	0.0336/0.0669	0.0303/0.0546	0.0390/ 0.0819	**R1/wR2 (I>2σ(I))[a]**
0.0281/0.0617	0.0306/0.0515	0.0251/0.0384	0.0497/0.0751	0.0492/0.0593	0.0729/ 0.0927	**R1/wR2 (all data)[a]**
1.071	1.04	1.026	1.113	1.022	1.007	**GOF (on F^2)[a]**
0.708/-0.878	1.368/-0.745	0.797/-0.515	0.094/-0.646	0.435/-0.403	1.054/ -0.959	**Largest diff peak and hole (e Å^{-3})**

Continuation Table 6. Crystallographic data for compounds **16a**, **16b**, **19a**, **20a**, **18b**, **19b** and **20b**.

	***T*, K**	***D*$_{calcd}$, g cm^{-3}**	***μ*, mm^{-1}**	***F*(000)**	**ϑ range, deg**	**Index ranges (*h*, *k*, *l*)**	**No. of rflns collected**	**No. of independent rflns/*R*$_{int}$**	**No. of observed rflns (*I*>2σ(*I*))**	**No. of data/restraints/parameters**	**R1/wR2 (*I*>2σ(*I*))[a]**	**R1/wR2 (all data)[a]**	**GOF (on *F*^{2})[a]**	**Largest diff peak and hole (e Å^{-3})**
20b	123	1.819	5.716	1315	2.32 – 25.35	±13, ±14, ±21	24095	4452/0.0461	4266	4452/6/320	0.0201/0.0501	0.0210/0.0506	1.208	1.803/-0.745

[a] R1 = $\sum(||F_o|-|F_c||)/\sum|F_o|$; wR2 = $\{\sum [w(F_o^2-F_c^2)^2]/ \sum[w(F_o^2)^2]\}^{1/2}$; GOF = $\{\sum[w(F_o^2-F_c^2)^2]/(n-p)\}^{1/2}$

Table 7. Selected bond lengths (Å) and bond angles (º) for rhodium and iridium complexes.

Complex		**19a**[a]	**19b**[b]	**20a**[a]	**20b**[b]
Bond lengths (Å)	M(1)–C(1)	2.023(3)	2.0263(11)	2.018(3)	2.021(2)
	M(1)–N(3)	2.128(3)	2.118(10)	2.122(2)	2.107(2)
	M(1)–Cl(1)	2.4065(8)	2.4053(3)	2.4090(7)	2.4088(6)
	M(1)–C(12)[b] or M(1)–C(13)[a]	2.155(3)	2.1992(11)	2.165(3)	2.173(2)
	M(1)–C(13)[b] or M(1)–C(14)[a]	2.213(3)	2.1566(12)	2.232(3)	2.227(3)
	M(1)–C(14)[b] or M(1)–C(15)[a]	2.236(3)	2.2264(12)	2.250(3)	2.233(2)
	M(1)–C(15)[b] or M(1)–C(16)[a]	2.154(3)	2.2159(11)	2.163(2)	2.166(3)
	M(1)–C(16)[b] or M(1)–C(17)[a]	2.181(3)	2.1673(11)	2.180(3)	2.198(2)
Bond angles (º)	C(1)–M(1)–N(3)	76.78(12)	76.82(4)	76.33(10)	76.22(9)
	C(1)–M(1)–Cl(1)	85.53(9)	86.28(3)	85.20(7)	86.12(7)
	N(3)–M(1)–Cl(1)	89.03(8)	87.99(3)	86.78(6)	86.02(5)
	C(1)–M(1)–C(12)[a] or C(1)–M(1)–C(13)[b]	117.04(13)	102.54(4)	117.33(11)	124.35(10)
	C(1)–M(1)–C(13)[a] or C(1)–M(1)–C(14)[b]	155.12(13)	113.39(4)	155.12(11)	163.12(10)
	C(1)–M(1)–C(14)[a] or C(1)–M(1)–C(15)[b]	154.84(13)	149.56(4)	156.47(10)	150.05(10)
	C(1)–M(1)–C(15)[a] or C(1)–M(1)–C(16)[b]	117.07(13)	162.11(5)	118.51(10)	114.26(9)
	C(1)–M(1)–C(16)[a] or C(1)–M(1)–C(17)[b]	100.50(13)	123.12(5)	101.47(10)	103.85(10)
Torsion angles (º)	C(1)–N(2)–C(4)–N(3)	-2.2(4)	-0.04(15)	-2.0(3)	-0.05(3)

Notations

Ar	Aromatic
arom	Aromatic
br	Broad signal
calcd.	Calculated
cat	Catalyst
$CDCl_3$	Deuterated chloroform
COSY	Correlation Spectroscopy
Cp*	1,2,3,4,5-Pentamethylcyclopentadiene
d	Doublet
dd	Doublet of doublets
ddd	Doublet of doublet of doublets
D_2O	Deuterium oxide
DCM	Dichloromethane
DFT	Density Functional Theory
DMSO	Dimethylsulfoxide
dt	Doublet of triplets
equiv.	Equivalents
Et_2O	Diethylether
g	Grams
GC-MS	Gas Chromatography – Mass Spectrometry
h	Hours
HMQC	Heteronuclear Multiple-Quantum Coherence
Hz	Herzt (h^{-1})
im	Imidazole
J	Coupling constant (in NMR)
m	Multiplet
M	Molar
mM	Milimolar
MeCN	Acetonitrile
MeOH	Methanol

min	Minutes
mL	Milliliter
MW	Molecular weight
NHC	N-Heterocyclic carbene
NMR	Nuclear Magnetic Resonance
NPs	Nanoparticles
ORTEP	Oak Ridge Thermal Elipsoid Plot
p	Pentet
ppm	Parts per million (unit of shift in NMR)
^{i}PrOD	Deuterated isopropanol
^{i}PrOH	Isopropanol
Py	Pyridine
q	Quartet
quat	Quaternary
RT	Room temperature
s	Singlet
t	Triplet
T	Temperature
TEM	Transmission Electron Microscopy
TH	Transfer hydrogenation
δ	Delta (NMR shift)

References

1. Glossary of terms used in physical organic chemistry (IUPAC Recommendations 1994). *IUPAC Compend. Chem. Terminol.* **66,** 1077 (1994).
2. Glossary of class names of organic compounds and reactivity intermediates based on structure (IUPAC Recommendations 1995). *IUPAC Compend. Chem. Terminol.* **67,** 1307 (1995).
3. Cardin, D. J., Cetinkaya, B. & Lappert, M. F. Transition metal-carbene complexes. *Chem. Rev.* **72,** 545–574 (1972).
4. Chugaev, L. & Skanavy-Grigorizeva, M. No Title. *J. Russ. Chem. Soc.* **47,** 776 (1915).
5. Burke, A., Balch, A. L., Enemark, J. H. & Amer., J. Palladium and platinum complex resulting from the addition of hydrazine to coordinated isocyanide. *Chem. Soc.* **92,** 2555 (1970).
6. Butler, W. M. & Enemark, J. H. No Title. *Inorg. Chem.* **10,** 2416 (1971).
7. Fischer, E. O. & Maasböl, A. Zur Frage eines Wolfram-Carbonyl-Carben-Komplexes. *Angew. Chemie* **76,** 645 (1964).
8. Fischer, E. 0. & Maasböl, A. On the Existence of a Tungsten Carbonyl Carbene Complex. *Angew. Chemie - Int. Ed. English* **3,** 580–581 (1964).
9. Wanzlick, H.-W. & Schönherr, H.-J. Direkt-Synthese eines Quecksilbersalz-Carben-Komplexes. *Angew. Chemie* **80,** 154–154 (1968).
10. Wanzlick, H. W. & Schonherr, H. J. No Title. *Angew. Chemie - Int. Ed.* **7,** 141 (1968).
11. Öfele, K. 1,3-Dimethyl-4-imidazolinyliden-(2)-pentacarbonylchrom ein neuer übergangsmetall-carben-komplex. *J. Organomet. Chem.* **12,** 42–43 (1968).
12. Schrock, R. R. Alkylcarbene complex of tantalum by intramolecular .alpha.-hydrogen abstraction. *J. Am. Chem. Soc.* **96,** 6796–6797 (1974).
13. Arduengo, A. J., Harlow, R. L. & Kline, M. A Stable Crystalline Carbene. *J. Am. Chem. Soc.* **113,** 361–363 (1991).
14. Arduengo, A. J., Dias, H. V. R., Harlow, R. L. & Kline, M. Electronic Stabilization of Nucleophilic Carbenes. *J. Am. Chem. Soc.* **114,** 5530–5534 (1992).
15. de Frémont, P., Marion, N. & Nolan, S. P. Carbenes: Synthesis, properties, and organometallic chemistry. *Coord. Chem. Rev.* **253,** 862–892 (2009).
16. Kaufhold, S., Petermann, L., Staehle, R. & Rau, S. Transition metal complexes with N-heterocyclic carbene ligands : From organometallic hydrogenation reactions toward water splitting. **305,** 73–87 (2015).
17. Herrmann, W. A. & Kocher, C. N-Heterocyclic Carbenes. *Angew. Chemie - Int. Ed. English* **36,** 2162–2187 (1997).
18. Boehme, C. & Frenking, G. N-Heterocyclic Carbene, Silylene, and Germylene Complexes of MCl (M = Cu, Ag, Au). A Theoretical Study [1]. *Organometallics* **17,** 5801–5809 (1998).
19. Fantasia, S., Petersen, J. L., Jacobsen, H., Cavallo, L. & Nolan, S. P. Electronic properties of N-heterocyclic carbene (NHC) ligands: Synthetic, structural, and spectroscopic studies

of (NHC)platinum(II) complexes. *Organometallics* **26,** 5880–5889 (2007).

20. Hock, S. J., Schaper, L.-A., Herrmann, W. A. & Kühn, F. E. Group 7 transition metal complexes with N-heterocyclic carbenes. *Chem. Soc. Rev.* **42,** 5073 (2013).
21. Alder, R. W., Allen, P. R. & Williams, S. J. Stable carbenes as strong bases. *J. Chem. Soc. Chem. Commun.* 1267 (1995). doi:10.1039/c39950001267
22. Magill, A. M., Cavell, K. J. & Yates, B. F. Basicity of nucleophilic carbenes in aqueous and nonaqueous solvents - Theoretical predictions. *J. Am. Chem. Soc.* **126,** 8717–8724 (2004).
23. Schwesinger, R., Mißfeldt, M., Peters, K. & von Schnering, H. G. Novel, Very Strongly Basic, Pentacyclic 'Proton Sponges' with Vinamidine Structure. *Angew. Chemie Int. Ed. English* **26,** 1165–1167 (1987).
24. Kaljurand, I., Rodima, T., Leito, I., Koppel, I. A. & Schwesinger, R. Self-consistent spectrophotometric basicity scale in acetonitrile covering the range between pyridine and DBU. *J. Org. Chem.* **65,** 6202–6208 (2000).
25. Peris, E. *Topics in Organometallic Chemistry, vol.21. N-Heterocyclic Carbenes in Transition Metal Catalysis*. (2007).
26. Schaper, L.-A., Hock, S. J., Herrmann, W. A. & Kühn, F. E. Synthesis and application of water-soluble NHC transition-metal complexes. *Angew. Chem. Int. Ed. Engl.* **52,** 270–89 (2013).
27. Levin, E., Ivry, E., Diesendruck, C. E. & Lemcoff, N. G. Water in N-Heterocyclic Carbene-Assisted Catalysis. *Chem. Rev.* Ahead of Print (2015). doi:10.1021/cr400640e
28. Kuwata, S. & Ikariya, T. Metal-ligand bifunctional reactivity and catalysis of protic N-heterocyclic carbene and pyrazole complexes featuring β-NH units. *Chem. Commun. (Camb).* **50,** 14290–14300 (2014).
29. Yang, L. & Wang, H. Recent advances in carbon dioxide capture, fixation, and activation by using N-heterocyclic carbenes. *ChemSusChem* **7,** 962–998 (2014).
30. Oehninger, L., Rubbiani, R. & Ott, I. N-Heterocyclic carbene metal complexes in medicinal chemistry. *Dalt. Trans.* **42,** 3269–3284 (2013).
31. Velazquez, H. D. & Verpoort, F. N-Heterocyclic carbene transition metal complexes for catalysis in aqueous media. *Chem. Soc. Rev.* **41,** 7032–60 (2012).
32. Peris, E. & Crabtree, R. H. Recent homogeneous catalytic applications of chelate and pincer N-heterocyclic carbenes. *Coord. Chem. Rev.* **248,** 2239–2246 (2004).
33. Godoy, F., Segarra, C., Poyatos, M. & Peris, E. Palladium Catalysts with Sulfonate-Functionalized-NHC Ligands for Suzuki−Miyaura Cross-Coupling Reactions in Water. *Organometallics* **30,** 684–688 (2011).
34. Tomás-Mendivil, E. *et al.* Water-Soluble Gold(I) and Gold(III) Complexes with Sulfonated N - Heterocyclic Carbene Ligands: Synthesis, Characterization, and Application in the Catalytic Cycloisomerization of γ - Alkynoic Acids into Enol-Lactones. *Am. Chem. Soc. Catal.* **3,** 3086–3098 (2013).
35. Azua, A., Sanz, S. & Peris, E. Sulfonate-Functionalized NHC-Based Ruthenium Catalysts for the Isomerization of Allylic Alcohols in Water. Recyclability Studies. *Organometallics* **29,** 3661–3664 (2010).

36. Gnanamgari, D. *et al.* Iridium and Ruthenium Complexes with Chelating N-Heterocyclic Carbenes : Efficient Catalysts for Transfer Hydrogenation , -Alkylation of Alcohols , and N-Alkylation of Amines. *Organometallics* **28,** 321–325 (2009).

37. Jantke, D., Cokoja, M., Drees, M., Herrmann, W. A. & Kühn, F. E. Ruthenium-Catalyzed Hydrogenation of Oxygen-Functionalized Aromatic Compounds in Water. *ChemCatChem* **5,** 3241–3248 (2013).

38. Horváth, H. *et al.* New Water-Soluble Iridium(I) − N-Heterocyclic Carbene − Tertiary Phosphine Mixed-Ligand Complexes as Catalysts of Hydrogenation and Redox Isomerization. *Organometallics* **33,** 6330–6340 (2014).

39. Azua, A., Sanz, S. & Peris, E. Water-soluble IrIII N-heterocyclic carbene based catalysts for the reduction of CO2 to formate by transfer hydrogenation and the deuteration of aryl amines in water. *Chem. - A Eur. J.* **17,** 3963–3967 (2011).

40. Biffis, A., Baron, M. & Tubaro, C. *Poly-NHC complexes of transition metals: Recent applications and new trends*. *Advances in Organometallic Chemistry* **63,** (Elsevier Inc., 2015).

41. Lindström, U. M. Stereoselective Organic Reactions in Water. *Chem. Rev.* **102,** 2751–2772 (2002).

42. Anastas, P. & Eghbali, N. Green chemistry: principles and practice. *Chem. Soc. Rev.* **39,** 301–12 (2010).

43. Schaper, L.-A., Hock, S. J., Herrmann, W. A. & Kühn, F. E. Synthesis and application of water-soluble NHC transition-metal complexes. *Angew. Chemie - Int. Ed.* **52,** 270–289 (2013).

44. Cornils, B. & Herrmann, W. A. *Aqueous-Phase Organometallic Catalysis*. (2004). doi:10.1002/3527602488

45. Kascatan-Nebioglu, A., Panzner, M. J., Tessier, C. A., Cannon, C. L. & Youngs, W. J. N-Heterocyclic carbene-silver complexes: A new class of antibiotics. *Coord. Chem. Rev.* **251,** 884–895 (2007).

46. Loch, J. A. *et al.* Palladium Complexes with Tridentate Pincer Bis-Carbene Ligands as Efficient Catalysts for C−C Coupling. *Organometallics* **21,** 700–706 (2002).

47. Masllorens, E. *et al.* Can the Disproportion of Oxidation State III Be Favored in RuII-OH2 / Ru IV=O Systems? *J. Am. Chem. Soc.* **128,** 5306–5307 (2006).

48. Cheng, Y. *et al.* Fused polycyclic nucleophilic carbenes – synthesis, structure, and function. *Dalt. Trans.* 7132–7140 (2009). doi:10.1039/b907211j

49. Tulloch, A. A. D., Danopoulos, A. A., Winston, S., Kleinhenz, S. & Eastham, G. N-Functionalised heterocyclic carbene complexes of silver. *J. Chem. Soc. Dalt. Trans.* **24,** 4499–4506 (2000).

50. Nolan, S. P. *N-Heterocyclic Carbenes Effective Tools for Organometallic Synthesis*. (WILEY-VCH Verlag GmbH & Co. KGaA, 2014).

51. Wong, C.-Y., Lai, L.-M., Pat, P.-K. & Chung, L.-H. Osmium Complexes Containing N-Heterocyclic Carbene-Based C,N,C-Pincer Ligands. *Organometallics* **29,** 2533–2539 (2010).

52. Chung, L.-H. *et al.* Ruthenium(II) and osmium(II) complexes bearing bipyridine and the N-heterocyclic carbene-based C^N^C pincer ligand: an experimental and density functional theory study. *Inorg. Chem.* **52,** 9885–96 (2013).

53. Wright, J. A. *et al.* 'Pincer' N-Heterocyclic Carbene Complexes of Rhodium Functionalised with Pyridyl and Bipyridyl Donors. *Eur. J. Inorg. Chem.* **23,** 4857–4865 (2006).

54. Andrew, R. E. & Chaplin, A. B. Synthesis and reactivity of NHC-based rhodium macrocycles. *Inorg. Chem.* **54,** 312–322 (2015).

55. Monti, F. *et al.* Charged Bis-Cyclometalated Iridium(III) Complexes with Carbene- Based Ancillary Ligands. *Inorg. Chem.* **52,** 10292–10305 (2013).

56. Syska, H., Herrmann, W. A. & Kühn, F. E. Water-soluble carbene complexes as catalysts for the hydrogenation of acetophenone under hydrogen pressure. *J. Organomet. Chem.* **703,** 56–62 (2012).

57. Jantke, D., Cokoja, M., Pöthig, A., Herrmann, W. A. & Kühn, F. E. Synthesis and Characterization of Highly Water Soluble Ruthenium(II) and Osmium(II) Complexes Bearing Chelating Sulfonated N - Heterocyclic Carbene Ligands. *Organometallics* **32,** 741–744 (2013).

58. Jantke, D. *et al.* Hydrogen Production and Storage on a Formic Acid/Bicarbonate Platform using Water-Soluble *N* -Heterocyclic Carbene Complexes of Late Transition Metals. *ChemSusChem* **9,** 2849–2854 (2016).

59. Raba, A. *et al.* Facile and scalable preparation of 2-imidazolylpyridines. *Tetrahedron Lett.* **54,** 3384–3387 (2013).

60. Claramunt, R. M., Elguero, J. & Meco, T. N-Polyazolylmethanes. III. Synthesis and proton NMR study of 1,1'- methylenediimidazole and 1,1'- methylenedibenzimidazole derivatives. *J. Heterocycl. Chem.* **20,** 1245–1249 (1983).

61. Diez-Barra, E., De la Hoz, A., Sanchez-Migallon, A. & Tejeda, J. Phase transfer catalysis without solvent. Synthesis of bisazolylalkanes. *Heterocycles* **34,** 1365–1373 (1992).

62. Gural'skiy, I. A., Molnar, G., Fritsky, I. O., Salmon, L. & Bousseksou, A. Synthesis of [Fe(hptrz)3](OTs)2 spin crossover nanoparticles in microemulsion. *Polyhedron* **38,** 245–250 (2012).

63. Sluijter, S. N., Warsink, S., Lutz, M. & Elsevier, C. J. Synthesis of palladium(0) and -(II) complexes with chelating bis(N-heterocyclic carbene) ligands and their application in semihydrogenation. *Dalt. Trans.* **42,** 7365–7372 (2013).

64. Papini, G., Pellei, M., Lobbia, G. G., Burini, A. & Santini, C. Sulfonate- or carboxylate-functionalized N-heterocyclic bis-carbene ligands and related water soluble silver complexes. *Dalton Trans.* 6985–90 (2009). doi:10.1039/b907211j

65. Jensen, S. B., Rodger, S. J. & Spicer, M. D. Facile preparation of η6-p-cymene ruthenium diphosphine complexes. Crystal structure of [(η6-p-cymene)Ru(dppf)Cl]PF6. *J. Organomet. Chem.* **556,** 151–158 (1998).

66. Werner, H. & Zenkert, K. XIII *. Osmium @) - und Osmium (O) -Komplexe mit p-Cymen als aromatischem Liganden. *J. Organomet. Chem.* **345,** 151–166 (1988).

67. White, C., Yates, A., Maitlis, P. M. & Heinekey, D. M. (η5-pentamethylcyclopentadienyl)Rhodium and -Iridium Compounds. *Inorg. Synth.* **29,** 228–

234 (1992).

68. Brown, M. K., May, T. L., Baxter, C. A. & Hoveyda, A. H. All-carbon quaternary stereogenic centers by enantioselective cu-catalyzed conjugate additions promoted by a chiral N-heterocyclic carbene. *Angew. Chem. Int. Ed. Engl.* **46,** 1097–100 (2007).

69. Almássy, A., Nagy, C. E., Bényei, A. C. & Joó, F. Novel Sulfonated N-Heterocyclic Carbene Gold(I) Complexes: Homogeneous Gold Catalysis for the Hydration of Terminal Alkynes in Aqueous Media. *Organometallics* **29,** 2484–2490 (2010).

70. Radloff, C. *et al.* Metal-dependent coordination modes displayed by macrocyclic polycarbene ligands. *Chem. - A Eur. J.* **16,** 13077–81 (2010).

71. Brown, D. H., Nealon, G. L., Simpson, P. V., Skelton, B. W. & Wang, Z. Silver and Palladium Complexes of a Bis (benzimidazolin-2-ylidene) pyridine Pincer Ligand. *Organometallics* **28,** 1965–1968 (2009).

72. Ye, J., Jin, S., Chen, W. & Qiu, H. Structural characterization of the first linearly arranged Ag3 complexes supported by naphthyridine-functionalized N-heterocyclic carbenes. *Inorg. Chem. Commun.* **11,** 404–408 (2008).

73. Pugh, D., Boyle, A. & Danopoulos, A. A. 'Pincer' pyridine dicarbene complexes of nickel and their derivatives. Unusual ring opening of a coordinated imidazol-2-ylidene. *Dalton Trans.* **8,** 1087–94 (2008).

74. Caballero, A. *et al.* Corrigendum to : '1,1'-(Pyridine-2,6-diyl)bis(3-benzyl-2,3-dihydro-1H-imidazol-2-ylidene), a new multidentate N-heterocyclic biscarbene and its silver(I) complex derivative'. *J. Organomet. Chem.* **627,** 263–264 (2001).

75. Baquero, E. A., Silbestri, G. F., Go, P., Flores, J. C. & Jesu, E. De. Sulfonated Water-Soluble N - Heterocyclic Carbene Silver(I) Complexes: Behavior in Aqueous Medium and as NHC-Transfer Agents to Platinum(II). *Organometallics* **32,** 2814–2826 (2013).

76. Moore, L. R. *et al.* Synthesis and Characterization of Water-Soluble Silver and Palladium Imidazol-2-ylidene Complexes with Noncoordinating Anionic Substituents. *Organometallics* **25,** 5151–5158 (2006).

77. Kriechbaum, M., List, M., J F Berger, R., Patzschke, M. & Monkowius, U. Silver and gold complexes with a new 1,10-phenanthroline analogue N-heterocyclic carbene: a combined structural, theoretical, and photophysical study. *Chem. - A Eur. J.* **18,** 5506–9 (2012).

78. Fliedel, C. & Braunstein, P. Thioether-Functionalized N-Heterocyclic Carbenes: Mono- and Bis-(S , C NHC) Palladium Complexes, Catalytic C−C Coupling, and Characterization of a Unique Ag 4 I 4 (S , C NHC) 2 Planar Cluster †. *Organometallics* **29,** 5614–5626 (2010).

79. Catalano, V. J., Malwitz, M. A. & Etogo, A. O. Pyridine Substituted N-Heterocyclic Carbene Ligands as Supports for Au (I) − Ag (I) Interactions : Formation of a Chiral Coordination Polymer. *Inorg. Chem.* **43,** 5714–5724 (2004).

80. Dinda, J. *et al.* Supporting Information N-heterocyclic carbene supported Au(i) and Au(iii) complexes: a comparison of cytotoxicities. *New J. Chem.* **38,** 1218–1224 (2014).

81. Zhang, X., Xi, Z., Liu, A. & Chen, W. Facile and Efficient Olefination of Aryl Halides Catalyzed by a Palladium Complex Containing a Heteroarene-Functionalized N-Heterocyclic Carbene. *Organometallics* **27,** 4401–4406 (2008).

82. Mann, J. B., Meek, T. L., Knight, E. T., Capitani, J. F. & Allen, L. C. Configuration Energies of the d-Block Elements. *J. Am. Chem. Soc.* **122,** 5132–5137 (2000).

83. Chung, L.-H., Chan, S.-C., Lee, W.-C. & Wong, C.-Y. Emissive osmium(II) complexes supported by N-heterocyclic carbene-based C^C^C-pincer ligands and aromatic diimines. *Inorg. Chem.* **51,** 8693–703 (2012).

84. Castarlenas, R., Esteruelas, M. A. & Oñate, E. Preparation of [C , N , O] -Pincer Osmium Complexes by Alkylidene Metathesis with a Methyl Group of 2 , 6-Diacetylpyridine. *Organometallics* **26,** 3082–3084 (2007).

85. Baya, M., Eguillor, B., Esteruelas, M. A., Oliván, M. & Oñate, E. Influence of the Anion of the Salt Used on the Coordination Mode of an N-Heterocyclic Carbene Ligand to Osmium. *Organometallics* **26,** 6556–6563 (2007).

86. Castarlenas, R., Esteruelas, M. A. & Oñate, E. N-Heterocyclic Carbene - Osmium Complexes for Olefin Metathesis Reactions. *Organometallics* **24,** 4343–4346 (2005).

87. Di Giuseppe, A., Castarlenas, R., Pérez-Torrente, J. J., Lahoz, F. J. & Oro, L. A. Hydride-rhodium(III)-N-heterocyclic carbene catalysts for vinyl-selective H/D exchange: a structure-activity study. *Chem. - A Eur. J.* **20,** 8391–403 (2014).

88. Zenkina, O. V, Keske, E. C., Kochhar, G. S., Wang, R. & Crudden, C. M. Heteroleptic rhodium NHC complexes with pyridine-derived ligands: synthetic accessibility and reactivity towards oxygen. *Dalton Trans.* **42,** 2282–93 (2013).

89. Wang, C.-Y., Liu, Y.-H., Peng, S.-M. & Liu, S.-T. Rhodium(I) complexes containing a bulky pyridinyl N-heterocyclic carbene ligand: Preparation and reactivity. *J. Organomet. Chem.* **691,** 4012–4020 (2006).

90. Stylianides, N., Danopoulos, A. A. & Tsoureas, N. 1Pyridine and phosphine functionalised N-heterocyclic carbene complexes of rhodium and iridium. *J. Organomet. Chem.* **690,** 5948–5958 (2005).

91. Mas-Marzá, E., Sanaú, M. & Peris, E. Coordination Versatility of Pyridine-Functionalized N-Heterocyclic Carbenes : A Detailed Study of the Different Activation Procedures . Characterization of New Rh and Ir Compounds and Study of Their Catalytic Activity. *Inorg. Chem.* **44,** 9961–9967 (2005).

92. Rahaman, S. M. W., Dinda, S., Sinha, A. & Bera, J. K. A Noninnocent Cyclooctadiene (COD) in the Reaction of an 'Ir(COD)(OAc)' Precursor with Imidazolium Salts. *Organometallics* **32,** 192–201 (2013).

93. Cowley, M. J. *et al.* Iridium N-Heterocyclic Carbene Complexes as Efficient Catalysts for Magnetization Transfer from para -Hydrogen. *J. Am. Chem. Soc.* **133,** 6134–6137 (2011).

94. Dastgir, S., Coleman, K. S., Cowley, A. R. & Green, M. L. H. Fused polycyclic nucleophilic carbenes - synthesis, structure, and function. *Dalton Trans.* **35,** 7203–14 (2009).

95. Peng, H. M., Webster, R. D. & Li, X. Quinoline-Tethered N-Heterocyclic Carbene Complexes of Rhodium and Iridium: Synthesis, Catalysis, and Electrochemical Properties. *Organometallics* **27,** 4484–4493 (2008).

96. Wang, C.-Y., Fu, C.-F., Liu, Y.-H., Peng, S.-M. & Liu, S.-T. Synthesis of iridium pyridinyl N-heterocyclic carbene complexes and their catalytic activities on reduction of nitroarenes. *Inorg. Chem.* **46,** 5779–86 (2007).

97. Gru, S., Kovacevic, A., Albrecht, M., Faller, J. W. & Crabtree, R. H. Abnormal Ligand Binding and Reversible Ring Hydrogenation in the Reaction of Imidazolium Salts with IrH 5 (PPh 3) 2. *J. Am. Chem. Soc.* **5,** 10473–10481 (2002).

98. Hillier, A. C., Lee, H. M., Stevens, E. D. & Nolan, S. P. Cationic Iridium Complexes Bearing Imidazol-2-ylidene Ligands as Transfer Hydrogenation Catalysts. *Organometallics* **20,** 4246–4252 (2001).

99. Schumacher, A., Bernasconi, M. & Pfaltz, A. Chiral N-heterocyclic carbene/pyridine ligands for the iridium-catalyzed asymmetric hydrogenation of olefins. *Angew. Chem. Int. Ed. Engl.* **52,** 7422–5 (2013).

100. Zhang, F. *et al.* The intramolecular π–π stacking interaction does not always work for improving the stabilities of light-emitting electrochemical cells. *Org. Electron.* **13,** 2442–2449 (2012).

101. Shibata, T., Hashimoto, H., Kinoshita, I., Yano, S. & Nishioka, T. Unprecedented diastereoselective generation of chiral-at-metal, half sandwich Ir(III) and Rh(III) complexes via anomeric isomerism on 'sugar-coated' N-heterocyclic carbene ligands. *Dalton Trans.* **40,** 4826–9 (2011).

102. Fawcett, J., Harding, D. A. J., Hope, E. G., Singh, K. & Solan, G. A. Stabilisation of iridium(III) fluoride complexes with NHCs. *Dalton Trans.* **39,** 10781–9 (2010).

103. Xiao, X.-Q. & Jin, G.-X. Functionalized N-heterocyclic carbene iridium complexes: Synthesis, structure and addition polymerization of norbornene. *J. Organomet. Chem.* **693,** 3363–3368 (2008).

104. Wang, L. *et al.* Transfer hydrogenation of acetophenone in an organic-aqueous biphasic system containing double long-chain surfactants. *R. Soc. Chem. Adv.* **4,** 1567–1569 (2014).

105. Li, J. *et al.* Surfactant-accelerated asymmetric transfer hydrogenation with recyclable water-soluble catalyst in aqueous media. *R. Soc. Chem. Adv.* **3,** 1825–1834 (2013).

106. Jung, Y. & Marcus, R. A. On the theory of organic catalysis 'on water'. *J. Am. Chem. Soc.* **129,** 5492–5502 (2007).

107. Garrison, J. C. & Youngs, W. J. Ag(I) N-heterocyclic carbene complexes: synthesis, structure, and application. *Chem. Rev.* **105,** 3978–4008 (2005).

108. Kühl, O. The chemistry of functionalised N-heterocyclic carbenes. *Chem. Soc. Rev.* **36,** 592–607 (2007).

109. Dixneuf, P. H. & Cadierno, V. *Metal-Catalyzed Reactions in Water*. (WILEY-VCH Verlag GmbH & Co. KGaA, 2013).

110. Kaufhold, S., Petermann, L., Staehle, R. & Rau, S. Transition metal complexes with N-heterocyclic carbene ligands: From organometallic hydrogenation reactions toward water splitting. *Coord. Chem. Rev.* **304–305,** 73–87 (2015).

111. Günay, M. E. & Gençay Çoğaşlioğlu, G. The role of N-heterocyclic carbene substituents on ruthenium (II) complexes in the catalytic transfer hydrogenation of acetophenone Ag-NHC. *Turkish J. Chem.* **40,** 296–304 (2016).

112. Csabai, P. & Joó, F. Synthesis and catalytic properties of new water-soluble ruthenium(II)-N-heterocyclic carbene complexes. *Organometallics* **23,** 5640–5643 (2004).

113. Vries, J. G. de & Elsevier, C. J. *The Handbook of Homogeneous Hydrogenation*. (WILEY-VCH Verlag GmbH & Co. KGaA, 2007).

114. Zhu, M. Integration of phase transfer catalysis into aqueous transfer hydrogenation. *Appl. Catal. A Gen.* **479,** 45–48 (2014).

115. Zhou, Z. & Sun, Y. Water-soluble chiral aminosulfonamides as ligands for ruthenium(II)-catalyzed asymmetric transfer hydrogenation. *Catal. Commun.* **10,** 1685–1688 (2009).

116. Gillet, S. *et al.* Lignin transformations for high value applications: towards targeted modifications using green chemistry. *Green Chem.* **19,** 4200–4233 (2017).

117. Astruc, D. *Nanoparticles and Catalysis*. (WILEY-VCH Verlag GmbH & Co. KGaA, 2008).

118. Ning, J., Shang, Z. & Xu, X. How Does the Hemilabile Group in Ruthenium-Cp* Picolyl-NHC Complexes Affect the Mechanism of Transfer Hydrogenation Reaction? A DFT Study. *Catal. Letters* **145,** 1331–1343 (2015).

119. Bäckvall, J.-E. Transition metal hydrides as active intermediates in hydrogen transfer reactions. *J. Organomet. Chem.* **652,** 105–111 (2002).

120. Clapham, S. E., Hadzovic, A. & Morris, R. H. Mechanisms of the H2-hydrogenation and transfer hydrogenation of polar bonds catalyzed by ruthenium hydride complexes. *Coord. Chem. Rev.* **248,** 2201–2237 (2004).

121. Gladiali, S. & Alberico, E. Asymmetric transfer hydrogenation: chiral ligands and applications. *Chem. Soc. Rev.* **35,** 226–236 (2006).

122. Samec, J. . S. M., Bäckvall, J.-E., Andersson, P. G. & Brandt, P. Mechanistic aspects of transition metal-catalyzed hydrogen transfer reactions. *Chem. Soc. Rev.* **35,** 237–248 (2006).

123. Torres, O., Martín, M. & Sola, E. Labile N -Heterocyclic Carbene Complexes of Iridium. *Organometallics* **28,** 863–870 (2009).

124. Jiménez, M. V. *et al.* Iridium(I) complexes with hemilabile N-heterocyclic carbenes: Efficient and versatile transfer hydrogenation catalysts. *Organometallics* **30,** 5493–5508 (2011).

125. Bonnet, L. G. *et al.* Synthesis, structure and reactivity of palladium(II) complexes of chiral N-heterocyclic carbene-imine and -amine hybrid ligands. *Dalt. Trans.* 3528–3535 (2004). doi:10.1016/j.poly.2004.06.031

126. Jiménez, M. V. *et al.* Rhodium(I) complexes with hemilabile N-heterocyclic carbenes: Efficient alkyne hydrosilylation catalysts. *Organometallics* **27,** 224–234 (2008).

127. Joó, F. *Aqueous Organometallic Catalysis*. (Kluwer Academic Publishers, 2002).

128. Abura, T., Ogo, S., Watanabe, Y. & Fukuzumi, S. Isolation and crystal structure of a water-soluble iridium hydride: A robust and highly active catalyst for acid-catalyzed transfer hydrogenations of carbonyl compounds in acidic media. *J. Am. Chem. Soc.* **125,** 4149–4154 (2003).

129. Lee, H. M. *et al.* Palladium complexes with ethylene-bridged bis (N -heterocyclic carbene) for C – C coupling reactions. *Tetrahedron* **60,** 5807–5825 (2004).

List of Schemes

Scheme 1. Synthesis of a ruthenium (II) NHC complex reported by Llobet *et al*.[47] 10

Scheme 2. Synthesis of a ruthenium (II) NHC complex reported by Zi-Ling Xue *et al*.[48]..... 10

Scheme 3. Synthesis of silver (I) complexes reported by Eastham *et al*.[49] 11

Scheme 4. Synthesis of ruthenium (II) and iridium (III) NHC complex reported by Crabtree *et al*.[36] 12

Scheme 5. Synthesis of gold NHC complexes..... 14

Scheme 6. Equilibria of gold (III) complexes dissolved in water. 14

Scheme 7. Synthesis of ruthenium, rhodium and iridium complexes developed by Kühn *et al*.[56] 17

Scheme 8. Synthesis of ruthenium, osmium, rhodium and iridium complexes developed by Kühn *et al.*[57,58] 17

Scheme 9. Synthesis of 2-(imidazole-1-yl)pyridine (**1**)..... 19

Scheme 10. Synthesis of bis(imidazol-1-yl) methane (**2**). 19

Scheme 11. Synthesis of bis(1,2,4-triazol-1-yl)methan (**3**). 20

Scheme 12. Synthesis of 2,6-Bis(imidazol-1-yl)pyridine (**4**). 20

Scheme 13. Synthesis of 1-(imidazole-1-yl-3-n-butyl)pyridine (**5**)..... 21

Scheme 14. Synthesis of 2,6-bis(imidazol-1-yl-3-n-butyl)pyridine (**6**). 21

Scheme 15. Synthesis of bis(imidazol-1-yl-3-butyl)methane dibromide (**7**) ligand. 21

Scheme 16. Synthesis of ruthenium (**12**) and osmium (**13**) metal precursors..... 24

Scheme 17. Synthesis of rhodium (**14**) and iridium (**15**) metal precursors. 24

Scheme 18. Synthesis of Ag-NHC complexes (**16a**-**b**). 25

Scheme 19. Synthesis of ruthenium(II) (**17a**), osmium(II) (**18a**), rhodium(III) (**19a**) and iridium(III) (**20a**) complexes. 28

Scheme 20. Synthesis of water-soluble NHC ruthenium(II) (**17b**), osmium(II) (**18b**), rhodium(III) (**19b**) and iridium(III) (**20b**) complexes. 30

Scheme 21. Transfer hydrogenation of acetophenone in a basic ^{i}PrOH solution (a), in an aqueous solution containing sodium formate and formic acid (b) and hydrogenation of acetophenone using H_2(g) as hydrogen source (c). 36

Scheme 22. Proposed mechanism for the transfer hydrogenation of acetophenone with 1-(2-pyridinyl)-3-*n*-butyl)imidazol-2-ylidene metal complexes. 50

Scheme 23. Proposed inner-sphere mechanism for the transfer hydrogenation of acetophenone with Rhodium complex **19b**. 59

Scheme 24. Possible pathways in the hydrogenation of acetophenone. 62

List of Figures

Figure 1. Fischer (a) first carbene compound, Wanzlick (b) and Öfele (c) first *N*-Heterocyclic compounds, first Schrock alkylidene–metal (d^0) complex (d) and first stable free carbene synthesized by Arduengo *et al*. (e)..... 2

Figure 2. Singlet (a) and triplet (b) forms of a carbene..... 2

Figure 3. Bond of a singlet carbene with a metal to form a Fischer carbene (a) and OM diagram of the π- contribution of the M-C bond (b)..... 3

Figure 4. Bond of a triplet carbene with a metal to form a Schrock carbene (a) and OM diagram of the π- contribution of the M-C bond (b)..... 3

Figure 5. Examples of synthesized water-soluble NHC-metal complexes containing different functionalization of the NHC moieties: carboxylate (a), sulfonate (b), ammonium (c), alcohol (d), water-soluble polymer (e), natural product based (f) and charged ligand (g)..... 8

Figure 6. Used NHC ligands for the synthesis of new catalysts..... 9

Figure 7. Some examples of chelating ruthenium NHC complexes. 12

Figure 8. Some examples of osmium, rhodium and iridium NHC complexes..... 13

Figure 9. Some examples of silver-NHC complexes containing sulfonate groups. 15

Figure 10. Some examples of palladium, ruthenium and iridium NHC complexes containing sulfonate groups. 16

Figure 11. ORTEP style representation of the cation of **16a** (thermal ellipsoids are shown at a 50% probability level). Hydrogen atoms and two PF6- are omitted for clarity. Selected bond lengths (Å) and angles(º): Ag(1)–C(1) 2.090(4), Ag(1)–C(13) 2.094(4), Ag(2)–C(25) 2.078(3), Ag(2)–N(3) 2.156(3), Ag(1)–Ag(2) 3.3456(4), C(1)–Ag(1)–C(13) 166.72(14), N(3)–Ag(2)–C(25) 158.87(13), C(13)–N(5)–C(16)–N(6) -10.60(5), C(1)–N(2)–C(4)–N(3) -67.6(4), C(25)–N(8)–C(28)–N(9) -13.7(5). 25

Figure 12. ORTEP style representation of **16b**·MeOH (thermal ellipsoids are shown at a 50% probability level). Hydrogen atoms and co-crystallized solvent are omitted for clarity. Selected bond lengths (Å) and angles(°): Ag(1)–C(1) 2.088(3), Ag(1)–C(12) 2.094(3), C(1)–Ag(1)–C(12)

173.21(12), C(1)–N(2)–C(4)–C(5) 28.6(4), C(1)–N(2)–C(4)–N(3) -153.2(3), C(12)–N(5)–C(15)–N(6) -10.9(4). 26

Figure 13. View of the crystal structure **16b**·MeOH along the crystallographic *a* axis. 27

Figure 14. ^{13}C NMR shifts of the aromatic carbon resonances of complexes **17a** and **18a**. 28

Figure 15. ^{13}C NMR shifts of the aromatic carbon resonances of complexes **19a** and **20a**. 29

Figure 16. ^{13}C NMR shifts of the aromatic carbon resonances of complexes **17b** and **18b**..... 31

Figure 17. ^{13}C NMR shifts of the aromatic carbon resonances of complexes **19b** and **20b**..... 32

Figure 18: ORTEP style representation of the cation in **18b**·MeOH (thermal ellipsoids are given at a 50% probability level). Hydrogen atoms and co-crystallized solvent are omitted for clarity. Selected bond lengths (Å) and angles (°): Os(1)–C(1) 2.037(3), Os(1)–N(3) 2.103(3), Os(1)–Cl(1) 2.4006(8), Os(1)–C(12) 2.197(4), Os(1)–C(13) 2.161(4), Os(1)–C(14) 2.199(4), Os(1)–C(15) 2.199(4), Os(1)–C(16) 2.241(4), Os(1)–C(17) 2.233(4), C(1)–Os(1)–N(3) 75.60(12), C(1)–Os(1)–Cl(1) 81.84(10), C(1)–Os(1)–C(13) 96.01(14), N(3)–Os(1)–C(15) 92.89(12), Cl(1)–Os(1)–C(17) 87.95(10), N(3)–Os(1)–Cl(1) 84.25(8), C(1)–N(2)–C(4)–N(3) 0.7(5). 33

Figure 19. ORTEP style representation of the cations **19a**, **19b**·2.10H_2O, **20a** and **20b**·2.10H_2O (ellipsoids are set at 50% probability). Hydrogen atoms and co-crystallized solvent are omitted for clarity. 34

Figure 20. TH of acetophenone catalyzed by ruthenium (II) carbonyl chloride complexes containing pyridine-functionalized NHCs described by Zi-Ling Xue *et al*.[48] 37

Figure 21. TH of acetophenone catalyzed by iridium (III) and ruthenium (II) complexes with chelating pyridine-functionalised NHCs described by Crabtree *et al*.[36] 37

Figure 22. TH of acetophenone catalyzed by ruthenium (II) complexes without chelating functionalised NHCs described by Gençay Çoğaşlioğlu *et al.*[111] 38

Figure 23. Structure of a ruthenium (II) complex (a), its equilibrium in water (b) and ketone catalytic hydrogenation of acetophenone (c) developed by Péter Csabai and Ferenc Joó.[112] ... 38

Figure 24. Catalytic transfer hydrogenation of ketones in water developed by Zhongqiang Zhou and Yong Sun[115] 40

Figure 25. Some examples of catalytic applications of palladium (a)[33], iridium (b)[39] and ruthenium (c)[35] complexes containing a chelating alkanesulfonated NHC ligand. 41

Figure 26. Catalytic hydrogenation of acetophenone by ruthenium, rhodium and iridium water-soluble catalysts developed by Kühn *et al.*[56] 41

Figure 27. Catalytically active Ru, Rh and Ir complexes with sulfonate functionalized NHC ligand (a), hydrogen production and storage formic acid/bicarbonate platform (b), hydrogenation of phenol (c) and acetophenone (d) developed in our research group.[37,58] 43

Figure 28. ^{1}H NMR spectrum of **17a** in ^{i}PrOD. 46

Figure 29. ^{1}H NMR spectrum of **17a** in the mixture KOH/^{i}PrOD. 46

Figure 30. ^{1}H NMR spectrum **19a** in the mixture KOH/^{i}PrOD. 47

Figure 31. ^{1}H NMR spectrum of **18a** in neat ^{i}PrOD. 48

Figure 32. ^{1}H NMR spectra of **17b** measured after stirring the samples in D_2O at RT (a) and at 80°C (b). 53

Figure 33. ^{1}H NMR spectra of **18b** measured after stirring the samples in D_2O at RT (a) and at 80°C (b). 53

Figure 34. ^{1}H NMR spectra of **17b** measured after stirring the sample in HCO_2Na/HCO_2H aqueous solution at RT (a) and 80°C (b) for 20 h. 54

Figure 35. ^{1}H NMR spectra of **18b** measured after stirring the sample in HCO_2Na/HCO_2H aqueous solution at RT (a) and 80°C (b) for 20 h. 55

Figure 36. ^{1}H NMR spectra of **20b** measured after stirring the sample in HCO_2Na/HCO_2H aqueous solution at RT (a) and 80°C (b) for 7 h. 56

Figure 37. 1H NMR spectra of **19b** measured after stirring the sample in HCO_2Na/HCO_2H aqueous solution at RT (a) and 80°C (b) for 15 min. 57

Figure 38. ^{1}H NMR spectra of **19b** measured at 5°C in HCO_2Na/HCO_2H aqueous solution after (a) 1.7 min, (b) 30 min, (c) 1 h, (d) addition of more HCO_2Na/HCO_2H solution, (e) 30 min after the latter addition. 58

Figure 39. Plot of the conversion of acetophenone vs. time using catalysts **17b** and **19b**..... 63

Figure 40. Black suspension observed after catalysis for **17b** (right) and **19b** (left)..... 63

Figure 41. TEM micrographs of the active Ru (left) and Rh (right) solution after 3 h reaction time. 65

Figure 42. New synthesized pyridine-functionalized NHC complexes. 67

Figure 43. ^{1}H (MeOD-d_4, 400 MHz) and ^{13}C (MeOD-d_4, 100 MHz) NMR spectra of **16a**. 89

Figure 44. ^{1}H (DMSO-d_6, 400 MHz) and ^{13}C (DMSO-d_6, 100 MHz) NMR spectra of **16b**. 90

Figure 45. ^{1}H (MeOD-d_4, 400 MHz) and ^{13}C (MeOD-d_4, 100 MHz) NMR spectra of **17a**. 91

Figure 46. ^{1}H (MeOD-d_4 , 400 MHz) and ^{13}C (MeOD-d_4 , 100 MHz) NMR spectra of **18a**. 92

Figure 47. ^{1}H (DMSO-d_6, 400 MHz) and ^{13}C (DMSO-d_6, 100 MHz) NMR spectra of **19a**. 93

Figure 48. ^{1}H (DMSO-d_6, 400 MHz) and ^{13}C (DMSO-d_6, 100 MHz) NMR spectra of **20a**. 94

Figure 49. ^{1}H (MeOD-d_4, 400 MHz) and ^{13}C (MeOD-d_4, 100 MHz) NMR spectra of **17b**. 95

Figure 50. ^{1}H (MeOD-d_4, 400 MHz) and ^{13}C (MeOD-d_4, 100 MHz) NMR spectra of **18b**. 96

Figure 51. ^{1}H (D_2O, 400 MHz) and ^{13}C (D_2O, 100 MHz) NMR spectra of **19b**. 97

Figure 52. ^{1}H (D_2O, 400 MHz) and ^{13}C (D_2O, 100 MHz) NMR spectra of **20b**. 98

List of Tables

Table 1. Overview of the synthesis of the different water-soluble ligands (**8**-**11**)..... 22

Table 2. Catalytic transfer hydrogenation with water-insoluble catalysts **17a**-**20a**. 45

Table 3. Catalytic transfer hydrogenation with water-soluble catalysts **17b**-**20b**..... 51

Table 4. Optimization of reaction conditions for the hydrogenation of acetophenone with catalysts **17b**-**20b**. 61

Table 5. Optimization of reaction conditions for the hydrogenation of acetophenone by **17b** and **19b** with previous preparation of the active NPs solution. 64

Table 6. Crystallographic data for compounds **16a**, **16b**, **19a**, **20a**, **18b**, **19b** and **20b**. 100

Table 7. Selected bond lengths (Å) and bond angles (º) for rhodium and iridium complexes. 103